TERNARY NANOCOMPOSITES OF HIGH DENSITY, LINEAR LOW DENSITY AND LOW DENSITY POLYETHYLENES

A THESIS SUBMITTED TO
THE GRADUATE SCHOOL OF NATURAL AND APPLIED SCIENCES
OF
MIDDLE EAST TECHNICAL UNIVERSITY

BY

EGEMEN UÇAR

IN PARTIAL FULFILLMENT OF THE REQUIREMENTS
FOR
THE DEGREE OF MASTER OF SCIENCE
IN
POLYMER SCIENCE AND TECHNOLOGY

JUNE 2007

Approval of Graduate School of Natural and Applied Sciences

Prof. Dr. Canan Özgen
Director

I certify that this thesis satisfies all the requirements as a thesis for degree of Master of Science.

Associate Prof. Dr. Göknur Bayram
Head of the Department

This is to certify that we have read this thesis and that in our opinion it is fully adequate, in scope and quality, as a thesis for the degree of Master of Science.

Prof. Dr. Ülkü Yılmazer
Supervisor

Examining Committee Members

Head of Jury: Prof. Dr. Leyla Aras	(METU, CHEM)	
Supervisor: Prof. Dr. Ülkü Yılmazer	(METU, CHE)	
Prof. Dr. Duygu Kısakürek	(METU, CHEM)	
Prof. Dr. Ali Usanmaz	(METU, CHEM)	
Prof. Dr. Teoman Tinçer	(METU, CHEM)	

I hereby declare that all information in this document has been obtained and presented in accordance with academic rules and ethical conduct. I also declare that, as required by these rules and conduct, I have fully cited and referenced all material and results that are not original to this work.

Name, Last name: Egemen Uçar

Signature

ABSTRACT

TERNARY NANOCOMPOSITES OF HIGH DENSITY, LINEAR LOW DENSITY AND LOW DENSITY POLYETHYLENES

Uçar, Egemen
M.S., Department of Polymer Science and Engineering
Supervisor: Prof. Dr. Ülkü YILMAZER

June 2007, 145 pages

In this study, the effects of organoclay loading, compatibilizer loading and polyethylene type on the morphology, rheology, thermal properties and mechanical properties of polyethylene/compatibilizer/organoclay nanocomposites were investigated. As compatibilizer, terpolymer of ethylene-methacrylate-glycidyl methacrylate (Lotader® AX8900), as organoclay Cloisite® 15A were used. All samples were prepared by a co-rotating twin screw extruder, followed by injection molding.

Considering ternary nanocomposites, highest impact strength results were obtained with 10% compatibilizer plus 2% organoclay; highest yield stress, elastic modulus, flexural strength, flexural modulus were obtained with 5% compatibilizer plus 4-6% organoclay.

DSC data indicated that addition of organoclay and compatibilizer did not change the melting point remarkably; on the other hand it affected the crystallinity. The organoclay used had no nucleation effect on polyethylene, and the compatibilizer decreased the crystallinity of the matrix.

X-ray diffraction showed that in all ternary nanocomposites and in binary nanocomposite of high density polyethylene with organoclay, layer separation associated with intercalation of the clay structure occurred,. The highest increase of interlayer gallery spacing was obtained with 10% compatibilizer plus 2% organoclay, which were 25%, 28% and 27% for HDPE, LLDPE and LDPE matrices respectively.

Keywords: Nanocomposite, organically modified clay, compatibilizer, melt compounding, ethylene-methyl acrylate-glycidyl methacrylate

ÖZ

YÜKSEK YOĞUNLUK, LİNEER ALÇAK YOĞUNLUK VE ALÇAK YOĞUNLUK POLİETİLENLERİN ÜÇLÜ SİSTEM NANOKOMPOZİTLERİ

Uçar, Egemen

Yüksek Lisans, Polimer Bilimi ve Teknolojisi Bölümü

Tez Yöneticisi: Prof. Dr. Ülkü Yılmazer

Haziran 2007, 145 sayfa

Bu çalışmada organik modifiyeli kil, uyumlaştırıcı ve polietilen çeşidinin morfolojik, reolojik, ısıl ve mekanik özellikler üzerindeki etkileri incelenmiştir. Uyumlaştırıcı olarak etilen-metil akrilat-glisidil metakrilat (Lotader® AX8900), organik modifiyeli kil olarak Cloisite® 15A kullanılmıştır. Bütün numuneler aynı yönde dönen çift vidalı ekstrüder ve bunu takiben enjenksiyonla kalıplama yöntemiyle hazırlanmıştır.

Üçlü sistem nanokompozitler göz önünde bulundurulduğunda, %10 uyumlaştırıcı ve %2 kil içeren kompozisyonlar en yüksek darbe dayanımını göstermiştir. En yüksek akmada gerilme dayanımı, elastik modül, bükülme direnci ve bükülme modülü değerleri ise %5 uyumlaştırıcı ve %4-6 kil içeren numunelerde görülmüştür.

DSC verileri, uyumlaştırıcı ve kil eklenmesinin erime sıcaklığına görülür şekilde etki etmediğini, fakat kristal yüzdesini etkilediğini göstermiştir. Kil polietilen içinde kristallenme başlatıcı bir etki göstermemiştir ve uyumlaştırıcı matrisin kristal yüzdesini düşürmüştür.

X-ışını kırınımı analizi, tüm üçlü sistem nanokompozitlerde ve ikili sistem kil/yüksek yoğunluk polietilende kil tabakalarının ayrıldığını göstermiştir. Tüm sistemler arasında tabakalar arası artış en çok %10 uyumlaştırıcı ve %2 kil içeren kompozisyonlarda görülmüştür. Bu artış sırasıyla YYPE, LAYPE ve AYPE matrisli nanokompozitler için %25,%28 ve %27 dir.

Anahtar Kelimeler: Nanokompozit, organik modifiyeli kil, uyumlaştırıcı, eriyik halde karıştırma, etilen-metil akrilat-glisidil metakrilat

To my beloved wife for sacrificing her career for me and for her love, and to my family for trusting me in their heart and giving me freedom for establishing my path

ACKNOWLEDGEMENTS

I would like to express my deepest gratitude to my supervisor Prof. Dr. Ülkü Yılmazer, for his continuous support, encouragement and guidance throughout this study.

I am very grateful to Assoc. Prof. Dr. Göknur Bayram from the Department of Chemical Engineering for giving me every opportunity to use the instruments in her laboratory.

Special thanks go to Cengiz Tan and Evren Tan from Department of Metallurgical and Materials Engineering for SEM analysis, Necmi Avcı from Department of Metallurgical and Materials Engineering for X-ray diffraction analysis and Central Lab of METU for DSC analysis.

I am also thankful to all my friends in Polymer Research Group for their cooperation and friendship.

I want to thank my beloved wife, for the sacrifices she made, the support she gave, for her help with the experiments and for loving me in heart.

Last but not the least; I wish to express my sincere thanks to Uçar-Olgun family for supporting and encouraging me through my life.

TABLE OF CONTENTS

LIST OF TABLES

LIST OF FIGURES

NOMENCLATURE

A_0	Original, undeformed cross-sectional area, mm2
b	Width of beam tested, mm
d	Depth of beam tested, mm
d	Plane spacing, Å
E	Modulus of Elasticity, MPa
F	Tensile Load, N
g	Grafted
ΔH_f	Heat of fusion measured, J/g
ΔH_f^0	Heat of fusion of 100% crystalline polymer, J/g
L	Support span, mm
L_0	Initial gauge length, mm
ΔL	Change in sample length, mm
m	Slope of the tangent to the initial straight-line portion of the load deflection curve, N/mm
n	Order of diffraction
P	Load at a given point on the load-deflection curve, N
R	Maximum strain in the outer fibers, mm/mm
S	Stress in the outer fibers at midspan, MPa
T	Thickness, mm
Tc	Crystallization temperature, °C
Tg	Glass transition temperature, °C
Tm	Melting temperature, °C
w	Weight fraction of clay

Greek Letters

Є	Tensile strain, mm/mm
λ	Wavelength, nm
σ	Tensile stress(nominal), MPa
σ_m	Tensile strength, MPa
θ	Scattering angle, °

Abbreviations

ASTM	American Society for Testing and Materials
CEC	Cation Exchange Capacity
DSC	Differential Scanning Calorimetry
E-MA-GMA	Ethylene-Methyl Acrylate-Glycidyl Methacrylate
GMA	Glycidyl Methacrylate
HDPE	High Density Polyethylene
HT	Hydrogenated Tallow
LDPE	Low Density Polyethylene
LLDPE	Linear Low Density Polyethylene
MFI	Melt Flow Index
MMT	Montmorillonite
PE	Polyethylene
PLS	Polymer Layered Silicate
PLSN	Polymer Layered Silicate Nanocomposite
SEM	Scanning Electron Microscopy
TEM	Transmission Electron Microscopy
OMLS	Organically Modified Layered Silicate
XRD	X-Ray Diffraction

CHAPTER I

INTRODUCTION

A composite, in general, is defined as a combination of two or more components differing in form or composition on a macroscale, with two or more distinct phases having recognizable interfaces between them. Proper combination of materials into composites gives rise to properties which transcend those of the constituents, as a result of the principle of combined action [1].

Composites usually consist of a reinforcing material embedded in a matrix (binder). The effective method to increase the strength and to improve overall properties is to incorporate dispersed phases into the matrix. Polymer matrix composites (PMC) are the most developed composite materials group and they have found widespread applications [1].

The field of nanocomposites involves the study of multiphase material where at least one of the constituent phases has one dimension less than 100 nm. The promise of nanocomposites lies in their multifunctionality, the possibility of realizing unique combinations of properties unachievable with traditional materials. The challenges in reaching this promise are tremendous. They include control over the distribution in size and dispersion of the nano size constituents, tailoring and understanding the role of interfaces between structurally or chemically dissimilar phases on bulk properties [2].

The main reason for these improved properties is interfacial interaction between the polymer matrix and organically modified layered silicate as opposed to conventional composites. Layered silicates have layer thickness in the order of 1 nm and very high aspect ratios (e.g., 10-1000). A few weight percent of organically modified layered

silicate that is properly dispersed throughout the matrix creates a much higher surface area for polymer-filler interfacial interactions than in conventional composites [3].
The preferred layered materials at nanocomposites are phyllosilicate clays of the 2: 1 type, more precisely smectites, and in particular montmorillonite (MMT). The layer surface has 0.25 to 0.9 negative charges per unit cell and a commensurate number of exchangeable cations in the interlamellar galleries. The amount of this high aspect ratio nanomaterial that needs to be added to a polymeric matrix to engender clay containing polymeric nanocomposite with improved performance can be as little as 5 ppm. The aim is to totally exfoliate the platelets, but frequently doublets and short stacks (tactoids) may also be present [4].

Polyethylene (PE) is used more than any other thermoplastic polymer. There is a wide variety of grades and formulations available that have an equally wide range of properties. In general, the outstanding characteristics of PE are toughness, ease of processing, chemical resistance, abrasion resistance, electrical properties, impact resistance, low coefficient of friction, and near-zero moisture absorption. This material evolved into two forms, LDPE and HDPE. PE's dominance can be explained by the fact that it offers a combination of characteristics that are ideally suited to various applications, such as good flow, good thermal stability, broad density range, and excellent chemical resistance [5].

Even after organic modification of the clays, polyethylene does not wet the surface of clays because it is nonpolar. It is necessary to blend in a functionalized polymer that wets the modified clay surface more readily and is also miscible with the bulk polymer [6].

Melt mixing is the preferred method for the preparation of nanocomposites with thermoplastic matrix polymers. Usually, the polymer is melted and compounded with intercalated clay using an extruder, an internal mixer, a kinetic-energy mixer, etc [4].Melt mixing method has great advantages over either in situ intercalative polymerization or polymer solution intercalation. Firstly, this method is environmentally benign due to the absence of organic solvent. Secondly, it is compatible with current industrial processes [3].

The aim of this study was to investigate the effect of content of organoclay, content of compatibilizer and polyethylene type on the final properties of PE based nanocomposites. In the experiments, terpolymer of ethylene-methacrylate-glycidyl methacrylate Lotader® AX8900 was used as the compatibilizer and organically modified montmorillonite clay Cloisite® 15A was used as the reinforcement.

Nanocomposites were produced by means of melt intercalation method using a co-rotating twin screw extruder, followed by injection molding. In order to characterize the nanocomposites, rheological properties, thermal properties and mechanical properties and morphology were investigated.

XRD was performed to investigate the extent of dispersion of the clay in the matrix. SEM was performed to investigate dispersion and distribution of the clay in the matrix. DSC was used to determine thermal behavior and MFI measurements were made to determine the flow behavior. Mechanical tests were performed to investigate the flexural strength, flexural modulus, tensile strength, elastic modulus and elongation at break. Notched charpy tests were done to observe the resistance to impact.

CHAPTER II

BACKGROUND

2.1 Composites

A composite is a combined material created by the synthetic assembly of two or more components; selected filler or reinforcing agent and a compatible matrix binder in order to obtain specific characteristics and properties. The components of a composite do not dissolve or otherwise merge completely into each other, but nevertheless do act in concert. The components as well as the interface between them can usually be physically identified, and it is the behavior and properties of the interface that generally control the properties of the composite. The properties of a composite cannot be achieved by any of the components acting alone [7]. Therefore composites help us with the most challenging engineering applications. There are two phases in a composite; one of them is the matrix and the other is the reinforcement phase.

2.1.1 Matrix Phase

The matrix usually comprises 30%-40% of a composite structure. It has a number of functions:

a) it binds the components together and determines the thermo-mechanical stability of the composite,

b) it protects the reinforcements from wear/ abrasion and environment,

c) it helps to distribute the applied load by acting as a stress-transfer medium,

d) it provides durability, inter-laminar toughness and shear/ compressive/ transverse strengths to the system in general, and,

e) it maintains the desired fiber orientations and spacings in specific structures [1].

2.1.2 Reinforcement Phase

The reinforcing component in a composite structure can be discontinuous (either in the form of dispersions/ particles, flakes, whiskers, discontinuous short fibers with different aspect ratios) or continuous (long fibers and sheets); although the most commonly employed reinforcing component is in particulate or in fibrous form [1].

2.1.3 Types of Composites

Many classifications can be made according to the matrix and reinforcements. Matrix can consist of metal, ceramic, carbon or polymer [1].

Composites can be also classified on the basis of the form of their structural components: fibrous (composed of fibers in a matrix), laminar (composed of layers of materials), and particulate (composed of particules in a matrix) [7].

2.2 Polymer-Matrix Composites

Typical resins include polyester, phenolic, epoxy, silicone, alkyd, melamine, polyimide, fluorocarbon, polycarbonate, acrylic, acetal, polypropylene, ABS (acrylonitrile-butadiene-styrene) copolymer, polyethylene, and polystyrene. Resins can be classified as thermoplastic (capable of being repeatedly hardened and softened by increases and decreases, respectively, in temperature) or thermoset (changing into a substantially infusible and insoluble material when cured by the application of heat or by chemical means) [7].

2.3 Nanocomposites

The diameter short fibers (e.g., glass or carbon) or ceramic particles are usually in the range of several micrometers, and they provide an increase in thermal stability, stiffness and strength of the polymer matrix used. There are, however, some drawbacks by such fillers, as for example a reduction in strain failure, impact strength and, sometimes also in fracture toughness. To overcome this problem, an innovative approach takes advantage of particles with diameters in the range of several nanometers [8].

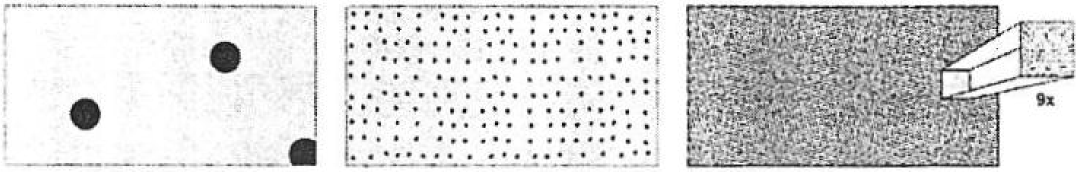

Figure 2.1 Correlation between the relative number (n) particles and the particle size (d) At a constant filler content of 3 vol. % within a reference volume. Left: d=10 μm, n ~ 2.8; center: d=1 μm, n= 2860; right: d=100nm, n=2860000 particles homogeneously distributed [9]

Figure 2.1 explains schematically why one must expect different, or even superior properties in the case of nanocomposites, when compared to traditional composites containing micro- or macro particles, their size and specific surface area is demonstrated for a constant filler content of 3 vol.%. Within a reference volume of 50000 $\mu m^{3,}$ one can detect only three particles when their diameter is 10μm (
Figure 2.1, left). However, the particle number increases enormously to more than 3 million, if nanoparticles of 100 μm diameter are used (
Figure 2.1, Right). Obviously, nanoparticles can provide a much higher interface area than the ''large'' particles. One can indeed speak of ''interface-dominated'' materials in this case, and it becomes clear that such increased interface area may widely determine the composite properties [9].

2.3.1 Polymer-Layered Silicate Nanocomposites

The polymer matrix and the fillers are bonded to each other by weak intermolecular forces, and chemical bonding is rarely involved. If the reinforcing material in the composite could be dispersed on a molecular scale (nanometer level) and interacted with the matrix by chemical bonding, then significant improvements in the mechanical properties of the material or unexpected new properties might be realized. These are the general goals of polymer nanocomposite studies. In order to achieve this purpose, clay minerals (montmorillonite, saponite, hectorite, etc.) have been discussed as candidates for the filler material [6].

2.3.2 Layered Silicates

A layer of silicate clay mineral is about 1 nm in thickness and consists of platelets of around 100 nm in width, so it represents a filler with a significantly large aspect ratio. For comparison, a glass fiber 13 nm in diameter with a length of 0.3 mm is 4×10^9 times the size of a typical silicate layer. In other words, if the same volumes of glass fiber and silicate were evenly dispersed, there would be a roughly 10^9 fold excess of silicate layers, with an exponentially higher specific surface available [6].

2.3.2.1 Montmorillonite (Smectite) Clay

Montmorillonite is 2:1 smectite; i.e., it has three atomic lattice layers in each of the nanolayers with an aluminum-oxygen-hydroxyl octahedral sheet sandwiched between two silicon-oxygen tetrahedral sheets. Individual nanolayers are 1nm thick and their lateral dimensions are about 100 nm [6].

2.3.3 Organically Modified Layered Silicates

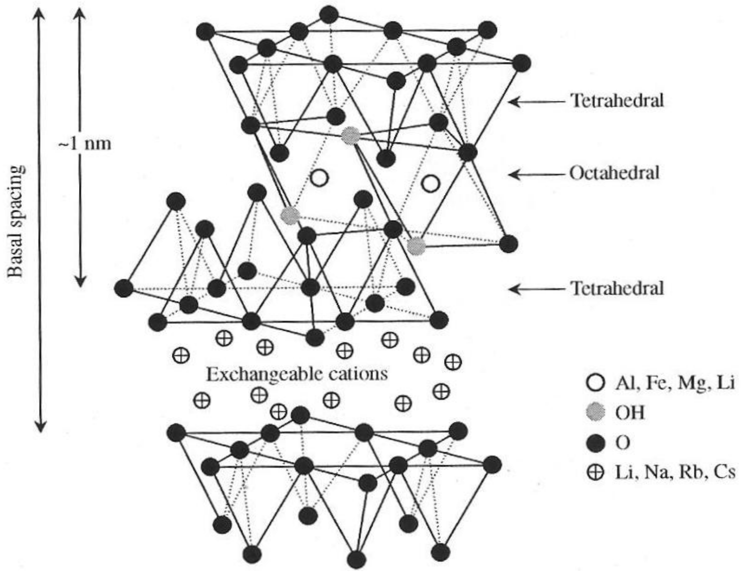

Figure 2.2 Structure of 2:1layared (phyllosilicates) [6]

Figure 2.2 shows structure of 2:1 layered (phyllosilicates) [3].There are hydroxyl groups at the nanolayer edges, which are part of the aluminum lattice layer. The interlayer galleries contain exchangeable cations (usually sodium) because of the charge imbalance created by isomorphic substitution of aluminum. The hydrophilic face of the clay platelets is modified by pre-intercalating long chain alkyl ammonium ions as surfactants, in order to enhance the interaction between the mineral and the organic polymer. The onium ion interacts with the surface of the clay while the hydrocarbon tails swell the clay and improve its dispersibility in organic materials. Other layered silicates with larger lateral dimensions have been investigated but they are harder to disperse, requiring much higher shear stresses for delamination and running the risk of damaging the particles [6].

2.3.4 Types of Polymer Layered Silicate Nanocomposite Structures

Depending on the strength of interfacial interaction between polymer matrix and layered silicate (modified or not), three different types of PLS nanocomposites are thermodynamically achievable, which is shown at Figure 2.3 [3].

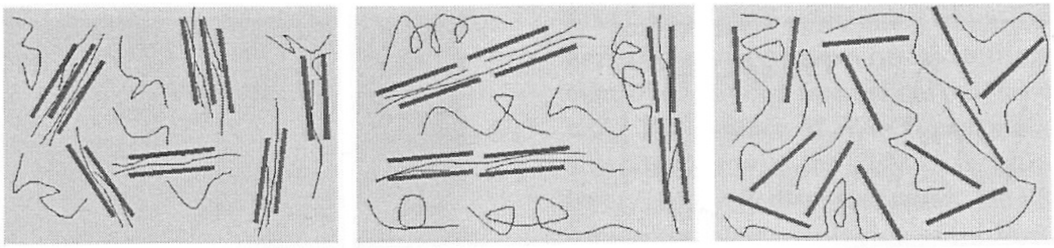

Intercalated Intercalated-and-flocculated Exfoliated

Figure 2.3 Schematic illustration of three different types of thermodynamically achievable polymer/clay nanocomposites [3]

1) Intercalated nanocomposites: in an intercalated nanocomposite, the insertion of polymer matrix into the layered silicate structure occurs in a crystallographically regular fashion, regardless of the silicate layer (clay) to polymer ratio. Properties of the composites typically resemble those of ceramic materials [3].

2) Flocculated nanocomposites: conceptually this is the same as with intercalated nanocomposites, however, silicate layers are sometimes flocculated due to hydroxylated edge-edge interaction of the silicate layers. The length of the oriented collections in the range of 300-800 nm is far larger than the original silicate layer (mean diameter 150 nm). Such flocculation presumably is governed by an interfacial energy between polymer matrix and organoclays and controlled by ammonium cation-matrix polymer interaction. The polarity of the matrix polymer is of fundamental importance in controlling the nanoscale structure [3].

3) Exfoliated nanocomposites: in exfoliated nanocomposites, the individual silicate layers are separated in a continuous polymer matrix by an average distance that totally depends on the layered silicate loading. Usually, the clay content of an exfoliated nanocomposite is much lower than that of an intercalated nanocomposite [3].

2.3.5 Synthesis of Polymer Layered Silicate Nanocomposites

2.3.5.1 In-Situ Intercalative Polymerization Method

In this method, the organically modified layered silicate is swollen within the liquid monomer or a monomer solution so that the polymer formation can occur in between the intercalated sheets. Polymerization can be initiated either by heat or radiation, by the diffusion of a suitable initiator, or by an organic initiator or catalyst fixed through cation exchange inside the interlayer before the swelling step by the monomer [3].

2.3.5.2 Solution Intercalation Method

This is based on a solvent system in which polymer or pre-polymer is soluble and the silicate layers are swellable. The layered silicate is first swollen in a solvent, such as water, chloroform or toluene. When the polymer and layered silicate solutions are mixed, the polymer chains intercalate and displace the solvent within the interlayer of the silicate. Upon solvent removal, the intercalated structure remains, resulting in polymer layered silicate nanocomposites [3].

2.3.5.3 Melt Intercalation Method

This method involves annealing, statically or under shear, a mixture of the polymer and organically modified layered silicate above the softening point of the polymer. This method has great advantages over either *in situ* intercalative polymerization or polymer solution intercalation. Firstly, this method is environmentally benign due to the absence of organic solvents. Secondly, it is compatible with current industrial processes, such as extrusion and injection molding. The melt intercalation method allows the use of polymers which were previously not suitable for *in situ* polymerization or the solution intercalation method. This solvent-free method is much preferred for practical industrial material production because of its high efficiency and possibility of avoiding environmental hazards [3].

2.4 Polyethylene

Polyethylene (PE) was discovered in 1933 by Reginald Gibson and Eric Fawcett at the British industrial giant, Imperial Chemical Industries (ICI). Although it is more than 70 years since it was first produced, it is still a very promising material. This widely used plastic is a polymer of ethylene, $CH_2=CH_2$, having the formula $(-CH_2-CH_2-)_n$. It is produced at high pressures and temperatures in the presence of anyone of several catalysts, depending on the desired properties of the end-use product. Other structures (leading to long and short branches) may be present, depending on the procedure used in the synthesis. PE is the largest volume polymer consumed in the world. It is a versatile material that offers high performance compared to other polymers and alternative materials such as glass, metal or paper [5].

2.4.1 Polymerization of PE

Despite ethylene's simple structure, the field of PE is a complex one with a wide range of types and many different manufacturing processes, which offer the possibility of a versatile tailor-made range of products, see Figure 2.4 [5].

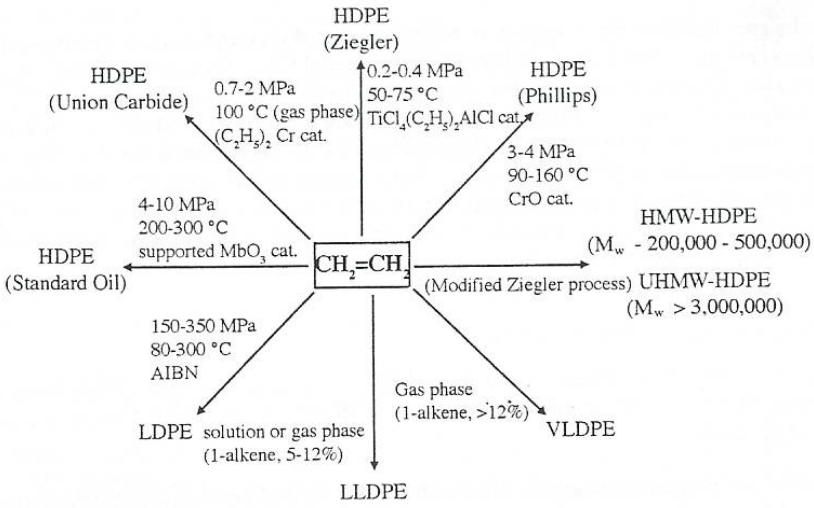

Figure 2.4 Different preparative routes for commercial PE [5]. M_w: molecular weight, AIBN: azo iso butyronitrile

The polymerization processes are classified with respect to the physical state of the medium, namely in suspension, in solution, in gaseous phase, and in bulk, and with respect to the reactor type, as in autoclave, tubular, loop, or fluidized bed [5].

2.4.2 Types of Polyethylene

PE grades are mainly classified according to their density. Figure 2.5 shows classification of PE grades [5].

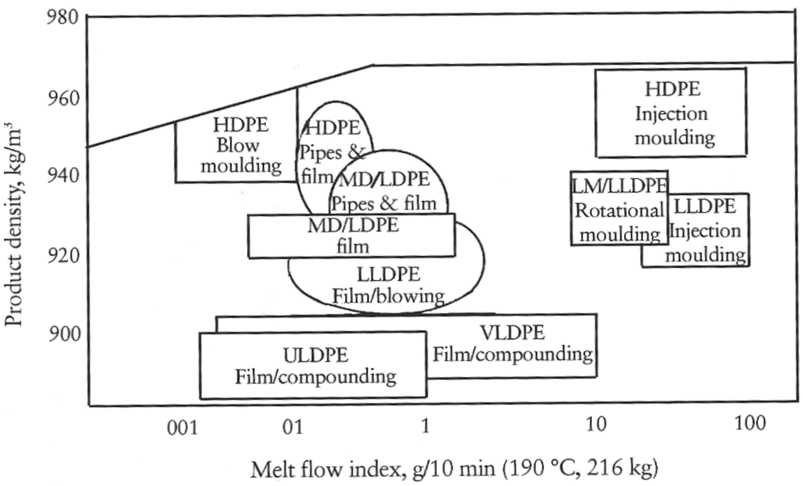

Figure 2.5 Classification of PE Grades [5]. MDPE: Medium density PE, ULDPE: Ultra low density PE, VLDPE: Very low density PE, LMDPE: Low medium density PE

2.4.2.1 Low Density Polyethylene

Originally referred to homopolymers of density 0.915-0.940 g cm^{-3}. However, use of Ziegler-type catalysts in low pressure processes produces copolymers of density 0.900-0.964 g cm^{-3}, and use of these catalysts in the high pressure processes can achieve densities of 0.870-0.960 g cm^{-3}. The M_W, M_W distribution and frequency and distribution of long and short chain branching all affect the physical and mechanical properties. Owing to the customizable nature of polyethylene, and differences between manufacturing processes, data given here tend to be overall ranges. Specific manufacturer's grades will normally have closer tolerances or, with certain processes, even be available outside the ranges quoted [12].

2.4.2.2 Linear Low Density Polyethylene

LLDPE designation is usually applied to ethylene copolymers in the density range 0.915-0.925 g cm^{-3}, with a co-monomer (normally butene, hexene or octene) content of approx. 2.5-3.5 mol%. As with LDPE properties are affected by M_W, M_W distribution and frequency type, and distribution of branches (co-monomer). The structural regularity and narrow M_W distribution achieved by the use of metallocene catalysts is having a major impact, a 'new' non-metallocene LLDPE has also been reported [12].

2.4.2.3 High Density Polyethylene

The most molecularly regular polyethylene grade is HDPE. It approximates to structural unit with five Me groups per 1000 carbon atoms. Metallocene catalysts are used to improve chain regularity. Virtually no branches or a small number of branches are introduced by copolymerization with another α-olefin. The number (or degree) of branches varies from 0.5-10 branches per 1000 carbon atoms. One chain end is a methylene group and the other is either a methylene or a vinyl group. The degree of branching, M_W and the M_W distribution influence most physical and mechanical properties [10,11].

2.4.3 Polyethylene – Organoclay Interaction

In spite of the organic treatment of the clay, polymers that do not include any polar group in their backbone, such as polyethylene (PE) and polypropylene, do not lead to a homogeneous dispersion of the clay. Only when the in situ polymerization was performed the PE/clay nanocomposite formation was achieved [13,14,15]. Initial attempts to create the polymer layered silicate nanocomposite from non polar polymers by simple melt mixing were based on the introduction of modified oligomers to mediate the polarity between the clay surface and the polymer matrix [16,17].

2.4.3.1 Glycidyl Methacrylate (GMA) Functionality

Glycidyl methacrylate (GMA) monomer has dual functionality, containing both methacrylic and epoxy groups. Both of these groups readily react with a wide range of monomers and functionalized molecules to provide the user with maximum freedom and flexibility in polymer design. The dual functionality of GMA also brings together the desirable properties of both methacrylics and epoxies [18]. Figure 2.6 shows the chemical formula of GMA.

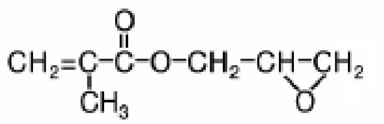

Figure 2.6 Chemical Formula of GMA

Glycidyl methacrylate gives reactivity (versus OH, COOH and NH_2 groups), leading to optimal dispersion during melt mixing with engineering thermoplastics.

2.4.3.2 Methyl Acrylate (MA) Functionality

Acrylic Ester shown in Figure 2.7 brings softness and polarity, while keeping high thermal stability during processing. The high content of acrylic ester leads to high flexibility (low crystallinity) and high impact absorption behavior.

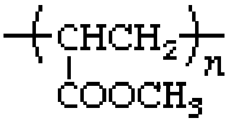

$$-\!\!\left(\underset{\displaystyle COOCH_3}{\underset{|}{C}}HCH_2\right)_n\!\!-$$

Figure 2.7 Chemical Formula of MA

2.5 Polymer Processing

There is great diversity among those industries associated with polymeric materials. Some industries are principally concerned with the production of polymers from the raw (monomeric) materials. Others are concerned with the physical conversion of a polymeric material into a finished article. The diversity arises both from the wide range of properties of the multitude of commercially available polymers and from the great variety of physical processes that can transform a polymer to an article of commerce [19].

2.5.1 Extrusion

Extrusion is basically the transformation of a raw material into a continuous, specifically shaped product by forcing the material through a die [20]. An extruder is a pump. It is a versatile machine, capable of performing other operations in concert with its pumping function. Figure 2.8 shows details of a typical screw extruder. If the extruder is fed with solid polymer chips or beads, a melting operation is normally achieved within a few diameters downstream of the feed inlet. This operation is often referred to as *plasticizing,* and such an extruder is a *plasticizing extruder.* If the feed is a fluid, usually a molten polymer, the extruder is called a *melt extruder.* If dissimilar polymers, or polymer plus another fluid, or polymer plus pigment or filler is fed to the extruder, the machine serves the additional function of a mixer [19].

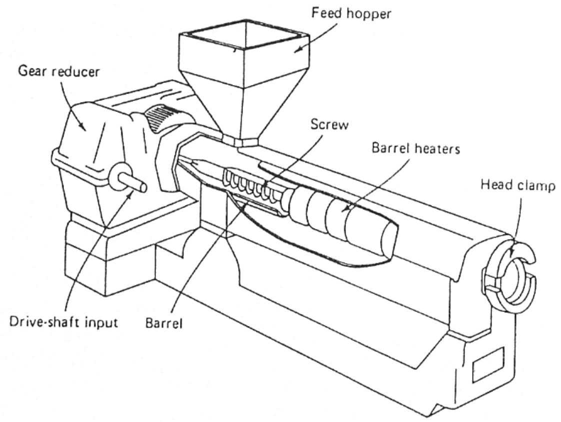

Figure 2.8 Cutaway view of a typical single-screw extruder [21]

Extruders in the polymer industry come in many different designs. The main distinction between the various extruders is their mode of operation: continuous or discontinuous. The latter type extruder delivers polymer in an intermittent fashion and, therefore, is ideally suited for batch type processes, such as injection molding and blow molding. As mentioned earlier, continuous extruders have a rotating member, whereas batch extruders have a reciprocating member. A classification of the various extruders is shown in Table 2.1 [21].

Table 2.1 Classification of Polymer Extruders [21]

Screw Extruders (Continuous)	Single Screw Extruders	- Melt Fed or Plasticating - Single Stage or Multi Stage - Plastic vs. Rubber Extruder
	Multi-Screw Extruders	- Twin Screw Extruder - Gear Pump - Planetary Gear Extruder - Multi (>2) Screw Extruder
Disk or Drum Extruders (Continuous)	Viscous Drag Type Extruders	- Spiral Disk Extruder - Drum Extruder - Diskpack Extruder - Stepped Disk Extruder
	Elastic Melt Extruders	- Screwless Extruder (Maxwell) - Screw/Disk Extruder (USSR)
Reciprocating Extruders (Discontinuous)	Ram Extruders	- Melt Fed Extruder - Plasticating Extruder (Capillary Rheometer)
	Reciprocating Screw Extruders	- Plasticating Unit in Molding Machines - Compounding Extruders (Ko-Kneader, Pulsating Action)

2.5.2 Twin Screw Extruders

A twin screw extruder is a machine with two Archimedean screws. Admittedly, this is a very general definition. However, as soon as the definition is made more specific, one limits it to a specific class of twin screw extruders. There is a tremendous variety of twin screw extruders, with vast differences in design, principle of operation, and field of application. It is, therefore, difficult to make general comments about twin screw extruders. The differences between the various twin screw extruders are much larger than the differences between single screw extruders. This is to be expected, since the twin screw construction substantially increases the number of design variables, such as direction of rotation, degree of intermeshing, etc. A classification of twin screw extruders is shown in Table 2.2 [21].

Table 2.2 Classification of Twin Screw Extruders [21]

Intermeshing Extruders	Corotating Extruders	- Low Speed Extruders (profile extrusion) - High Speed Extruders (compounding, devolatilization)
	Counterrotating Extruders	- Conical Extruders (profile extrusion) - Cylindrical Extruders (profile extrusion)
Nonintermeshing Extruders	Counterrotating Extruders	- Equal Screw Length - Unequal Screw Length
	Corotating Extruders	- Not used in practice
	Coaxial Extruders	- Inner Melt Transport Forward - Inner Melt Transport Rearward - Inner Solids Transport Rearward - Inner Plasticating, Rearward Transport

This classification is primarily based on the geometrical configuration of the twin screw extruder shown in Figure 2.9. Some twin screw extruders function much in the same fashion as single screw extruders. Other twin screw extruders operate quite differently from single screw extruders and are used in very different applications [21].

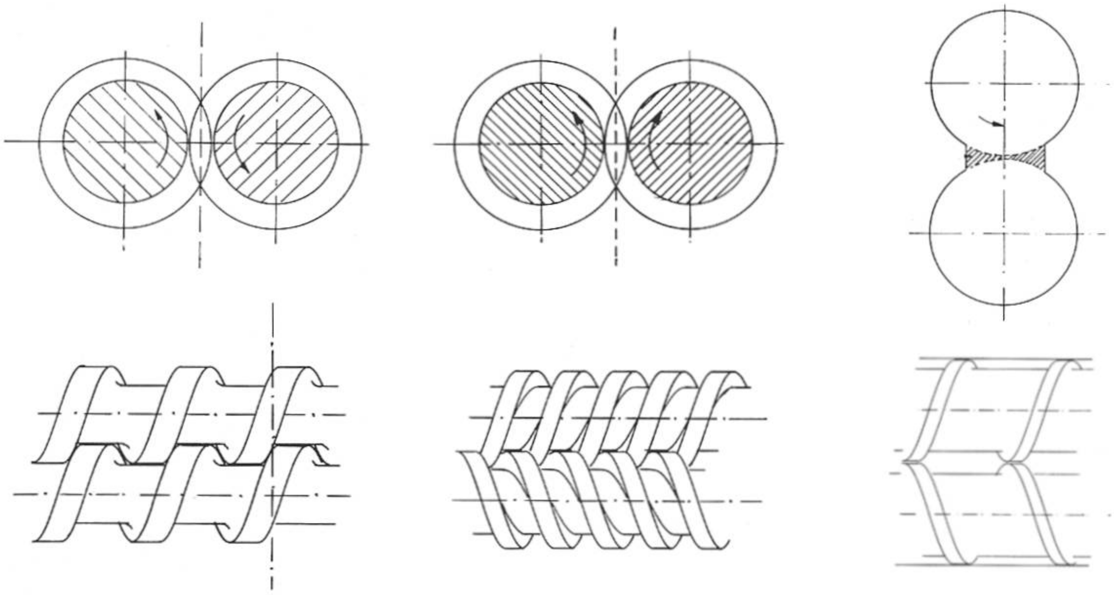

Intermeshing Co-Rotating

Intermeshing Counter-Rotating

Non-Intermeshing Counter-Rotating

Figure 2.9 Screw Types of Twin Screw Extruders [21]

2.5.3 Injection Molding

Injection molding is a major processing technique for converting thermoplastics, and now thermosetting materials, into all types of products [22].

Most thermoplastic materials are molded by the process of *injection molding.* Here the polymer is preheated in a cylindrical chamber to a temperature at which it will flow and then is forced into a relatively cold, closed mold cavity by means of quite high pressures applied hydraulically, traditionally through a plunger or ram, but today almost invariably by means of a reciprocating screw that serves the dual purposes of providing the molten polymer mass and forcing it into the mold [23].

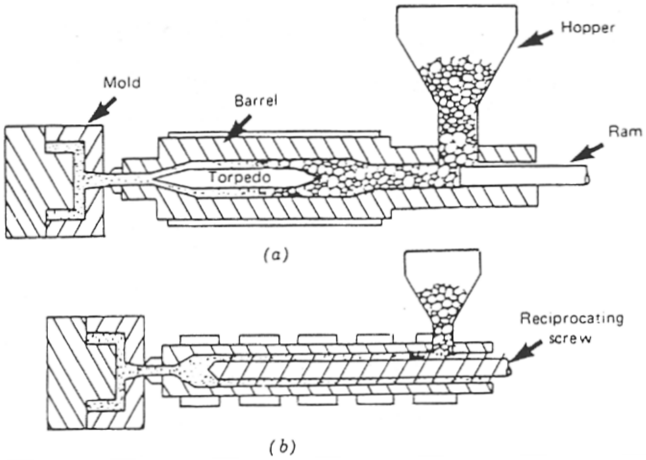

Figure 2.10 (a) a ram-fed (b) a screw fed injection molding machine [23]

With reference to Figure 2.10, the screw rotates to pick up the particulate polymer, compact and melt it, mix the melt, and deliver it to the entrance to the mold. The screw then moves forward, to force a fixed volume of the molten polymer into the closed mold. The melt temperature may be considerably higher than in compression molding, and pressures of hundreds to thousands of tons are common. After the polymer melt has solidified in the cool mold, the screw rotates and moves backward to ready the charge of polymer for the next cycle. Meanwhile the mold is opened and the molded article is removed [23].

An outstanding feature of injection molding is the speed with which finished articles can be produced. Cycle times of 10-30 sec are common, as are multicavity molds allowing the production of many parts per cycle. Articles weighing up to many kilograms can be produced [23].

2.6 Characterization of Nanocomposites

The structure of the PLS nanocomposites has typically been established using wide-angle X-ray diffraction (XRD) analysis and scanning electron microscopy (SEM) observations.

2.6.1 Morphological Analysis

There are several techniques that are used to elucidate the nanostructure of polymer layered silicate nanocomposites, including atomic force microscopy, NMR, and neutron-scattering methods; however, wide-angle X-ray diffraction (XRD) and transmission electron microscopy (TEM) are the most commonly used techniques [24]. Since there was no opportunity for TEM available, SEM was performed.

2.6.1.1 X-Ray Diffraction (XRD)

In 1913, Bragg showed that the positions of the discrete X-ray spots in the diffraction pattern can be explained by assuming that the diffracted X-ray photons behave as if they were “reflected” from certain families of equally spaced parallel planes passing through the crystal lattice. Figure 2.11 illustrates the principle known as Bragg's law. The two paths, A and B, for the incident and diffracted beams differ in length by $2d\sin\theta$; where d is the perpendicular distance between two adjacent parallel planes. The parameter θ is equal to the angle between the incident beam and each plane and is equal to the angle between the diffracted beam and each plane. For constructive interference to take place, this difference must be equal to a whole number of wavelengths. Bragg showed that diffraction takes place only if all the lattice points of the crystal are on the parallel planes [41].

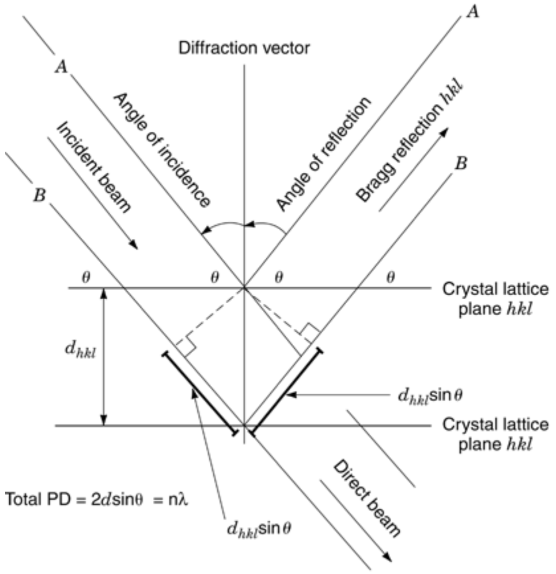

Figure 2.11 Geometry of diffraction and its relationship to Bragg's law [41]

Where n is an integer. An example of parallel planes that pass through all of the lattice points is shown in Figure 2.12 [41].

$$n\lambda = 2\ d\ \sin(\theta) \tag{2.1}$$

where, n is degree of diffraction, λ is wavelength, θ is the measured diffraction angle and d refers to interlayer spacing.

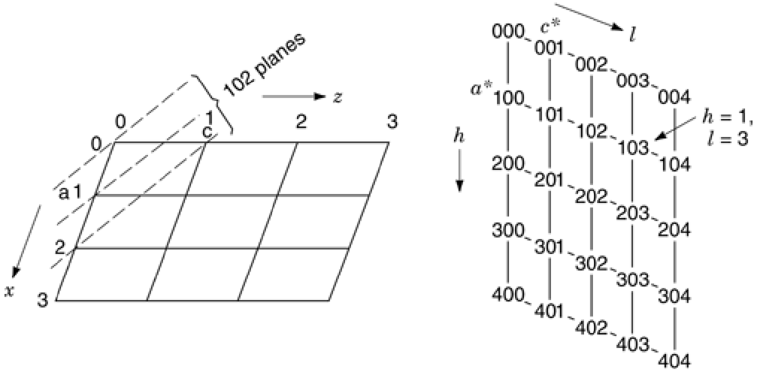

Figure 2.12 Indexes of reflections and the reciprocal lattice [41]

After the clay is organically modified, the most common technique used to analyze the clay with XRD, which allows the interlayer *d*-spacing (the distance between the basal layers of the MMT clay, or of any layered material) to be measured. Increased spacing between basal layers and a hydrophobic, organophilic surface make it more likely for the polymer to enter between the layers (referred to as the *gallery*) of the clay. Because XRD has been successfully used to analyze organically modified clays, it has been employed to look at changes in *d*-spacings when PLSN materials are prepared. The *d*-spacing observed by XRD for PLSN materials has been used to describe the nanoscale dispersion of the clay in the polymer [24].

With XRD, *immiscible* materials have no change in *d*-spacing, meaning that no polymer has entered the gallery and that the spacing between clay layers is unchanged. *Intercalated* nanocomposites have an increased *d*-spacing, indicating that polymer has entered the gallery, expanding the layers. *Exfoliated* PLSNs show no peak by XRD, suggesting that a great amount of polymer has entered the gallery space, expanding the clay layers so far apart that diffraction cannot be observed with wide-angle ($2\theta > 1°$) XRD techniques. Furthermore, the clay layers are sufficiently disordered such that they no longer give a coherent XRD signal [22].

2.6.1.2 Scanning Electron Microscopy (SEM)

Electron microscopy is done in one of two ways: SEM or TEM. SEM is the most common and well-known electron microscopy method for the physical imaging of surfaces. This technique is based on the interaction with a surface of a primary beam of electrons with energy typically in the range of 0.5–40 keV. This primary electron beam is first demagnified by a condenser lens and then focused onto the sample surface using a series of objective lenses where it is rastered across the surface using a series of scanning coils. SEM must be done in vacuum so that the electrons can travel unimpeded for adequate distances. The typical surface magnification realized is of the order of 10–100,000 times depending on the energy of the primary electron beam in traditional SEM instruments. However, modern SEMs can achieve a lateral resolution of 1.5 nm at a primary electron voltage of only 1.5 keV [41].

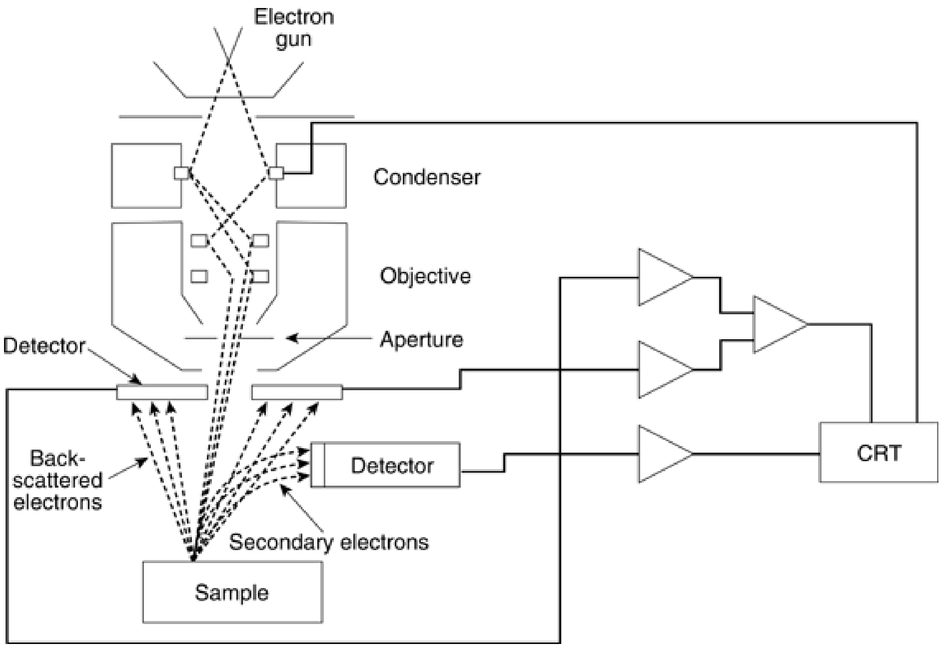

Figure 2.13 Block diagram of scanning electron microscope [41]

2.6.2 Mechanical Tests

Most polymers are subjected to the effect of external load during their application; thus, the exact determination of their mechanical properties and the proper interpretation of the results are important for both theory and practice. Numerous mechanical characteristics are measured routinely under various loading conditions, and the results are used for characterization, product development, quality control, and for engineering purposes. Mechanical testing is frequently used for the study of structure/property correlations in polymers and modified polymer systems. The techniques, methods, and procedures used for homopolymers also are often applied without any modification for the characterization of polymer blends [20].

2.6.2.1 Tensile Test

Tensile loading occupies a special position among the widely used mechanical tests. Because of its simplicity, it is used for the characterization of all kinds and forms of materials. Tensile characteristics of products prepared from thermoplastic or thermoset polymers, as well as rubbers, are routinely measured in the form of bars, films, tubes, and so on. Various properties are determined with the technique, such as fracture and tear resistance, yield stress and strain, as well as many others.

Although stress-strain curves are registered in a tensile test, usually Young's modulus, yield, and ultimate characteristics are understood under the term *tensile properties* [20].Since the true stress and strain are difficult to measure in practice, the *nominal* or *engineering* stress and strain are usually obtained on the basis of the original dimensions of the test specimen. Referring to typical stress-strain curves for plastics, shown in Figure 2.14, the tensile properties may be defined as follows:

1. *Tensile stress* is the tensile load/unit area of minimum original cross section within the gage boundaries carried by the test specimen at any given moment. It is expressed in force per unit area.

$$\sigma = F/ A_0 \tag{2.2}$$

2. *Tensile strength* is the maximum tensile stress supported by the specimen during a tension test.

3. *Tensile strength at break* is the tensile stress at the moment of rupture of the test specimen.

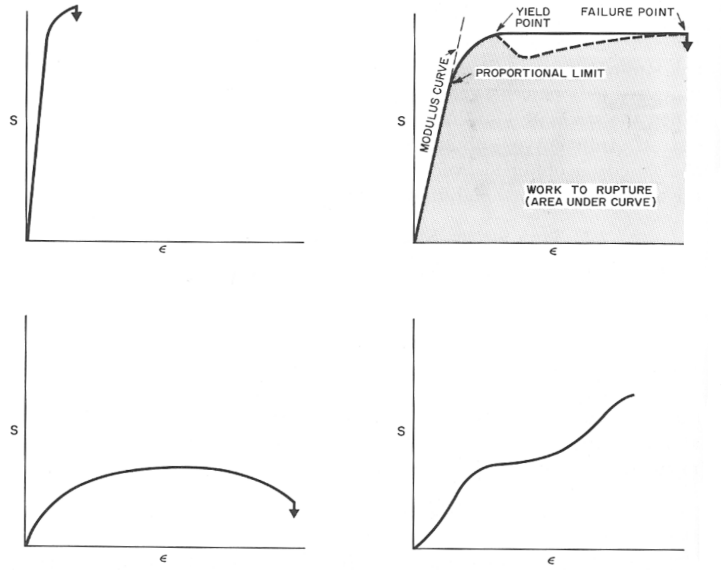

Figure 2.14 Typical stress-strain curves of plastics [20]

Typical stress-strain curve for brittle plastics (upper left). Typical stress-strain curve for plastics showing a yield point and cold drawing (upper right). Typical stress-strain curve for some elastomeric plastics (lower left). Typical stress-strain curve for some rubbers (lower right).

4. *Elongation* is the increase in length produced in the gage length of the test specimen by a tensile load. It is expressed in units of length, commonly as a percentage.

5. *Elongation at break* is the elongation at the moment of rupture of the test specimen.

6. *Strain* is the ratio of the elongation to the gage length of the test specimen; that is, the change in length per unit of original length. It is expressed as a dimensionless ratio.

$$\varepsilon = \Delta L/L_0 \qquad (2.3)$$

7. *Yield point* is the first point on the stress-strain curve at which an increase in strain occurs without an increase in stress.
8. *Proportional limit* is the greatest stress or strain which a material is capable of sustaining without any deviation from proportionality of stress to strain.
9. *Modulus of elasticity* is the ratio of stress to corresponding strain below the proportional limit of a material. It is expressed as force per unit area.

$$E = \sigma/ \varepsilon \qquad (2.4)$$

10. *Work to cause rupture* is the area under the stress-strain curve. It is a measure of the amount of energy or work which must be done to rupture secondary (yield point) and primary (rupture) bonds.

In some special cases, with crystalline polymers such as nylon, polypropylene, or linear polyethylene, the specimens may undergo what is called *necking* where highly localized strain takes place. This is illustrated in Figure 2.14 (upper right) for a specimen of polypropylene. The cold drawing that takes place in all such crystalline materials is usually accompanied by considerable increase in the strength of the specimen as orientation of molecules and realignment of crystallites takes place, Necking, or cold drawing, invariably continues until all of the narrow center section has become oriented or until some serious flaw is encountered. If allowed to continue, the necking process encounters the greatly increased cross section of the ends of the specimen. The strength of the highly oriented center section is usually not great enough to overcome the resistance of the enlarged sections at the ends of the specimen; at this point the necking process stops and rupture occurs [20].

2.6.2.2 Flexural Test

Because of the increasing importance of plastics in structural applications, much attention has been devoted to standardized methods and procedures for determining their physical properties. One of the more important mechanical properties of interest in any basic comparison of rigid materials is that of flexural strength [25]. ASTM D790M-92 test method covers the determination of flexural properties of polymers using a three-point or four-point loading system.

Three-point loading system utilizes center loading on a simply supported beam. A bar of rectangular cross-section is tested in flexure as a beam. The bar rests on two supports and is loaded by means of a loading nose midway between the supports Figure 2.15.

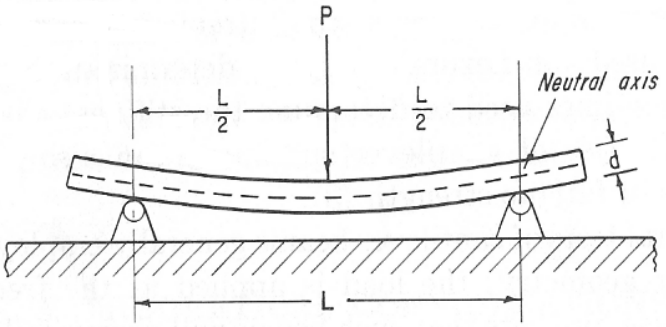

Figure 2.15 Three point bending test schematic drawing

When the specimen is tested in flexure as a simple beam supported at two points and loaded at the midpoint, the maximum stress in the outer fibers occurs at midspan. This stress may be calculated for any point on the load-deflection curve by the following equation.

$$S = 3PL/2bd^2 \qquad (2.5)$$

where S is stress in the outer fibers at midspan (MPa), P is load at a given point on the load-deflection curve (N), L is support span (mm), b is width of beam tested (mm), and d is depth of beam tested (mm).

The maximum strain in the outer fibers occurs at midspan as well, and may be calculated as follows:

$$r = 6Dd/L^2 \quad (2.6)$$

where r is maximum strain in the outer fibers (mm/mm), D is maximum deflection of the center of the beam (mm), d is depth of beam tested (mm), and L is support span (mm).

The tangent modulus of elasticity, often called flexural modulus, is the ratio within the elastic limit of stress to corresponding strain and shall be expressed in MPa. It is calculated by drawing a tangent to the steepest initial straight-line portion of the load-deflection curve and using Equation (2.7)

$$E_B = L^3m/4bd^3 \quad (2.7)$$

where E_B is modulus of elasticity in bending (MPa), L is support span (mm), b is width of beam tested (mm), d is depth of beam tested (mm), and m is slope of the tangent to the initial straight-line portion of the load-deflection curve (N/mm).[25,26]

2.6.2.3 Impact Test

The most widely used test methods are called charpy and izod. The methods in question differ in the way the specimen is gripped and how the stress is applied on them. In the first case, the charpy method, the specimen is supported as a horizontal beam and is broken by a single oscillation of the pendulum, where the line of impact is central to the two supports. In the second case, the izod method, the specimen is supported as an embedded beam and is broken by a single oscillation of the pendulum at a fixed distance from the specimen clamp and from the centre line of the impact. In either case, the specimens may or may not have a stress concentrator notch.

The measuring method is based on determining the amount of energy, expressed in Joules, needed to break the specimen under specified conditions, such as: location of the specimen, shape of the notch and speed of impact of the hammer on the specimen. As the maximum potential energy of the pendulum is known, and is in relation to the weight of the hammer used and the drop height, the latter in turn being in relation to the starting angle, it results that the energy absorbed by the specimen in order to break it can be determined by measuring the hammer rise angle after impact [20].

2.6.3 Thermal Analysis

It has long been considered that the most useful workhorse techniques, for a modestly equipped laboratory concerned with characterizing polymeric materials, are differential scanning calorimetry (DSC), dynamic mechanical thermal analysis (DMTA), wide and small angle X-ray diffraction (WAX and SAXS), thermo gravimetric analysis (TGA) and optical and electron microscopy [27].

2.6.3.1 Differential Scanning Calorimetry Analysis (DSC)

Differential scanning calorimetry (DSC) is the most useful indirect method for analysis of polymer blends. DSC is used to quantitatively measure phenomena associated with both thermodynamic and kinetic processes such as crystallization, melting, glass transition, curing, and aging of polymers and their blends. Interactions between polymers in a blend will change some of these thermal characteristics due to the morphological changes in the blend. Several important blend attributes need to be understood; in each case, DSC can provide a measure by means of the heat flow of the process. Direct means of characterization, such as optical and electron microscopies, X-ray diffraction, and various spectroscopies can measure the morphology and interactions of blends [20].

DSC allows determination of heat capacity versus temperature or time, measurement of heats of fusion, identification of crystalline and liquid crystalline phases, degrees of crystallinity, etc. Glass transition measurement allows characterization of ageing and blend compatibilities. Heats of reaction allow cure and degradation studies [27].

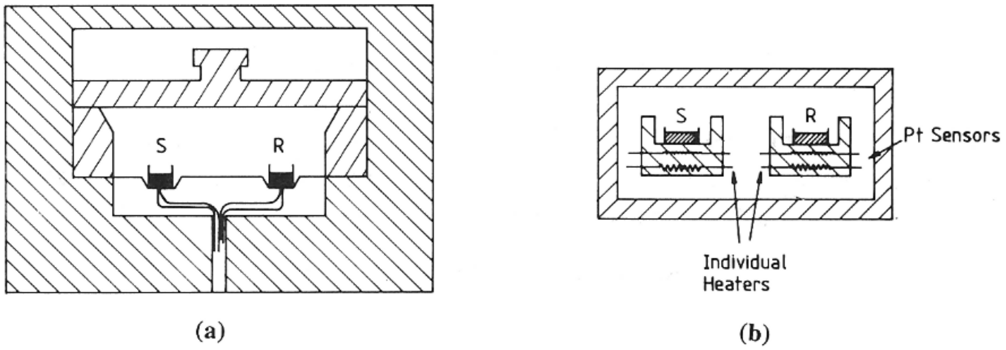

Figure 2.16 Schematic Diagram of working principle of (a) heat-flow (b) electrical-compensation DSC

There are two basic methods in use in commercial instrumentation. Figure 2.16(a) shows the power-compensation method employed by Perkin-Elmer. It was this method which first attracted the name 'DSC', because the difference in power required to ramp the sample and the reference at the same rates is measured. In reality, of course, a difference in temperature between sample and reference is required to drive the differential power requirement. This highly elaborate method is then seen to suffer from many of the same problems as the technique originally suggested by Boersma [28] which uses a heat-flow disc to quantify the difference in the heat flow to sample and reference (Figure 2.16(b)). With proper engineering, this heat-flow difference is just proportional again to the temperature difference between sample and reference (ΔT). In cells of the type used by polymer Laboratories, TA Instruments and others, ΔT can be kept small by appropriate cell design [27].

2.6.4 Flow Characteristics

2.6.4.1 Melt Flow Index (MFI) Test

The melt index tester is essentially a simple capillary rheometer. The piston is pushed down by placing a weight on top of it, see Figure 2.17.

The melt index is the number of grams of polymer extruded in a time period of 10 minutes. Details of the geometry and test procedures are described in ASTM D1238 [21].

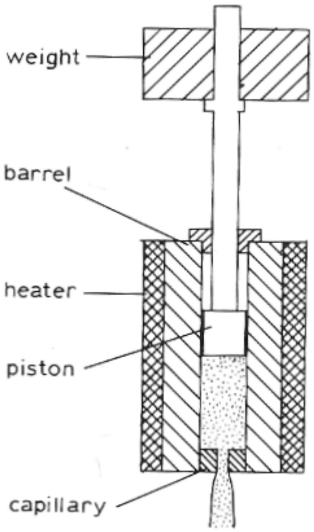

Figure 2.17 Melt Index Tester [21]

2.7 Previous Studies

Vaia et. al. [31] showed that polymer-clay nanocomposites could be developed by melt blending the polymer and organophilic clay in a twin-screw extruder. In this route both polymer and clay are either simultaneously fed, or separately premixed and then fed, to the twin-screw extruder. The heat and shear generated by the screw in the barrel of the extruder facilitates the intercalation/exfoliation of clay in the polymer matrix.

Wang et al. [32] prepared maleic anhydride grafted polyethylene/ clay nanocomposites by melt compounding. They investigated the effect of organic modifier type and maleic anhydride grafting level on the exfoliation and intercalation behavior. It was concluded that methylene group in alkylamine (organic modifier) should be higher than 16 and maleic anhydride grafting level should be higher than 0.1 wt% for exfoliated nanocomposite.

Dennis and co-workers [33] studied dispersion mechanism. It was reported that to optimize dispersion: both the clay treatment chemistry and process conditions need to be optimized. It was concluded that increasing residence time in general improves delaminated dispersion, but it is reported that there is an optimum of shear intensity that can be applied after which delaminated dispersion gets worse. It is concluded that in designing a screw configuration, one should take into account the proposed dispersion mechanism. However, it was concluded that shear is required to start the dispersion process, because shear promotes the intercalated ribbons to be reduced in size. Also, residence time in a non-shearing extruder environment is needed to allow the platelets to peel apart. At last, it was recommended that more work is needed to improve our understanding of screw design and then begin making the more traditional variable changes such as feed rate, screw speed, temperature profile and feed points for resin and clay.

Kato et al. [34] prepared polyethylene-clay hybrids successfully by melt compounding with maleic anhydride grafted polyethylene (MA-g-PE), organophilic clay and polyethylene. In these polyethylene-clay hybrids, the silicate layers of the clay were exfoliated and dispersed to the monolayers. The hybrids exhibit higher tensile yield strengths and tensile moduli than those of polyethylene matrices and those of polyethylene-inorganic clay composites. When 5 wt % clay was loaded, the tensile yield strength and the tensile modulus of the hybrid were, respectively, 1.4 and 1.8 times higher than those of the polyethylene/MA-g-PE mixture. The gas permeability of that clay hybrid decreased 30% compared with polyethylene/MA-g-PE mixture.

Liang et al. [35] prepared by direct melt blending and solution blending polyethylene (PE)/maleic anhydride grafted polyethylene (PE-*g*-MAH)/organic-montmorillonite(Org-MMT) nanocomposites. Three cationic surfactants hexadecyltrimethylammonium-chloride, hexadecyldimethylbenzylammonium chloride, and octadecyltrimethyl-ammonium chloride were used to modify montmorillonite. It was found that the intercalation effect of PE/PE-*g*-MAH/Org-MMT could be enhanced by increasing the content of PE-*g*-MMT, using the silicate modified by a cationic surfactant with a benzyl group or long alkyl chain, adopting the solution blending method or using high-density polyethylene as matrix. The maximum value in tensile strength was achieved when the concentration of PE-*g*-MAH was 6 wt %. The impact strength increased concomitantly with the content of PE-*g*-MAH.

Hotta and Paul [36] prepared polyethylene-clay nanocomposites by melt compounding various combinations of a maleic anhydride grafted linear low density polyethylene (LLDPE-*g*-MA), a linear low density polyethylene (LLDPE), and two organoclays. They have selected two types of organoclay to show the effect of the number of alkyl groups attached to the nitrogen of the organic modifier on exfoliation and improvement of mechanical properties. Nanocomposites derived from the organoclay having two alkyl tails, exhibited better dispersion and improvement of mechanical properties than nanocomposites based on the organoclay having one alkyl tail. In addition, the rheological properties and gas permeability of the nanocomposites derived from the organoclay having two alkyl tails, were investigated. Both melt viscosity and melt tension (melt strength) increased with increased content of clay (MMT) and LLDPE-*g*-MA. Gas permeability was decreased by the addition of MMT.

Isik [30] investigated the effects of compatibilizer type, organoclay type, and the addition order of components on the morphological, thermal, mechanical and flow properties of ternary nanocomposites based on low density polyethylene. Based on the results of the mechanical tests, compatibilizer and organoclay contents were determined as 5 wt. % and 2 wt % respectively. Among the investigated addition orders, mechanical test results showed that the best sequence of component addition was the one in which LDPE, compatibilizer and organoclay were simultaneously compounded in the first run of the extrusion. Considering the ternary nanocomposites, compositions of LDPE/ethylene-methyl acrylate-glycidyl methacrylate/ Cloisite® 15A, LDPE/ ethylene-glycidyl methacrylate /Cloisite® 15A and LDPE/ethylene-butyl acrylate-maleic anhydride/ Cloisite® 30B showed the highest improvement in mechanical properties.

CHAPTER III

EXPERIMENTAL

3.1 Materials

3.1.1 Polymer Matrix

3.1.1.1 LDPE

Low density polyethylene was purchased from Petkim Petrokimya Holding A.Ş, İzmir, Turkey. The trade name of the LDPE used is Petilen I22-19T and it is sold in the form of pellets in a 25 kg bags. Properties of LDPE obtained from the company are given in Table 3.1.

Table 3.1 Properties of polymer matrix, LDPE

Properties	Unit	Value	Test Method
Melt Flow Rate (2160 g, 190°C)	g/10 min	17-29	ASTM D-1238
Density, 23°C	g/cm^3	0.917-0.921	ASTM D-1505

3.1.1.2 LLDPE

Linear low density polyethylene was purchased from Ras Lanuf Oil and Gas Processing Company, Libya. The trade name of the LLDPE used is Lanufene LLI-2420 and it is sold in the form of pellets in a 25 kg bags. Properties of LLDPE obtained from the company are given in Table 3.2.

Table 3.2 Properties of polymer matrix, LLDPE. ESCR: Environmental Stress Cracking Resistance

Properties	Unit	Value	Test Method
Melt Flow Rate (2160 g, 190°C)	g/10 min	20.0	D1238
Density, 23°C	g/cm^3	0.924	D1505
Ultimate Tensile Strength	MPa	11	D638
Elongation at Break	%	450	D638
1% Secant Modulus	MPa	314	D638
Notched Izod Impact	J/m	500	D256/A
Vicat Softening Temperature	^{0}C	94	D1505
Low Temperature Brittleness	^{0}C	<-70	D746
ESCR, (F50)	hrs	150	D1693
Mold Shrinkage	%	1- 3	PE Method

3.1.1.3 HDPE

High density polyethylene was purchased from Petkim Petrokimya Holding A.Ş, İzmir, Turkey. The trade name of the HDPE used is Petilen I 668 and it is sold in the form of pellets in a 25 kg bags. Properties of HDPE obtained from the company are given in Table 3.3.

Table 3.3 Properties of polymer matrix, HDPE

Property	Unit	Value	Test Method
Melt Flow Rate (2160g, 190°C)	g/10 min	4.4-6.5	ASTM D-1238
Density, 23°C	g/cm^3	0.966-0.970	ASTM D-1505
Tensile Strength			
- At Yield	Kg/cm^2	295	ASTM D-638
- At Break	Kg/cm^2	240	ASTM D-638
- Elongation At Break	%	1250	ASTM D-638
Stiffness	Kg/cm^2	10450	ASTM D-747
Izod Impact Strength	Kg cm/cm	5	ASTM D-256
ESCR, (F50)	hour	4	ASTM D-1693

3.1.2 Organoclay

Cloisite® 15A is a natural montmorillonite modified with a quaternary ammonium salt. Organic modifier is shown in Figure 3.1.

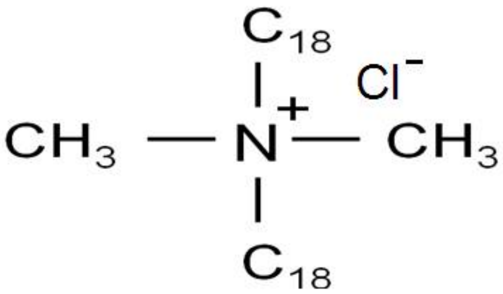

$$CH_3-\overset{\displaystyle C_{18}\ \ }{\underset{\displaystyle C_{18}}{\overset{|}{\underset{|}{N^+}}}}-CH_3 \quad Cl^-$$

Figure 3.1 Chemical Formula of Modifier used at Cloisite® 15A

Table 3.4 Properties of Cloisite® 15A

Properties	
Organic Modifier	dimethyl, dehydrogenated tallow, quaternary ammonium
Modifier Concentration	125 meq/100g clay
% Moisture	< 2%
% Weight Loss on Ignition	43%
Typical Dry Particle Sizes:	10% less than: 2μ
(microns, by volume)	50% less than: 6μ
	90% less than: 13μ
Color	off white
Loose Bulk, kg/m^3	172.8
Packed Bulk, kg/m^3	298.6
Specific Gravity, g/cc	1.66
d- spacing (X-Ray)	31.5Å

3.1.3 Compatibilizer

Lotader® AX 8900 is a random terpolymer of ethylene, acrylic ester and glycidyl methacrylate, polymerized under high pressure in an autoclave process. Co-monomer content is high.

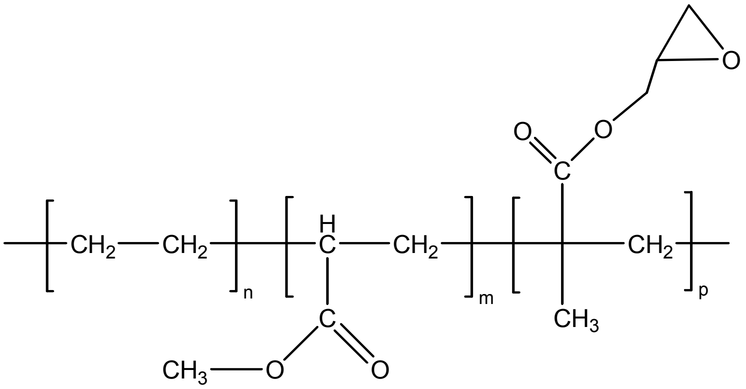

Figure 3.2 Chemical structure of Lotader® AX8900 (E-MA-GMA)

Table 3.5 Specifications of Lotader® AX8900

Properties	Unit	Value
Methyl Acrylate Content	wt %	25
Glycidyl Methacrylate Content	wt%	8
Melt Index (190°C, 2.1kg,ASTM 1238)	g/10min.	6
Melting Point (DSC)	°C	60
Vicat Softening Point (ASTM1525-1kg)	°C	< 40
Tensile Strength at Break (ASTM D638)	MPa	4
Elongation at Break (ASTM D638)	%	1100
Hardness Shore A (ASTM D2240)	-	70

Glycidyl methacrylate gives reactivity (versus OH, COOH and NH_2 groups), leading to optimal dispersion during melt mixing with engineering thermoplastics. As an ethylene copolymer, Lotader AX 8900 is compatible with LDPE in all proportions, and with almost all other ethylene copolymers.

3.2 Experimental Set-Up

3.2.1 Extruder

In the experiment, PRISM TSE 16 TC bench-top operation co-rotating twin screw extruder is used. The barrel has additional ports for feeding solids and liquids, or for venting. A simple manual control panel houses controls and instruments to operate the extruder and feeders. PRISM TSE 16 TC barrel length is 25:1 and can be used for research, development or small scale production. Some typical applications are polymer compounds, masterbatches, nanocomposites, biodegradable polymers and adhesives.

Table 3.6 Specifications of PRISM TSE 16 TC Extruder

PRISM TSE 16 TC	Units	Value
Barrel length	L/D	25:1
Barrel bore diameter	mm	16
Screw diameter	mm	15.6
Channel depth	mm	3.3
Centre-line spacing	mm	12.5
Centre-line to radius ratio		1.56
Maximum screw speed	rpm	500
Power at maximum screw speed	kW	1.25
Torque per shaft	Nm	12
Torque/ (C-line3)	Nm/cm^3	6.1
Barrel zones		4
Heater rating	W	15 x 300
Die heater rating	W	1 x 750
Extruder dimensions	L x W x H m	0.9 x 0.4 x 0.9
Scale-up data		
Internal free volume	cm^3	68
Peripheral surface area	cm^2	316
Surface area per unit free volume	m^2/l	0.47
Typical output	kg/h	0.5 to 10
Services		
Electrical power	Volt/ph/Amp	220V/1ph/32A
Cooling water 20 °C	Liters/min	5

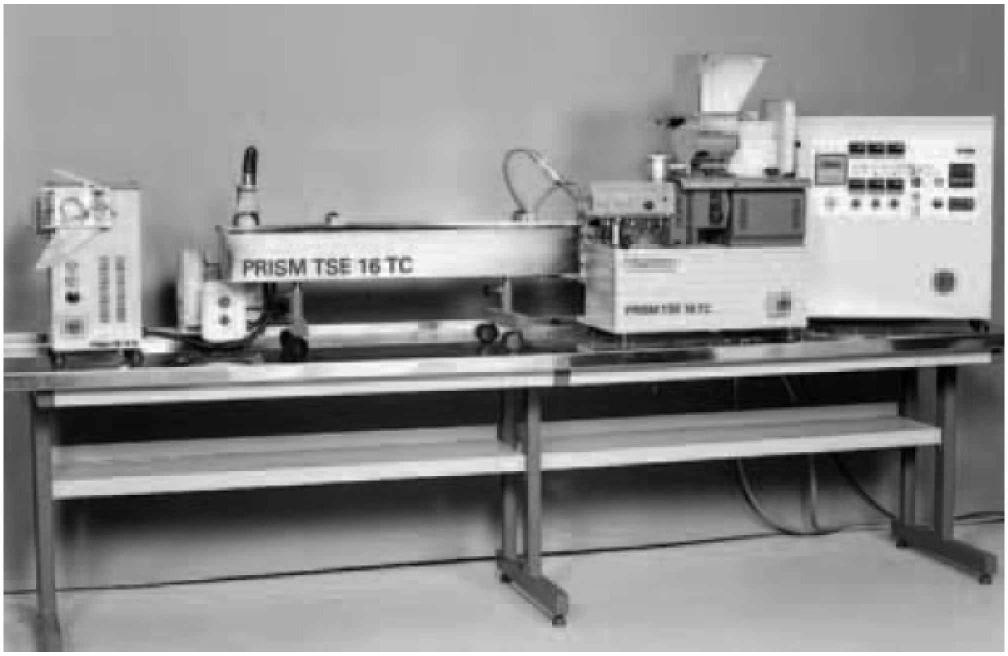

Figure 3.3 Thermo Prism TSE 16 TC twin screw extruder

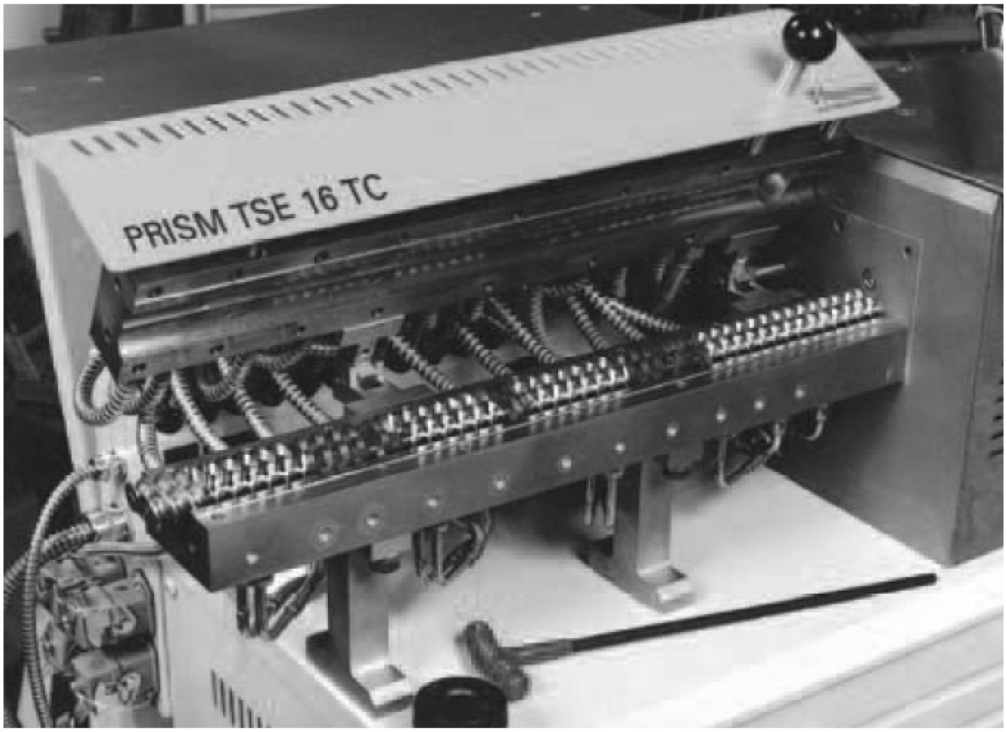

Figure 3.4 Screw Configuration of Thermo Prism TSE 16 TC twin screw extruder

3.2.2 Injection Molding Machine

DSM Micro Injection Molding Machine 10cc is used for the injection molding of test samples. The technical specifications of the injection molding machine are shown in Table 3.7.

Table 3.7 Technical specifications of the injection molding machine

		Unit
Dimensions W x H x D	900x400x350	mm
Barrel capacity	10	cm^3
Number of controlled heating zones	2	
Maximum temp. barrel	350	^{0}C
Maximum temp. mould	200	^{0}C
Warming-up time (20 to 240°C)	10	min.
Compressed air pressure	6-16	bar
Total heating power	0.7	kW
Weight	50	kg

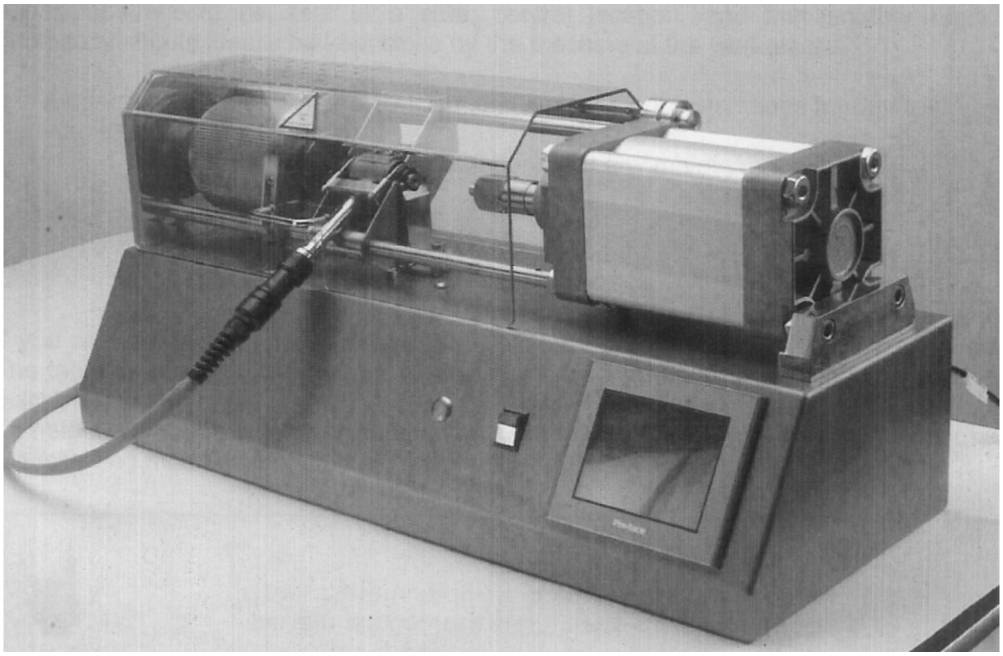

Figure 3.5 Micro Injection Molding Machine 10cc

3.3 Experimental Procedure

Flowchart of experimental procedure, characterization and testing is shown in Figure 3.6. The sample codes and their compositions are given in Table 3.8.

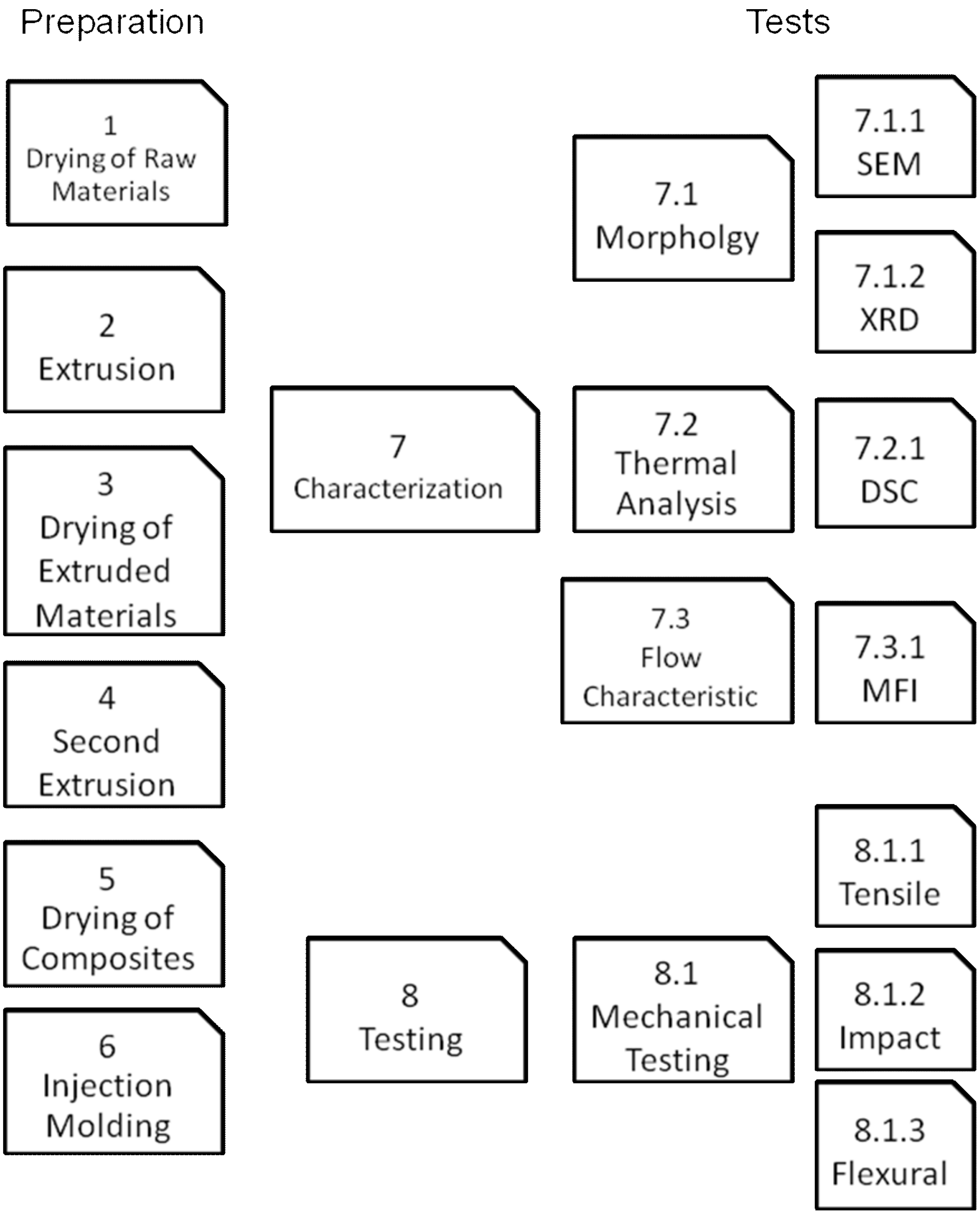

Figure 3.6 Flowchart of experimental procedure, characterization and testing

Table 3.8 Sample codes and their weight percentages

Sample Codes		HDPE %	Compatibilizer %	Organoclay %
HD1	HD	100	0	0
HD2	HD5E	95	5	0
HD3	HD10E	90	10	0
HD4	HD2C	98	0	2
HD5	HD4C	96	0	4
HD6	HD6C	94	0	6
HD7	HD5E2C	93	5	2
HD8	HD5E4C	91	5	4
HD9	HD5E6C	89	5	6
HD10	HD10E2C	88	10	2
HD11	HD10E4C	86	10	4
HD12	HD10E6C	84	10	6
		LLDPE %	Compatibilizer %	Organoclay %
LLD1	LLD	100	0	0
LLD2	LLD5E	95	5	0
LLD3	LLD10E	90	10	0
LLD4	LLD2C	98	0	2
LLD5	LLD4C	96	0	4
LLD6	LLD6C	94	0	6
LLD7	LLD5E2C	93	5	2
LLD8	LLD5E4C	91	5	4
LLD9	LLD5E6C	89	5	6
LLD10	LLD10E2C	88	10	2
LLD11	LLD10E4C	86	10	4
LLD12	LLD10E6C	84	10	6
		LDPE %	Compatibilizer %	Organoclay %
LD1	LD	100	0	0
LD2	LD5E	95	5	0
LD3	LD10E	90	10	0
LD4	LD2C	98	0	2
LD5	LD4C	96	0	4
LD6	LD6C	94	0	6
LD7	LD5E2C	93	5	2
LD8	LD5E4C	91	5	4
LD9	LD5E6C	89	5	6
LD10	LD10E2C	88	10	2
LD11	LD10E4C	86	10	4
LD12	LD10E6C	84	10	6

3.3.1 Drying

All materials are pre-dried under conditions shown in Table 3.9.

Table 3.9 Drying Conditions

Materials	Temperature (^{0}C)	Time (h)
	Before Extrusion	
PE Grades	100	12-15
Organoclay	120	12-15
Compatibilizer	40	12-15
	Before Second Extrusion	
All Compositions	100	4
	Before Injection Molding	
All Compositions	100	12-15

3.3.2 Extrusion

After drying, polyethylene, compatibilizer and organoclay are fed to the extruder. Polyethylene and, if any, compatibilizer are pre-mixed and fed from main feeder, the organoclay is fed from side feeder. After adjusting the proper feed rate for each material, extrusion is done at the fixed temperature profile, total flow rate and screw speed. The temperature profile in the barrel is 170, 210, 210, 210, 220 ^{0}C from hopper inlet to the die. The total flow rate and screw speed are 25 g/min and 200 rpm, respectively. The molten product is pelletized after cooled in the water bath.

3.3.3 Injection Molding

After nanocomposites are prepared by extrusion, test samples are injection molded. The mould and nozzle temperature are kept at 30^{0}C and 220 ^{0}C, respectively. The molding pressure is kept at 5 bars.

3.4 Characterization of Specimens

In order to investigate the effects of various compositions on the nanocomposite properties morphological and thermal analysis are done. Also, their performances are measured through mechanical testing.

3.4.1 Morphological Analysis

3.4.1.1 X-Ray Diffraction (XRD) Analysis

The composites are analyzed by using a RIGAKU D/MAX 2200/PC X-ray diffractometer. Cu Kα (λ = 1.54 Å) radiation, generated at a voltage of 40 kV and current of 40 mA is used as the X-Ray source. The diffraction angle 2θ is scanned from 1^o to 10^o at a scanning rate of 1^o/min and a step size of 0.01^o. XRD analysis is performed on tensile bars except for the organoclay which is in the powder form.

3.4.1.2 Scanning Electron Microscopy (SEM) Analysis

The fracture surfaces of the materials obtained by impact testing are examined by a low voltage Scanning Electron Microscope (JEOL JSM-6400).

3.4.2 Thermal Analysis

3.4.2.1 Differential Scanning Calorimetry (DSC) Analysis

Differential Scanning Calorimeter Perkin Elmer Diamond DSC (Figure 3.7) is used for obtaining DSC curves of the composites. The measurement is done under nitrogen atmosphere, temperature range is from 50 ^{0}C to 160 ^{0}C and the heating rate is 10 ^{0}C/min. Melting points and % crystallinities are determined from the experiment. The heat of fusion (ΔH) value for 100 % crystalline polyethylene is taken as 293 j/g [37].

Figure 3.7 Perkin Elmer Diamond DSC

3.4.3 Flow Characteristics

3.4.3.1 Melt Flow Index (MFI) Test

Melt Flow Index (MFI) tests are performed with Omega Melt Flow Indexer. Tests are performed according to ASTM D-1238, at 190°C and under a weight of 2.16 kg. The results are given as g/10min of material that passes from the die, see Figure 3.8.

Figure 3.8 Melt Flow Index Tester

3.5 Mechanical Tests

3.5.1 Tensile Tests

Tensile tests are performed for each composition according to ASTM D638M-91a [38], by using a Shimadzu type AG-100kNIS testing machine, shown in Figure 3.9.

Figure 3.9 Shimadzu mechanical testing machine

The dog bone shaped tensile sample is shown in Figure 3.10 and the dimensions are as follows: width of the narrow section (w), distance between grips (D), total length of the specimen (L_0) and thickness (T) are 4, 40, 74 and 2 mm, respectively.

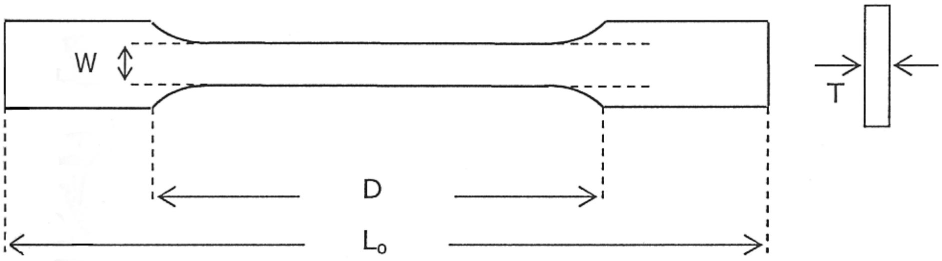

Figure 3.10 Dog bone shaped tensile sample

3.5.2 Flexural Tests

Flexural test is performed using the Lloyd LR 30K Universal Testing machine, according to Test Method – I Procedure of ASTM D790M-92. Length, width and depth of the injection molded specimen are 79, 10, and 4 mm, respectively. The support span and stain rate are taken 64 mm, 0.1 min^{-1}, respectively. Then, cross head speed is calculated as 17 mm/min to yield a strain rate of 0.1 min^{-1}.

3.5.3 Impact Test

Notched impact tests are performed according to ASTM E 23 Charpy standard using Ceast Resil Impactor machine Figure 3.11. The width, length, height and notch size of the specimen are 10, 78, 4 and 2 mm, respectively.

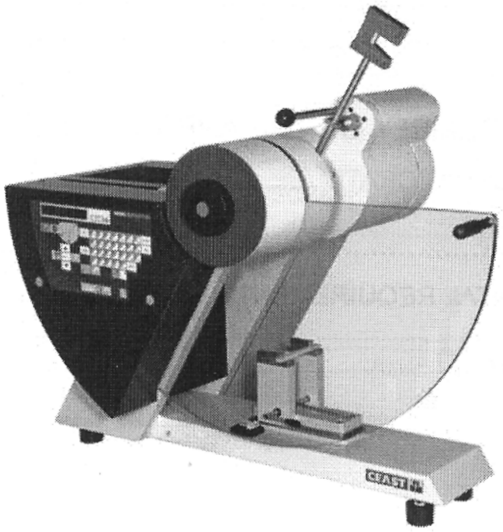

Figure 3.11 Ceast Resil Impactor Machine

CHAPTER IV

RESULTS AND DISCUSSION

4.1 Morphological Analysis

Wide Angle X-Ray Diffraction (XRD) and Scanning Electron Microscope (SEM) are two complimentary techniques used for characterization of nanocomposites.

4.1.1 X-Ray Diffraction (XRD)

Due to its ease of use and availability XRD is most commonly used to probe the polymer layered silicate nanocomposite structure and sometimes to study the kinetics of the polymer melt intercalation. By monitoring the position, shape and intensity of the basal reflections from the distributed silicate layers, the nanocomposite structure either intercalated or exfoliated may be identified [3].

From Bragg's law the interlayer spacings are calculated and given in Table 4.1 through Table 4.3. X-Ray diffraction pattern of organoclay powder is shown in Figure A.30. 2Θ for organoclay is found to be 2.76 degree, which is consistent with the manufacturer's specifications. Details of X-ray data are in Appendix A, Figures A.2 through A.29.

In Tables 4.1 through 4.3 d_1, d_2 and d_3 are referred to the first, second and third peak respectively. Δd_1 is the change in d_1 and Δd_2 is the change in d_2 of the Cloisite® 15A powder.

In Figures 4.1 through 4.9 XRD patterns of nanocomposites and the organoclay powder Cloisite® 15A are shown.

It is thought that in Cloisite® 15A powder there are some regions which are not ion exchanged with the quaternary ammonium salt. This is shown by the d-spacing at

1.28 nm which is close to the d-spacing of Na-montmorillonite given as 1.17 nm in the literature. When Cloisite® 15A is melt mixed with the polymer, the polymer chains also enter these regions and show intercalation. This theory is supported by the fact that upon melt mixing the original peak observed at 1.28 nm becomes lower in intensity and new peak, d_2, appears owing to the intercalation of the polymer into the regions which were not ion exchanged.

Table 4.1 d-spacing data of HDPE nanocomposites

	d_1 (nm)	d_2 (nm)	d_3 (nm)	Δd_1 (%)	Δd_2 (%)
Organoclay	3.20	1.28			
HD2C	3.73	1.97	1.32	16	54
HD4C	3.78	1.96	1.31	18	53
HD6C	3.67	1.91	1.32	15	49
HD5E2C	3.78	1.98	1.32	18	54
HD5E4C	3.82	1.98	1.32	19	54
HD5E6C	3.62	1.89	1.31	13	48
HD10E2C	4.00	1.97	1.38	25	54
HD10E4C	3.74	1.98	1.34	17	54
HD10E6C	3.78	1.98	1.31	18	55

Table 4.2 d-spacing data of LLDPE nanocomposites

	d_1 (nm)	d_2 (nm)	d_3 (nm)	Δd_1 (%)	Δd_2 (%)
Organoclay	3.20	1.28			
LLD2C	3.20	1.31	-	0	3
LLD4C	2.90	1.30	-	-10	1
LLD6C	2.91	1.29	-	-9	1
LLD5E2C	4.00	1.97	1.31	25	54
LLD5E4C	3.86	1.98	1.32	21	55
LLD5E6C	3.76	1.96	1.32	17	53
LLD10E2C	4.11	2.06	1.38	28	61
LLD10E4C	3.82	2.03	1.33	19	58
LLD10E6C	3.94	2.00	1.34	23	56

Table 4.3 d-spacing data of LDPE nanocomposites

	d_1 (nm)	d_2 (nm)	d_3 (nm)	Δd_1 (%)	Δd_2 (%)
Organoclay	3.20	1.28			
LD2C	2.94	1.32	-	-8	3
LD4C	2.93	1.31	-	-9	2
LD6C	2.94	1.30	-	-8	2
LD5E2C	3.87	2.03	1.34	21	58
LD5E4C	3.78	1.97	1.33	18	54
LD5E6C	3.76	1.96	1.31	17	53
LD10E2C	4.05	2.07	1.35	27	62
LD10E4C	3.78	2.02	1.37	18	58
LD10E6C	3.76	1.98	1.34	17	55

The results show that the highest increase of basal spacings are obtained for 10% compatibilizer plus 2% clay content, which are %25, %28, %27 increase for HDPE, LLDPE and LDPE, respectively. Also, 5% compatibilizer plus 2% clay compositions exhibit the second highest increase in d_1, except for HDPE.

In the case of exfoliated nanocomposites, the extensive layer separation associated with the delamination of the original silicate layers in the polymer matrix results in the eventual disappearance of any coherent X-ray diffraction from the distributed silicate layers [3]. No disappearance of coherent X-ray diffraction is observed in this study, thus no exfoliated nanocomposites are expected. However, as observed in Figures 4.1 through 4.9 the height of the peaks decreases in all compositions indicating partial exfoliation.

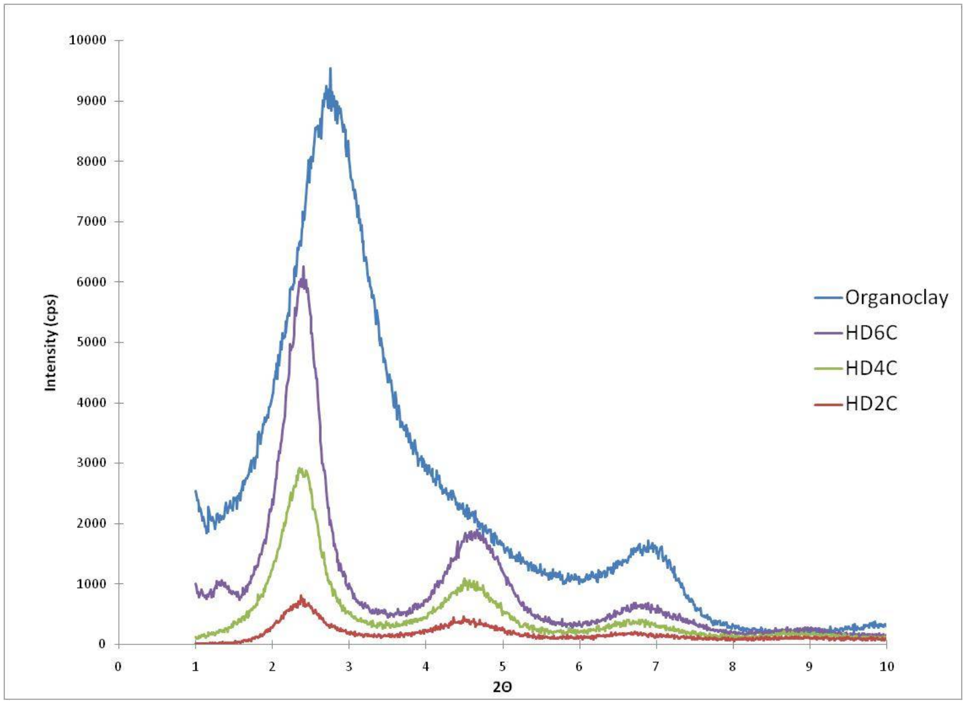

Figure 4.1 XRD patterns for HD2C, HD4C, HD6C and Cloisite® 15A

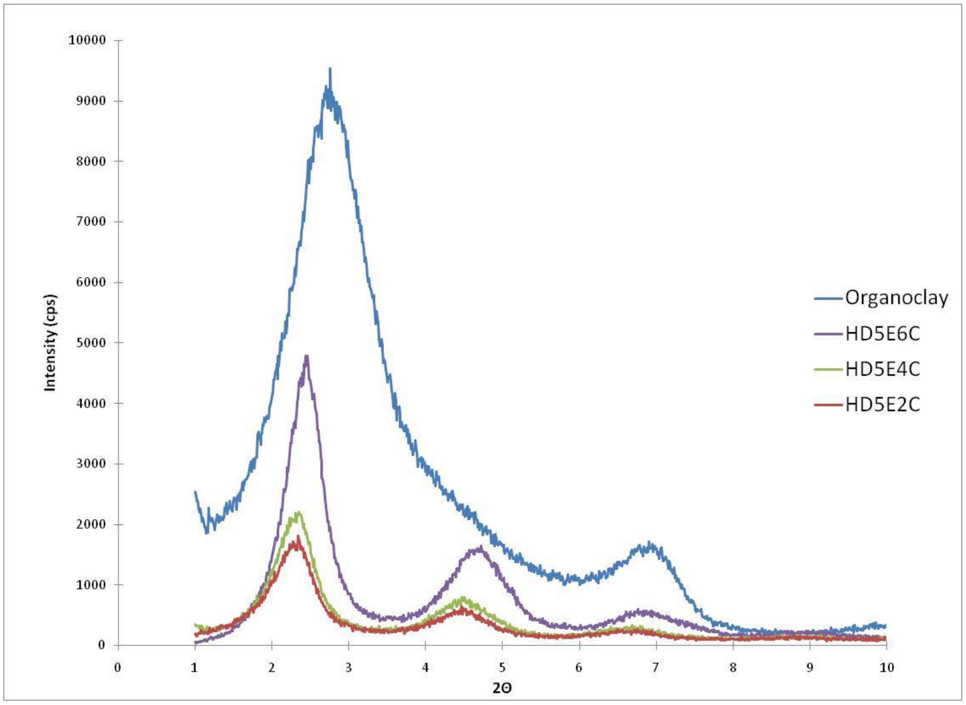

Figure 4.2 patterns for HD5E2C, HD5E4C, HD5E6C and Cloisite® 15A

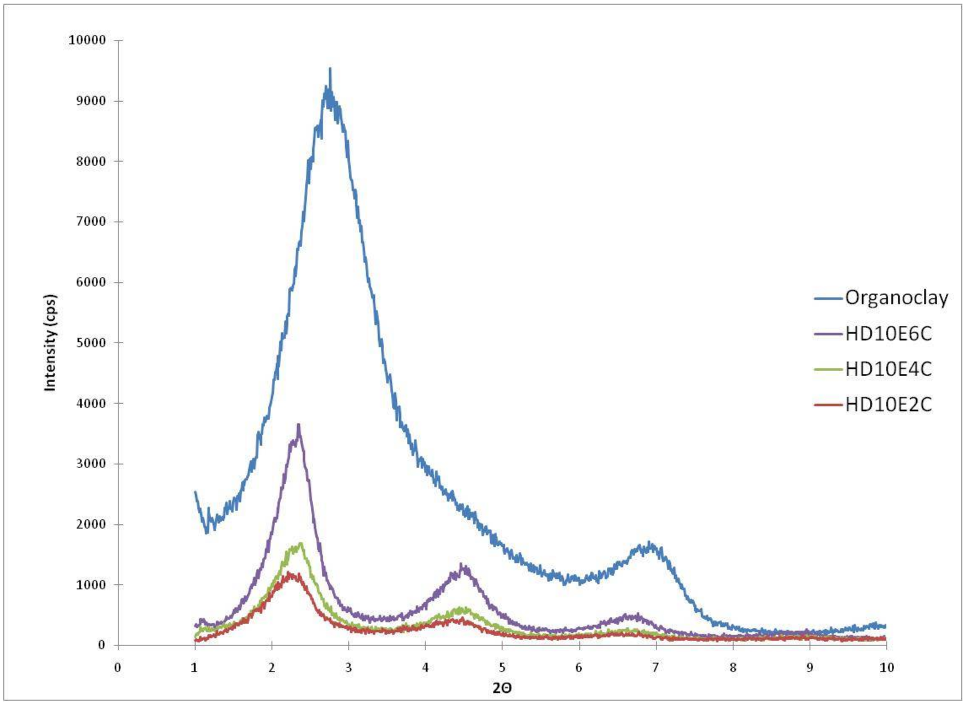

Figure 4.3 XRD patterns for HD10E2C, HD10E4C, HD10E6C and Cloisite® 15A

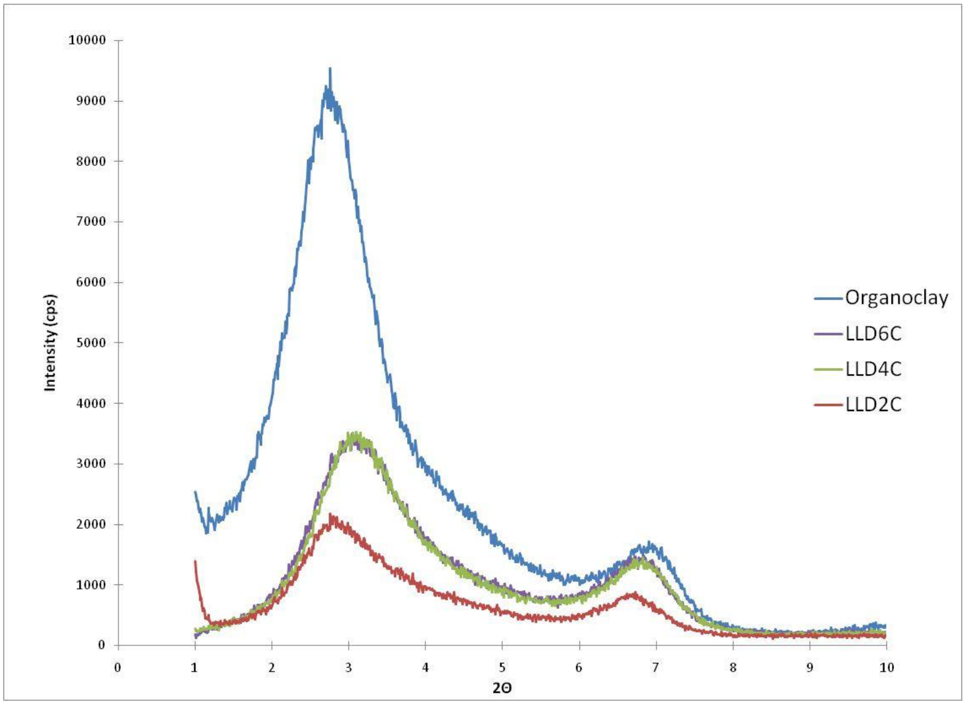

Figure 4.4 XRD patterns for LLD2C, LLD4C, LLD6C and Cloisite® 15A

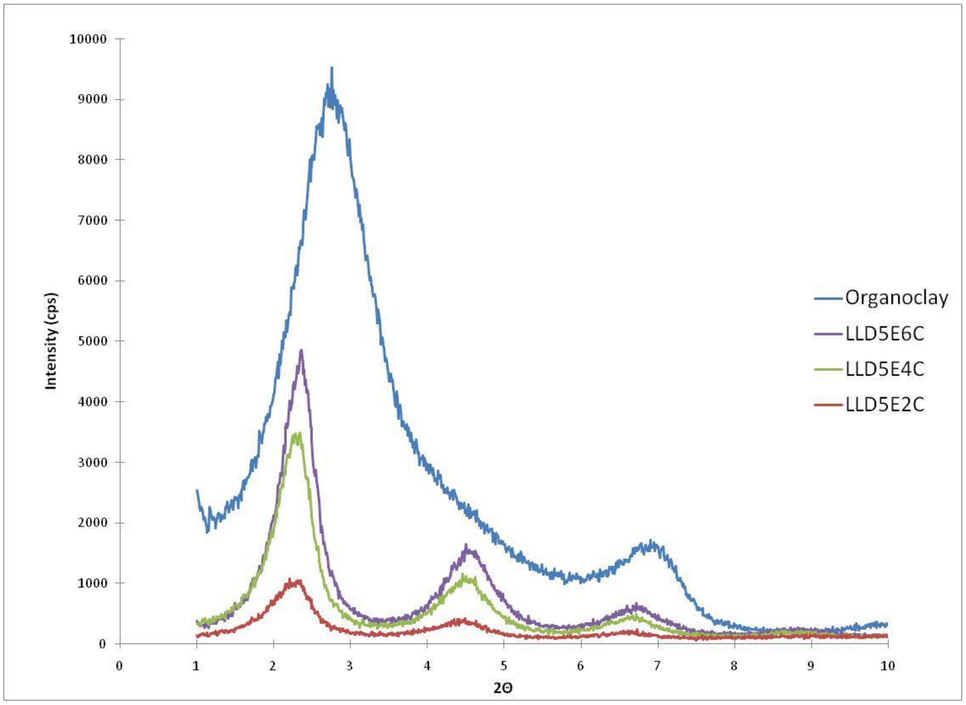

Figure 4.5 XRD patterns for LLD5E2C, LLD5E4C, LLD5E6C and Cloisite® 15A

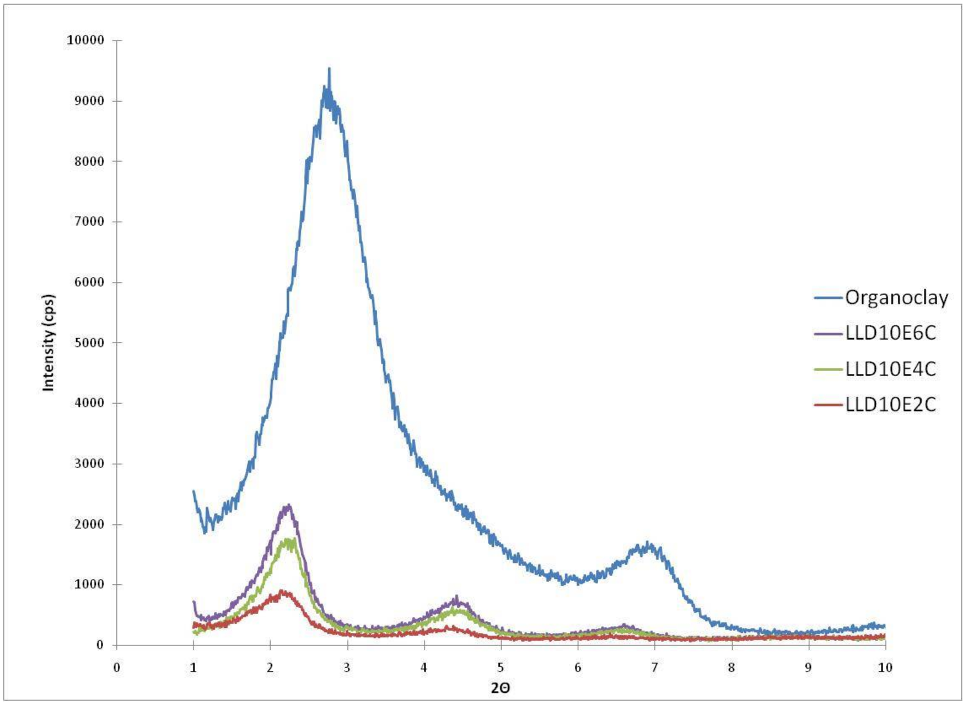

Figure 4.6 XRD patterns for LLD10E2C, LLD10E4C, LLD10E6C and Cloisite® 15A

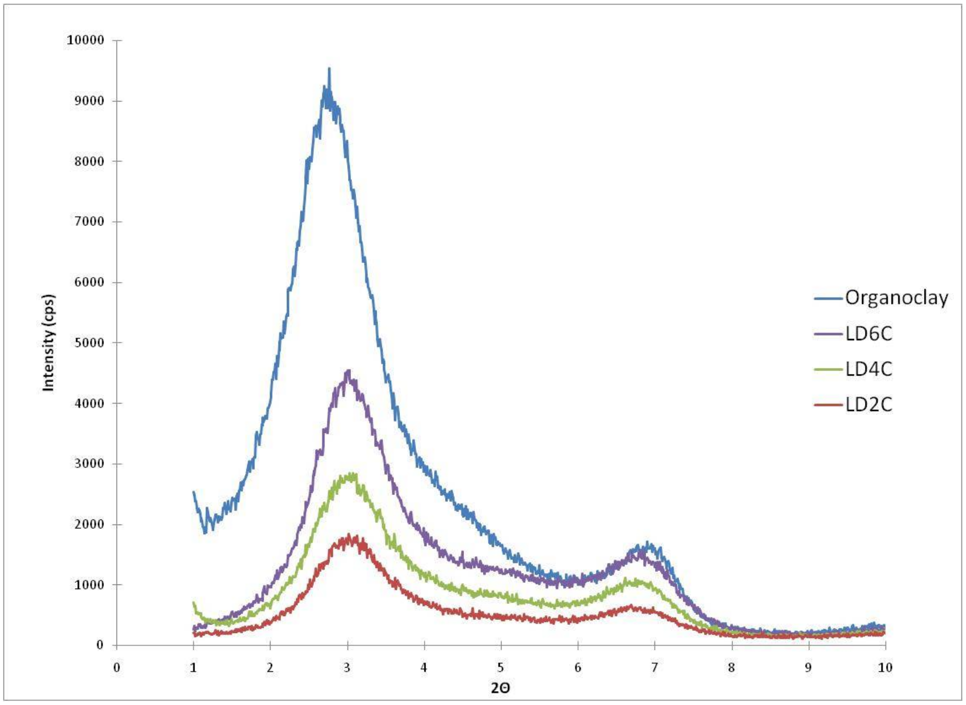

Figure 4.7 XRD patterns for LD2C, LD4C, LD6C and Cloisite® 15A

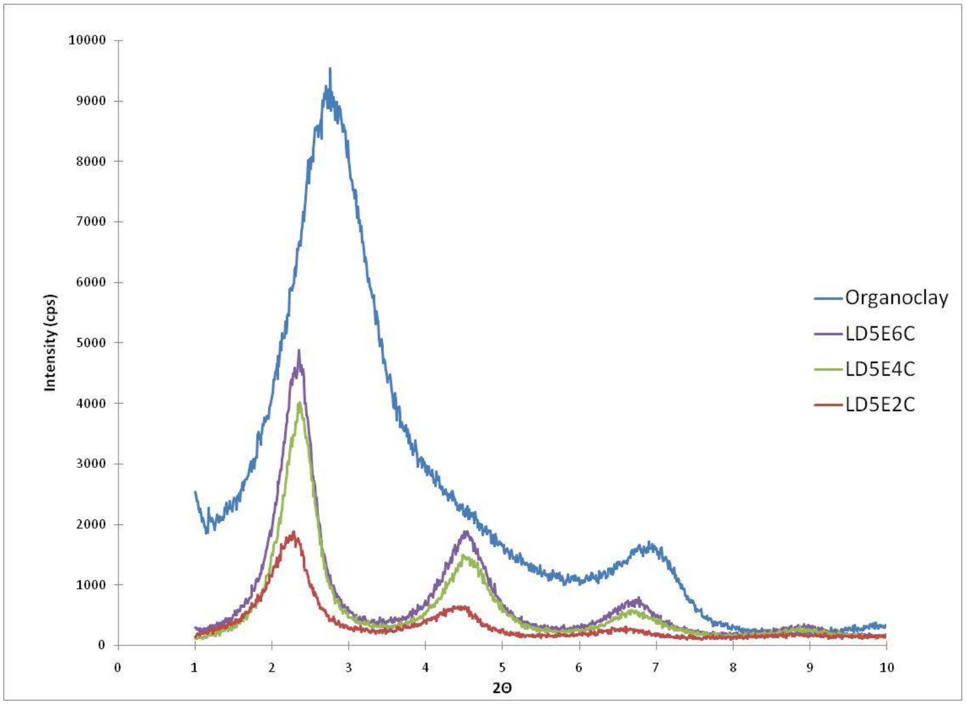

Figure 4.8 XRD patterns for LD5E2C, LD5E4C, LD5E6C and Cloisite® 15A

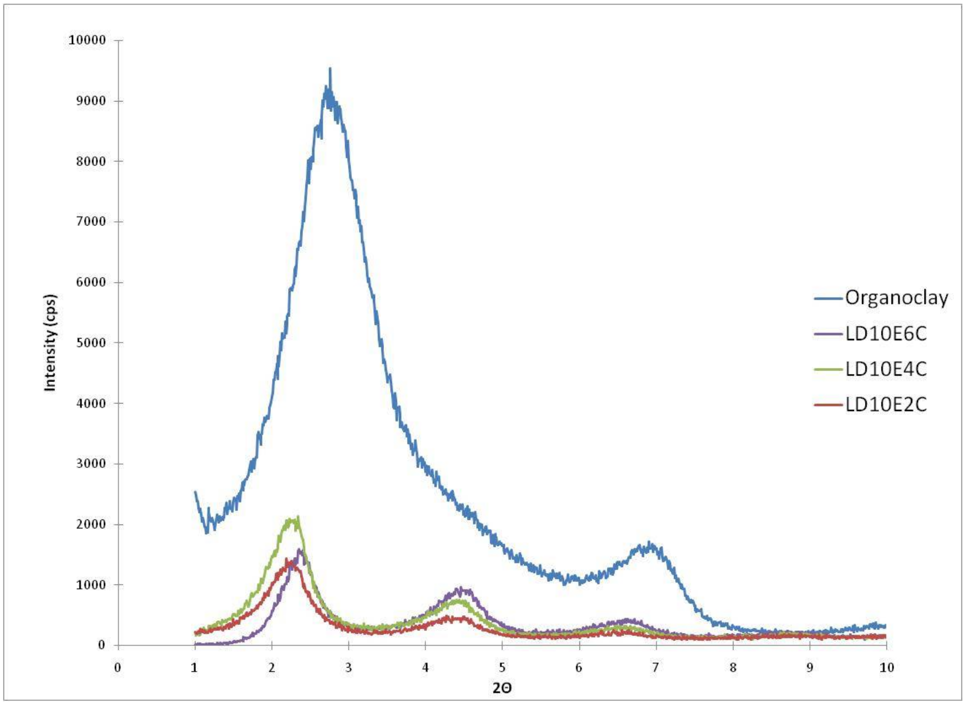

Figure 4.9 XRD patterns for LD10E2C, LD10E4C, LD10E6C and Cloisite® 15A

The broadened peaks with less intensity are a characteristic of a highly disordered intercalated structure, i.e., a decrease in the degree of coherent layer stacking [42]. It is seen from Figures 4.1 though 4.9 that heights of both the first and second peaks of pure organoclay decrease and peaks broaden, indicating decrease in the number of layers of individual clay particles.

For intercalated nanocomposites, the finite layer expansion associated with polymer intercalation results in the appearance of a new basal reflection corresponding to the larger gallery height [7]. At all compositions except LDPE/organoclay and LLDPE/organoclay, new basal reflections corresponding to the larger gallery height are observed, which imply intercalation of nanocomposites, see Figures 4.1, 4.2, 4.3, 4.5, 4.6, 4.8 and 4.9.

Binary blends of organoclay with LDPE as well as LLDPE at any composition did not give new basal reflections, see Figures 4.4 and 4.7, indicating again that compatibilizer is an essential component for LDPE and LLDPE nanocomposites. In the absence of compatibilizer, LDPE or LLDPE chains cannot enter into the clay galleries. On the contrary, basal spacings in Figures 4.4 and 4.7 are slightly decreased because of the high pressures applied on the composites during injection molding.

On the other hand, Figure 4.1 shows that HDPE with organoclay gives high order peaks; also increase in the interlayer spacings are observed. Also, when Figures 4.1, 4.2 and 4.3 are compared it is observed that HDPE nanocomposites need compatibilizer above 2% clay for intercalation of layers of clay. Below 2% clay, compatibilizer even makes the dispersion worse.

In nanocomposites of LDPE and LLDPE with 4-6% clay, more than 5% compatibilizer is needed to decrease d_1 peak height thus decrease the number of layers of individual clay particles, see Figures 4.5, 4.6, 4.8 and 4.9 . However, in HDPE nanocomposites, it is not possible to decrease d_1 peak by increasing compatibilizer content, see Figures 4.2 and 4.3.

Although, XRD offers a convenient method to determine the interlayer spacing of the silicate layers in the original layered silicates and in the intercalated nanocomposites (within 1-4 nm), however, little can be said about the spatial distribution of the silicate layers or any structural inhomogeneities in the polymer layered nanocomposites. Additionally, some layered silicates initially do not exhibit well-defined basal reflection. Thus, peak broadening and intensity decreases are very difficult to study systematically. Therefore, conclusions concerning the mechanism of nanocomposites formation and their structure based solely on XRD patterns are only tentative [3].

4.1.2 Scanning Electron Microscopy (SEM) Analysis

Figure 4.10 shows the SEM micrograph of HDPE. It is seen that neat HDPE shows smooth surface and also crack propagation lines can be seen. These lines are in straight pattern due to the homogenous nature of HDPE, because there is nothing to stop the crack propagation.

Figure 4.11 for HDPE with 10% compatibilizer shows continuous and interpenetrated lines indicating that the E-MA-GMA and HDPE are miscible and there is no phase separation.

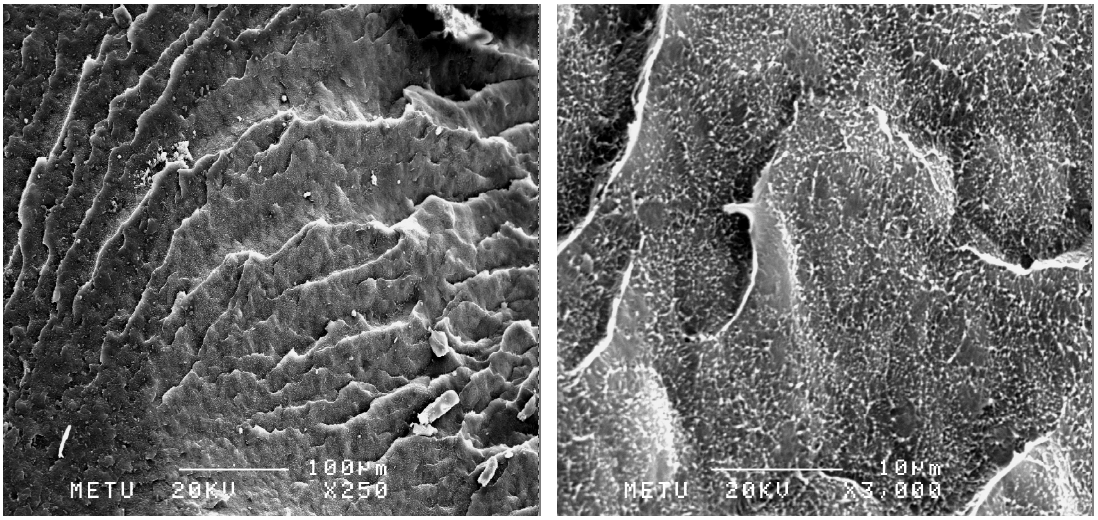

Figure 4.10 SEM micrographs of HDPE

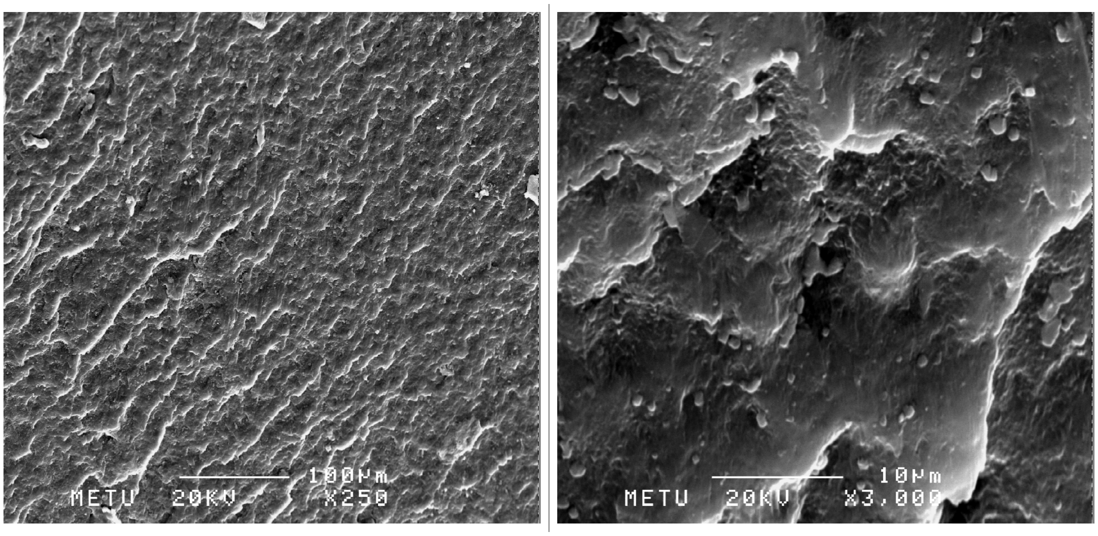

Figure 4.11 SEM micrographs of HD10E

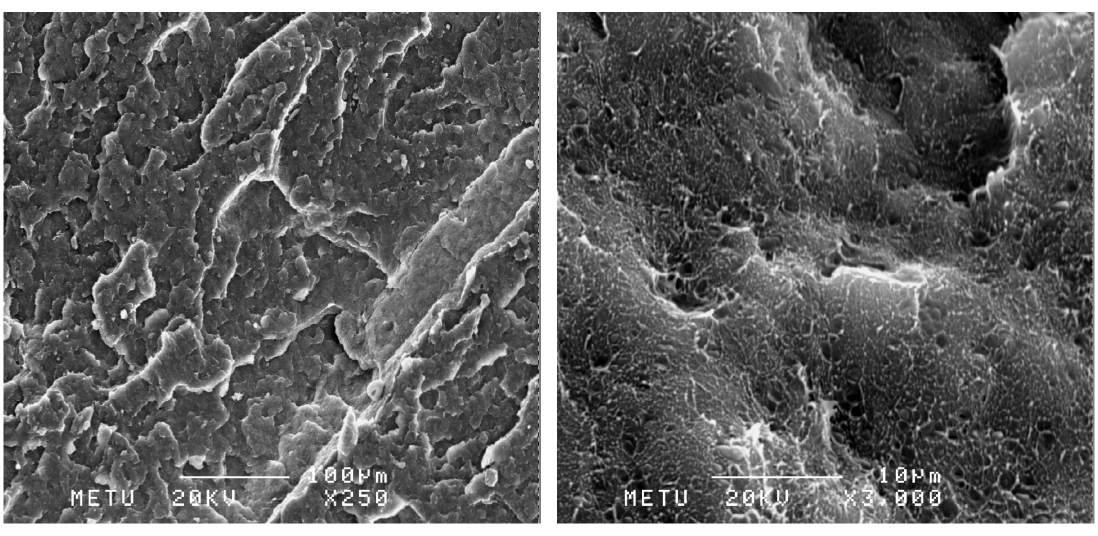

Figure 4.12 SEM micrographs of HD2C

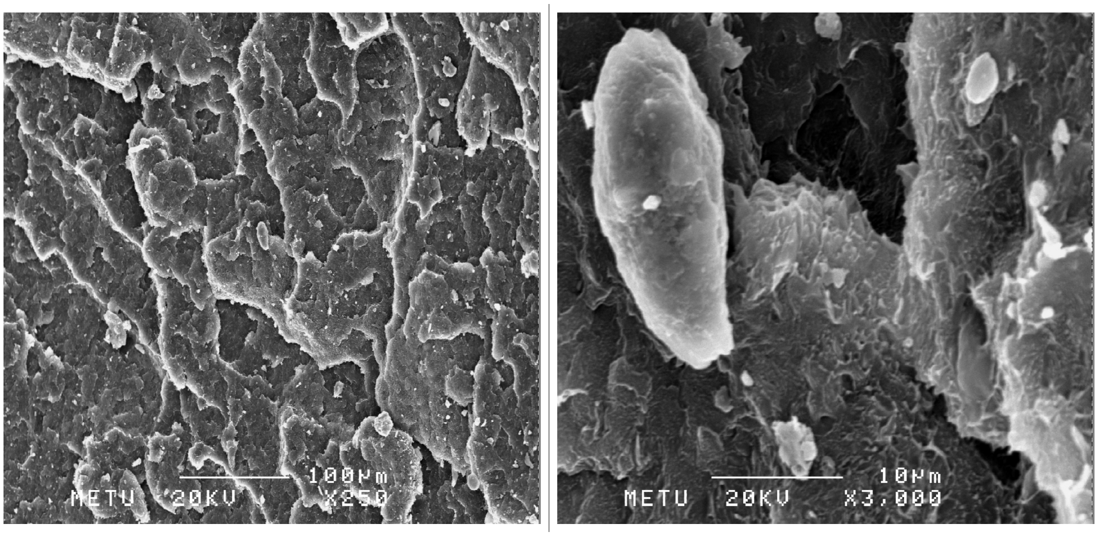

Figure 4.13 SEM micrographs of HD6C

Figure 4.12 for HDPE with 2% organoclay shows that introduction of clay to HDPE decreases the smoothness of the surface, but at low clay loading no agglomerated clay particles are observed. In contrast to Figure 4.12, in Figure 4.13 with higher clay loading, agglomerated clay particles can be seen indicating that dispersion of the clay is worse at 6% clay loading. At x3000 magnification clay agglomerates can be seen more clearly.

Figure 4.14 and Figure 4.15 show the ternary composition of HDPE with 10% elastomer with 2% and 6% clay respectively.

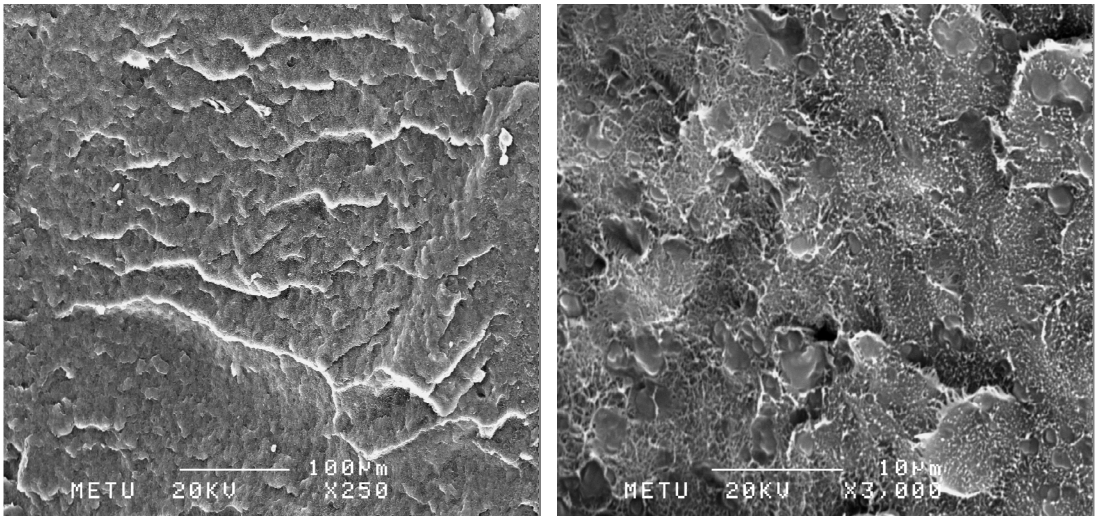

Figure 4.14 SEM micrographs of HD10E2C

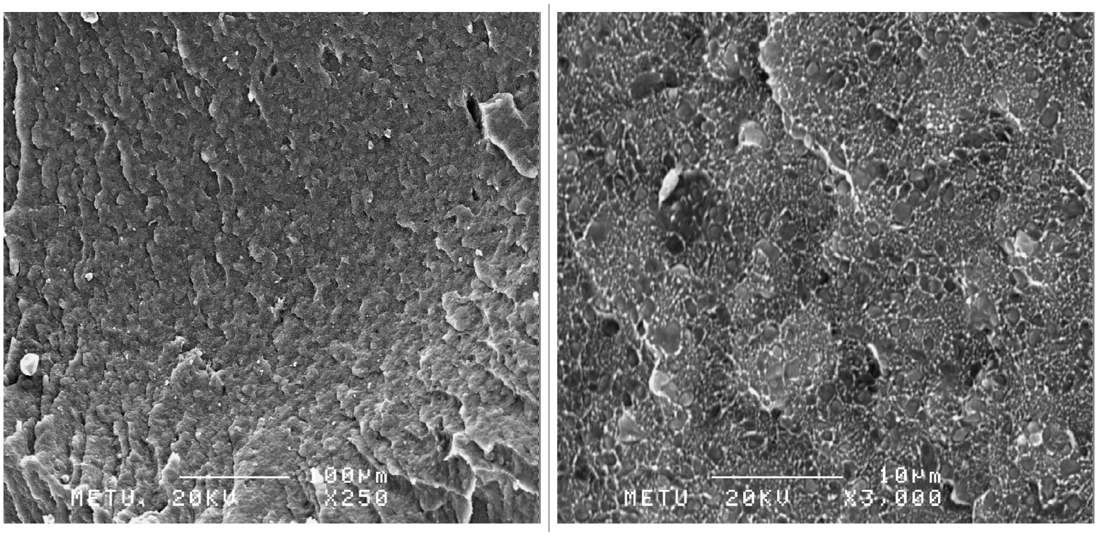

Figure 4.15 SEM micrographs of HD10E6C

When Figure 4.14 and Figure 4.15 are compared it is observed that introduction of higher clay content makes the crack propagation path more tortuous. Also, when Figure 4.13 (for HD6C) and Figure 4.15 (for HD10E6C) are compared, it can be concluded that introduction of compatibilizer makes the surface smoother and disperses the clay better in the matrix.

Figure 4.16 and Figure 4.17 show SEM micrographs of LLDPE and LLDPE with 10% compatibilizer respectively.

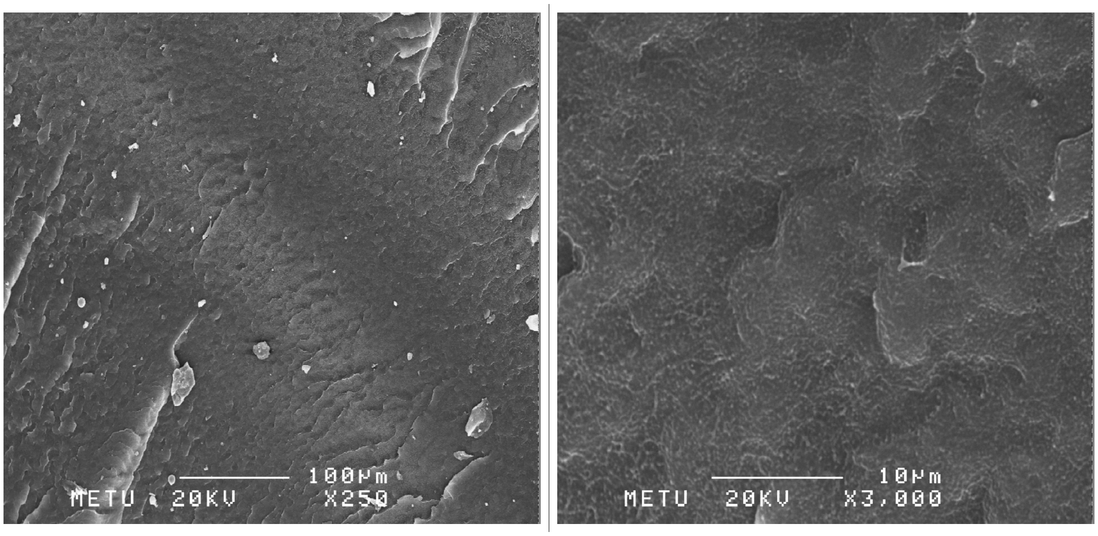

Figure 4.16 SEM micrographs of LLDPE

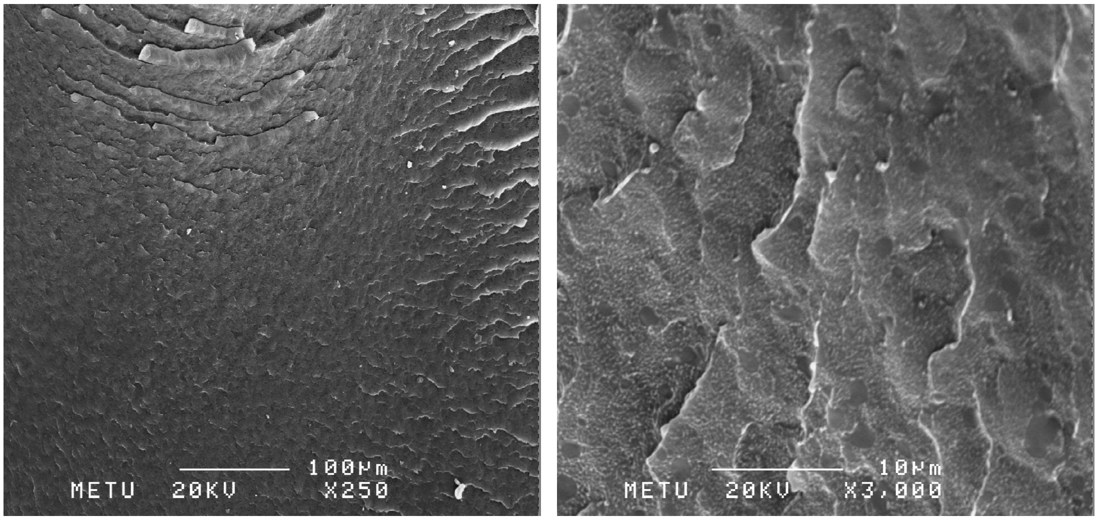

Figure 4.17 SEM micrographs of LLD10E

LLD10E as well as neat LLDPE show smooth surface signifying the compatibility of the LDPE and E-MA-GMA. Also, since there is no organoclay, the fracture surfaces are not tortuous.

Figure 4.18 shows the addition of 2% organoclay to LLDPE. When Figure 4.18 is compared with Figure 4.16 it is observed that the addition of organoclay makes the surface tortuous. Also, some clay agglomerates can be seen in Figure 4.18.

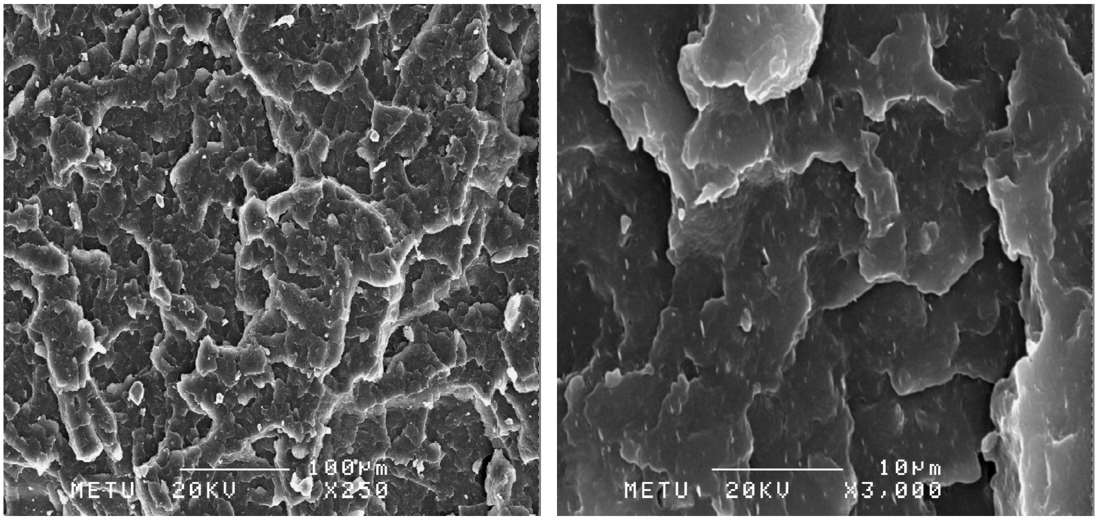

Figure 4.18 SEM micrographs of LLD2C

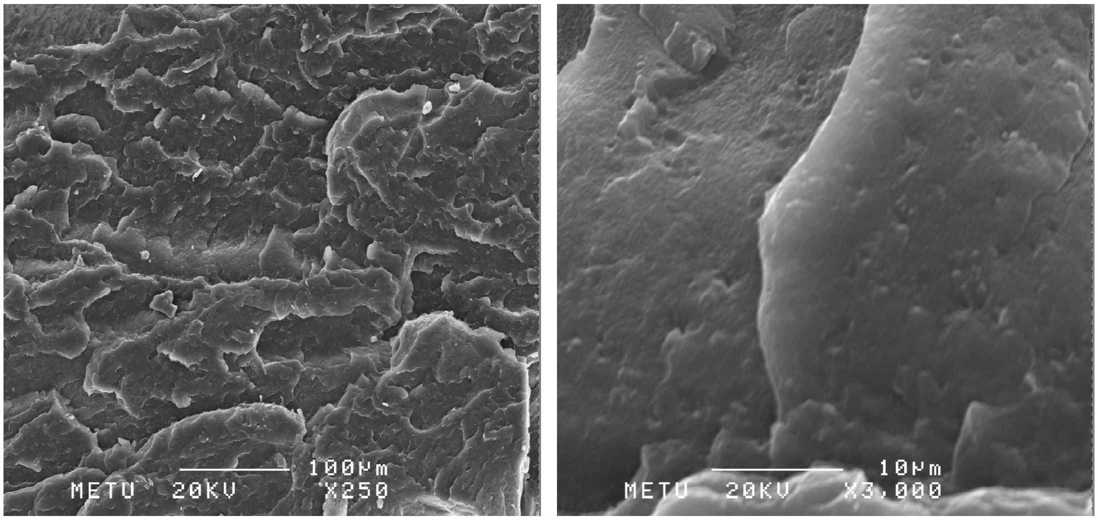

Figure 4.19 SEM micrographs of LLD10E2C

Figure 4.19 indicates the effect of addition of 10% compatibilizer to the composition given in Figure 4.18. It is observed that the addition of compatibilizer makes the fracture surface smoother.

Figure 4.20 shows the SEM micrographs of LLDPE with 6% organoclay. Figure 4.21 shows the effect of addition of 10% compatibilizer to the composition given in Figure 4.20.

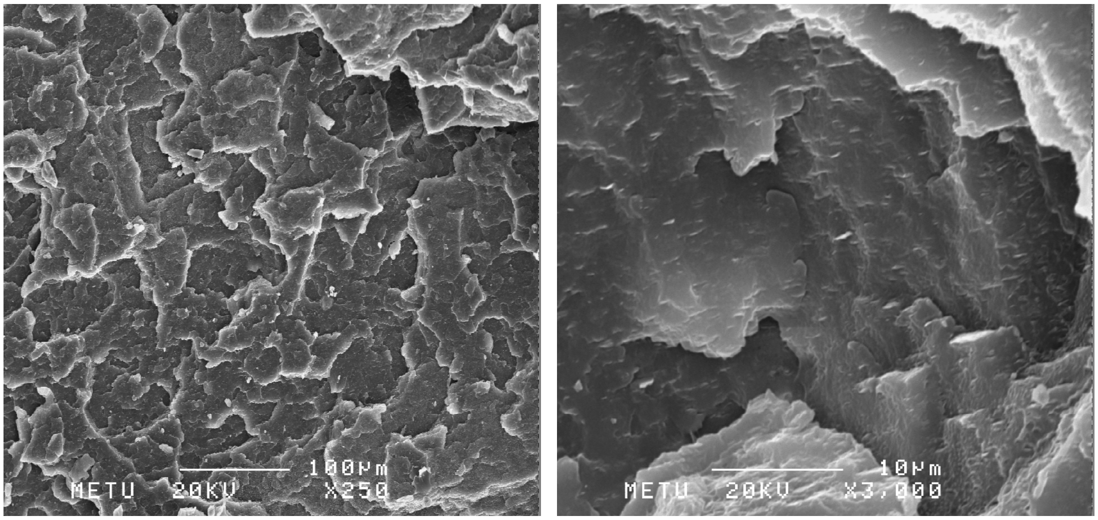

Figure 4.20 SEM micrographs of LLD6C

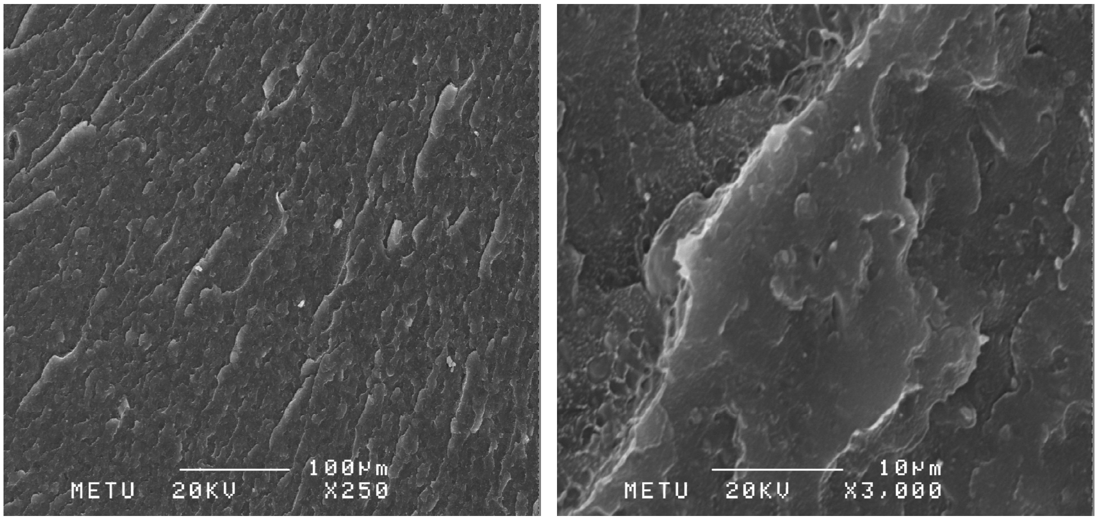

Figure 4.21 SEM micrographs of LLD10E6C

Comparison of Figure 4.18 and Figure 4.20 shows that, as clay loading increases in the absence of compatibilizer, crack propagation lines are more tortuous. Comparison of Figure 4.20 with Figure 4.21 indicates that, using compatibilizer helps dispersing the particles and makes the surface of the fracture surface smoother. In Figure 4.22 the SEM micrograph of LDPE is shown, where the smooth surface of the neat LDPE is observed.

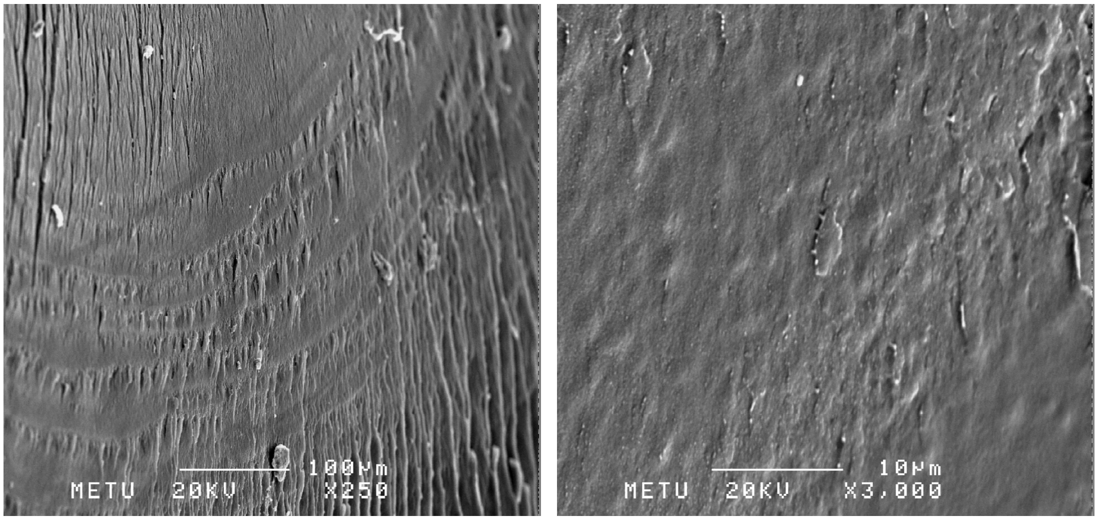

Figure 4.22 SEM micrographs of LDPE

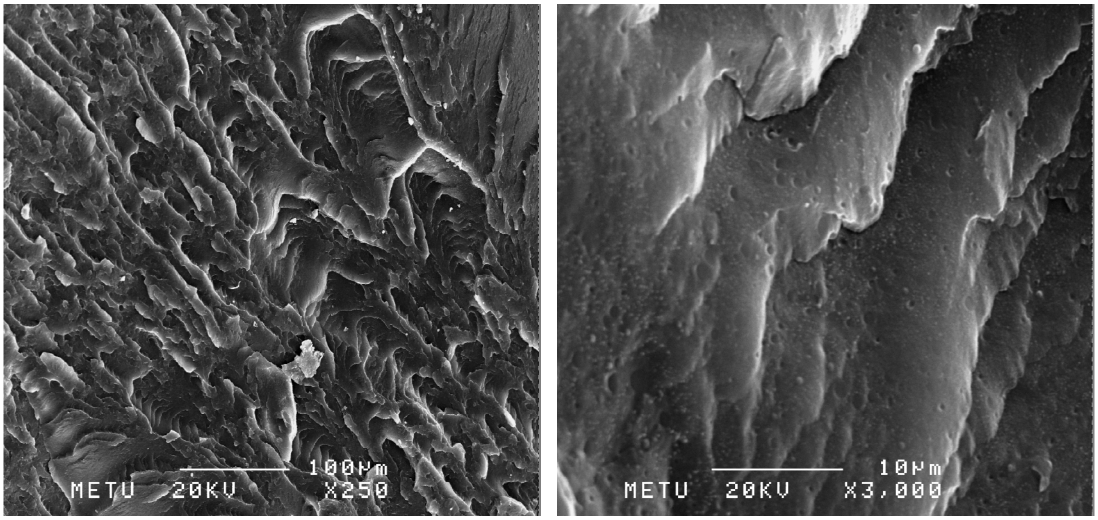

Figure 4.23 SEM micrographs of LD10E

Figure 4.23 shows the effect of addition of 10% compatibilizer to LDPE. By introducing 10% compatibilizer to LDPE, the crack propagation lines become coarser. The structure being coarser than HD10E and LLD10E, may indicate that the compatibilizer is less miscible with LDPE than it is with HDPE and LLDPE. Figure 4.24 shows the effect of addition of 2% organoclay to LDPE shown in Figure 4.22. This makes the surface tortuous with some clay agglomerates.

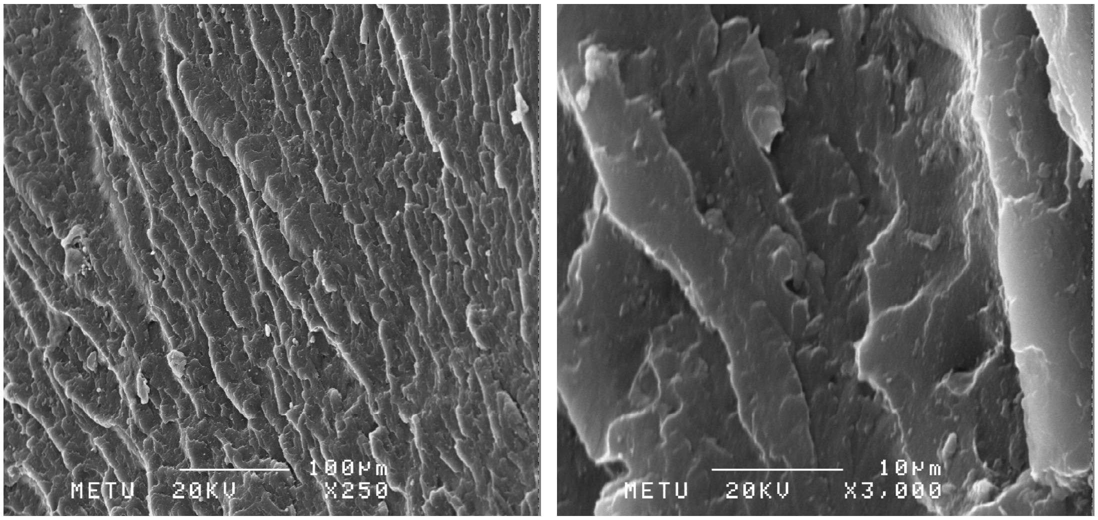

Figure 4.24 SEM micrographs of LD2C

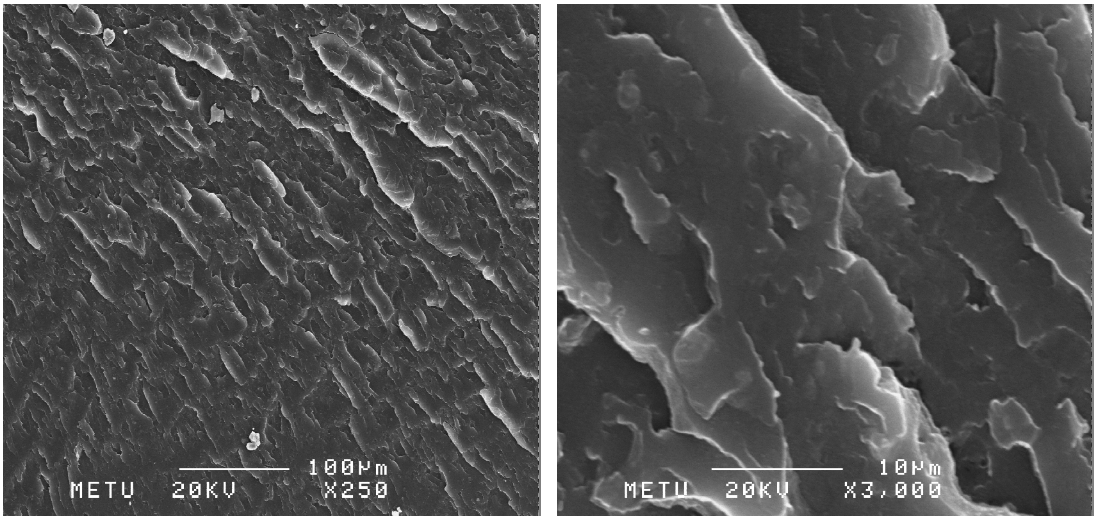

Figure 4.25 SEM micrographs of LD10E2C

Figure 4.25 shows that the addition of 10% compatibilizer to the previous composition makes the surface smoother showing better dispersion of the organoclay.

Figure 4.26 shows the fracture surface of LDPE with 6% clay. When it is compared with Figure 4.24 it is observed that higher clay content makes the surface rougher and some clay agglomerates can be seen.

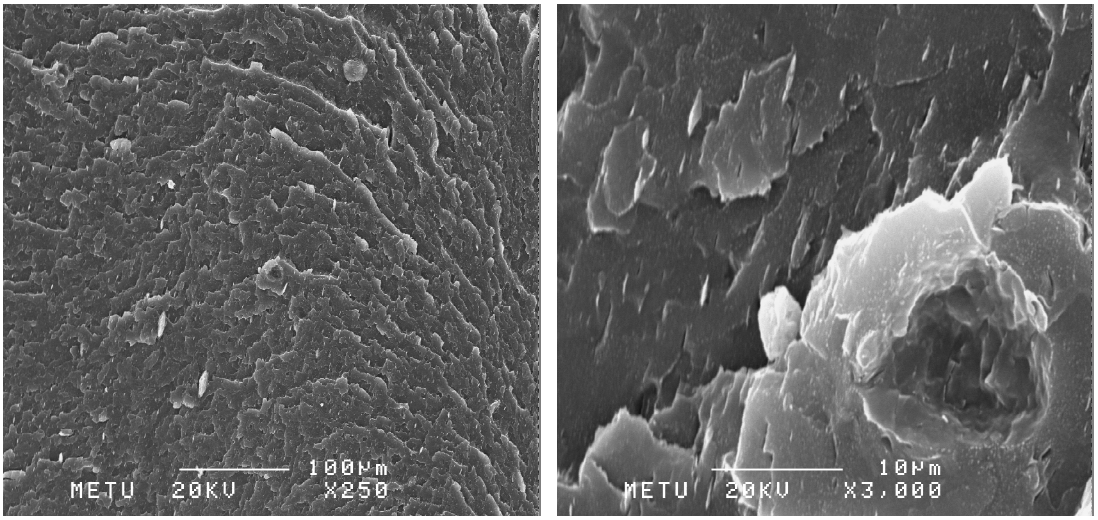

Figure 4.26 SEM micrographs of LD6C

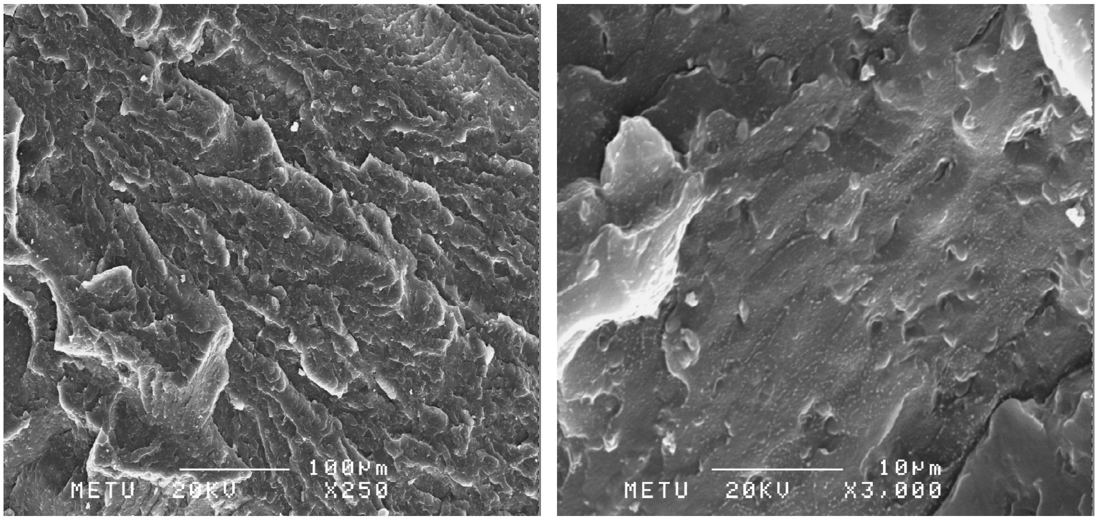

Figure 4.27 SEM micrographs of LD10E6C

Figure 4.27 shows the effect of addition of 10% compatibilizer to the previous composition. It is observed that addition of E-MA-GMA makes the surface smoother and helps deagglomeration of organoclay.

4.2 Thermal Characterization

4.2.1 Differential Scanning Calorimetry (DSC) Analysis

In order to investigate the crystallinity of the samples, DSC analysis is performed. The results are presented in Table 4.4 through Table 4.6 and DSC diagrams are given in Appendix B. Percent crystallinity is calculated from the following formula

$$\% \text{ crystallinity} = \Delta H_f / (\Delta H_f^0 \times (1-w)) \times 100 \qquad (4.1)$$

where ΔH_f is the heat of fusion measured, ΔH_f^0 is the heat of fusion of 100% crystalline PE and w is the weight fraction of clay. Here ΔH_f^0 is taken as 293 J/g.

Table 4.4 Percent crystallinity data of the HDPE matrix containing samples

Code	Compatibilizer %	Organoclay %	Melting Point ^{0}C	ΔH J/g	Crystallinity %
HD	0	0	132.7	165.0	56.3
HD5E	5	0	132.4	163.0	55.6
HD10E	10	0	133.4	148.9	50.8
HD2C	0	2	132.8	157.3	54.8
HD4C	0	4	134.6	149.5	53.1
HD6C	0	6	134.1	148.2	53.8
HD5E2C	5	2	135.4	153.1	53.3
HD5E4C	5	4	132.5	153.7	54.6
HD5E6C	5	6	135.2	145.0	52.6
HD10E2C	10	2	133.1	136.3	47.5
HD10E4C	10	4	132.8	143.1	50.9
HD10E6C	10	6	133.5	136.6	49.6

HDPE has very few branches and therefore it is capable of fitting in close packing, which results in higher percent crystallinity than LLDPE and LDPE. On the other hand LDPE has very large branches prohibiting close chain configuration, which results in mostly amorphous structure.

Table 4.5 Percent crystallinity data of the LLDPE matrix containing samples

Code	Compatibilizer %	Organoclay %	Melting Point ^{0}C	ΔH J/g	Crystallinity %
LLD	0	0	125.9	90.9	31.0
LLD5E	5	0	124.8	88.0	30.0
LLD10E	10	0	126.4	75.1	25.6
LLD2C	0	2	125.9	87.1	30.3
LLD4C	0	4	124.5	82.2	29.2
LLD6C	0	6	125.2	86.1	31.2
LLD5E2C	5	2	124.7	84.7	29.5
LLD5E4C	5	4	126.0	75.5	26.8
LLD5E6C	5	6	124.5	84.5	30.7
LLD10E2C	10	2	125.6	85.9	29.9
LLD10E4C	10	4	125.1	75.5	26.8
LLD10E6C	10	6	124.4	74.2	27.0

Table 4.6 Percent crystallinity data of the LDPE matrix containing samples

Code	Compatibilizer %	Organoclay %	Melting Point ^{0}C	ΔH J/g	Crystallinity %
LD	0	0	107.7	67.3	23.0
LD5E	5	0	107.7	74.0	25.3
LD10E	10	0	106.6	65.0	22.2
LD2C	0	2	107.6	68.7	23.9
LD4C	0	4	107.0	65.9	23.4
LD6C	0	6	106.8	65.5	23.8
LD5E2C	5	2	106.7	67.8	23.6
LD5E4C	5	4	105.3	63.4	22.5
LD5E6C	5	6	107.8	64.8	23.5
LD10E2C	10	2	107.3	64.4	22.4
LD10E4C	10	4	105.3	56.9	20.2
LD10E6C	10	6	105.9	56.7	20.6

The addition of E-MA-GMA decreases the crystallinity in general. As it is stated in compatibilizer manufacturer's data sheet, the high content of MA leads to low crystallinity, 10% compatibilizer leads to 6% decrease in crystallinity in binary mixtures, with the exception of LDPE which already has low crystallinity.

In the binary mixtures of clay and PE, slight decrease in crystallinity was observed in composites with HDPE matrix. Crystallinity of LLDPE and LDPE are not affected from clay loading. Anything that makes difficult for the chains to come close decreases crystallinity. However, in LLDPE and LDPE matrices there is already higher space between the chains, because of the branching, thus clay does not disturb the crystallinity significantly. It can be concluded that clay has no nucleation effect on polyethylene.

In ternary mixtures, the results are consistent with the statements made above for binary mixtures, with few exceptions. In general, compatibilizer and clay affect crystallinity negatively; however clay has less effect than the compatibilizer.

4.3 Mechanical Properties

Tensile, flexural and impact tests were performed on the injection molded samples, in order to see and compare the performances of nanocomposites, binary mixtures and neat polymers.

4.3.1 Tensile Properties

Tensile tests were performed for all the compositions. Five samples were used for each composition and stress-strain curves were obtained. All mechanical test results are presented in Appendix C. The curves obtained for pure polyethylenes are shown in Figure 4.28 and Figure 4.29.

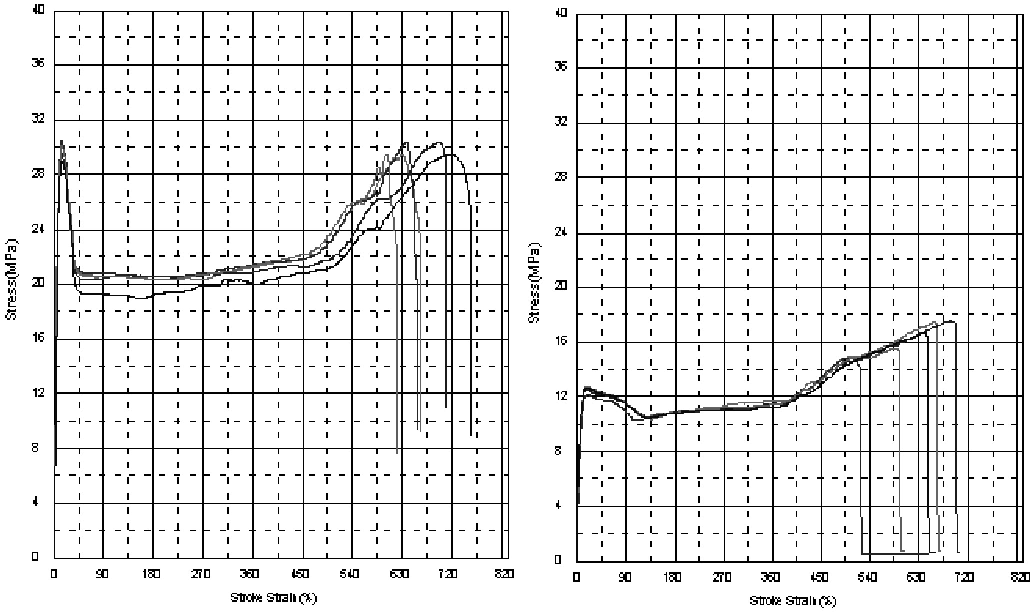

Figure 4.28 Stress-strain curve of pure HDPE (left) and LLDPE (right)

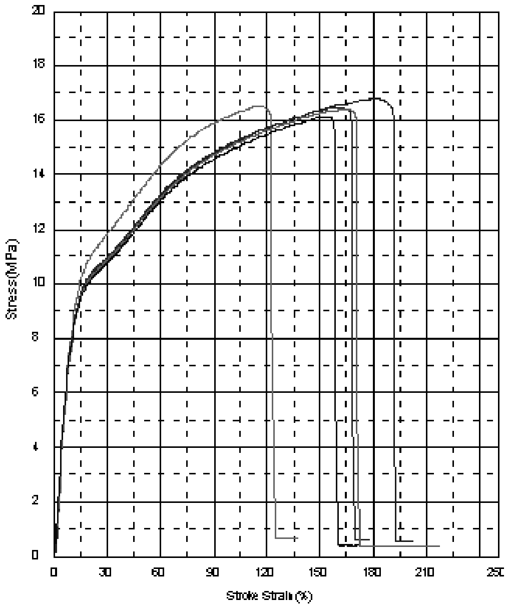

Figure 4.29 Stress-strain curve of pure LDPE

It can be observed that low branched HDPE and short branched LLDPE show different behavior than long branched LDPE. HDPE and LLDPE show yield, followed by cold drawing and strain hardening, whereas LDPE does not exhibit cold drawing.

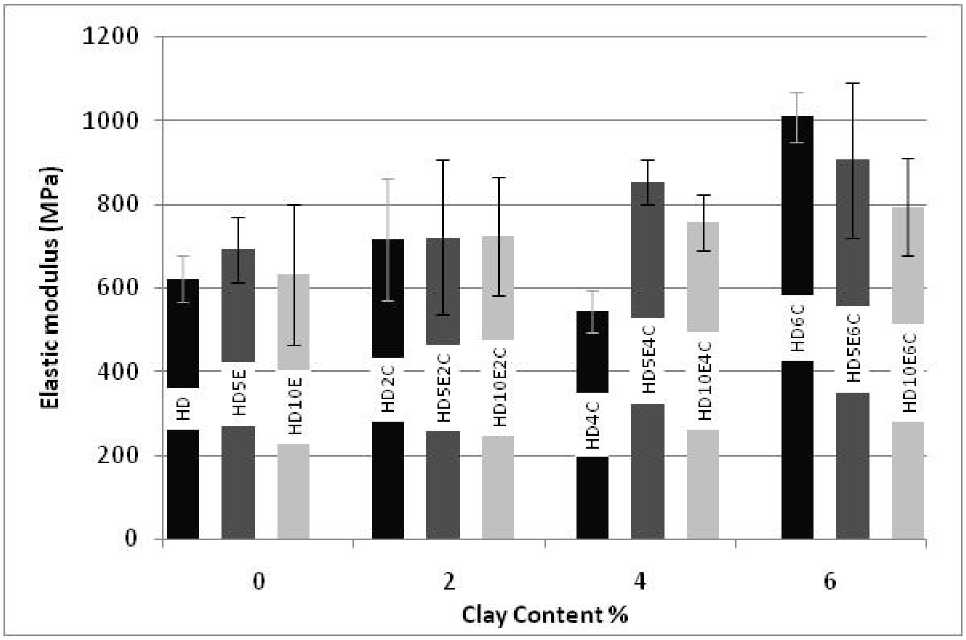

Figure 4.30 Elastic modulus values of HDPE nanocomposites

Elastic modulus values of nanocomposites with HDPE matrix composites are more than twice the elastic modulus values of nanocomposites with LLDPE matrix and nearly six times higher than the elastic modulus values of nanocomposites with LDPE matrix in general, however there is no systematic trend in HDPE nanocomposites, see Figure 4.30.

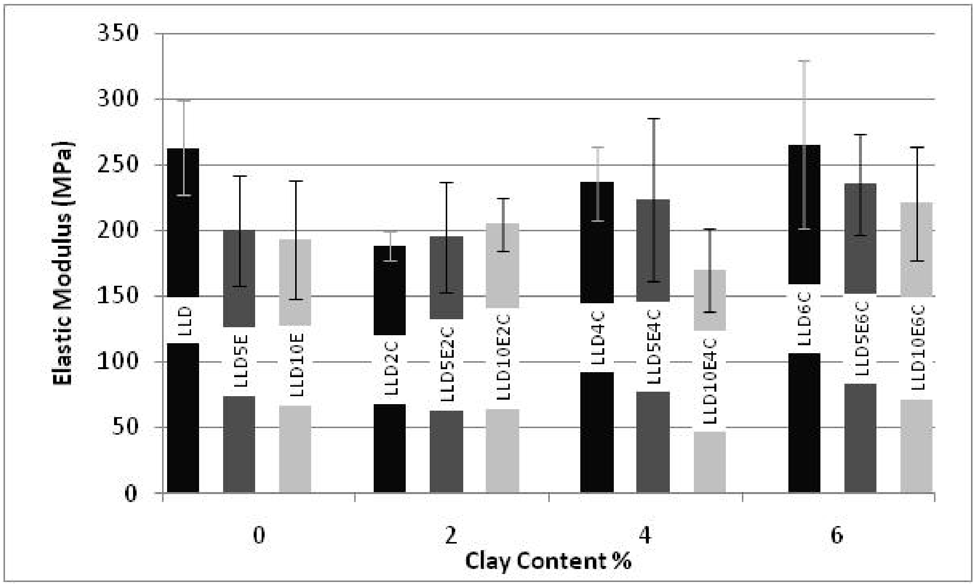

Figure 4.31 Elastic modulus values of LLDPE nanocomposites

In LLDPE nanocomposites, as compatibilizer content increases elastic modulus decreases and as clay content increases elastic modulus increases, see Figure 4.31.

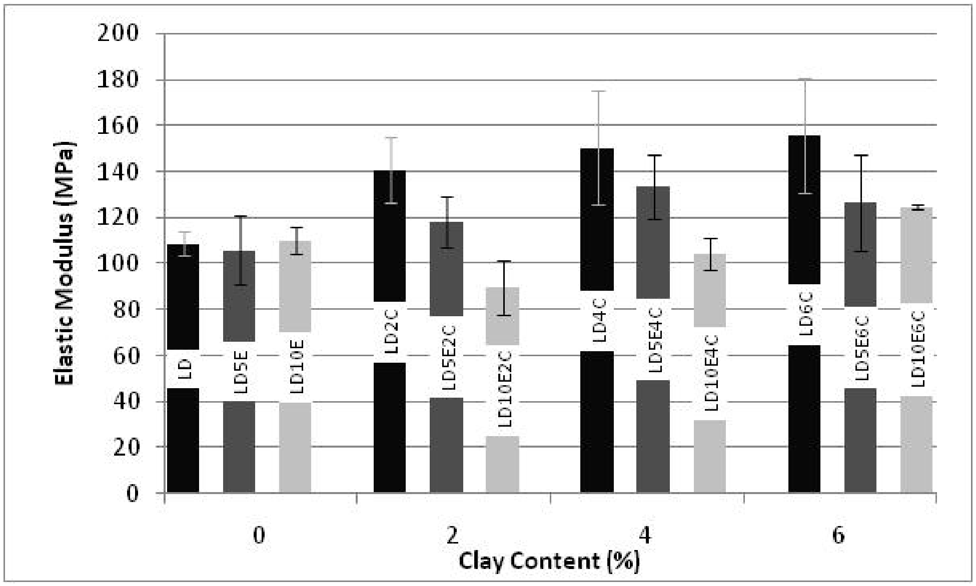

Figure 4.32 Elastic modulus values of LDPE nanocomposites

Elastic modulus values of LDPE nanocomposites show similar trend with LLDPE nanocomposites, see Figure 4.32. In all types of polyethylenes, highest increase are obtained at 6% clay content when compared with neat polymers.

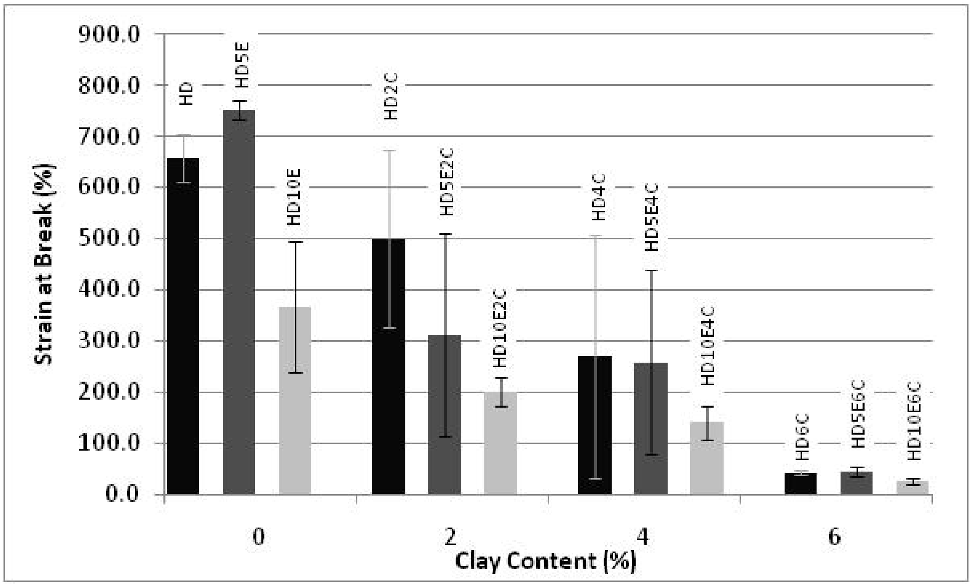

Figure 4.33 Strain at break values of HDPE nanocomposites

Strain at break values of HDPE nanocomposites, see Figure 4.33, which are related to toughness, dramatically decreases as clay content is increased. With the addition of clay sample cannot elongate and it fails. In general, strain at break values are also negatively affected from increasing compatibilizer content.

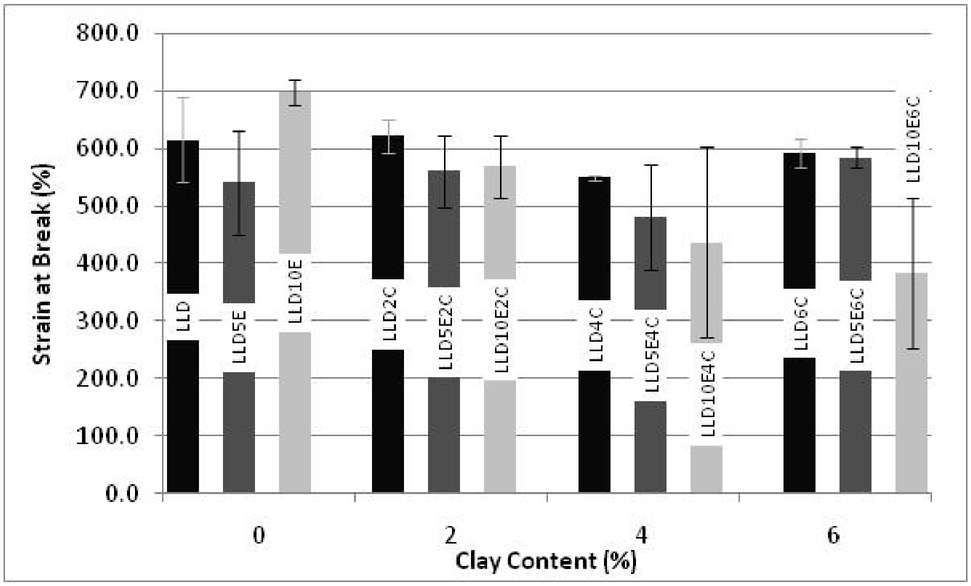

Figure 4.34 Strain at break values of LLDPE nanocomposites

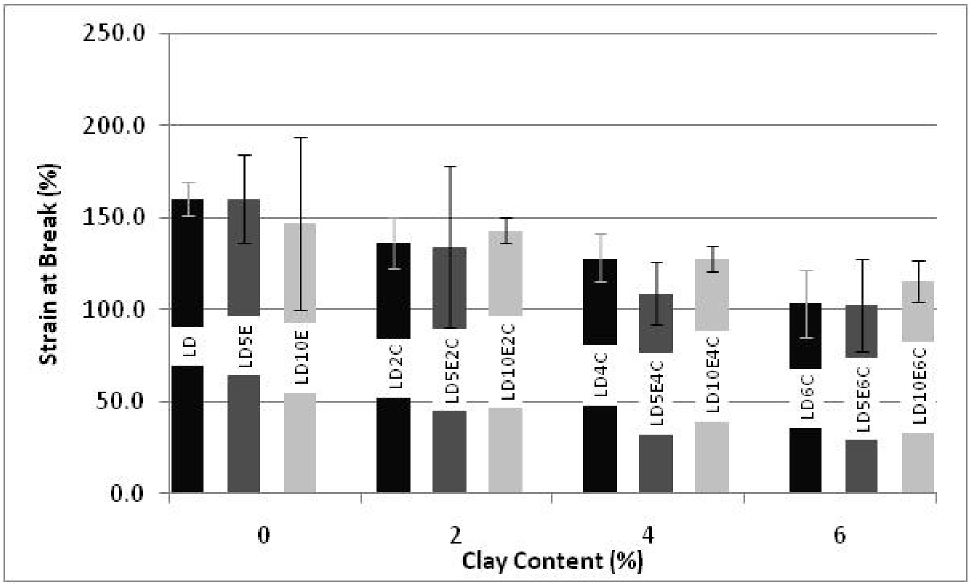

Figure 4.35 Strain at break values of LDPE nanocomposites

Strain at break values of LLDPE and LDPE nanocomposites, see Figure 4.33 through Figure 4.35, are very little affected from organoclay or compatibilizer.

Stress at yield values of nanocomposites increase with increasing clay content and decreases with increasing compatibilizer content, see Figure 4.36 and 4.38.

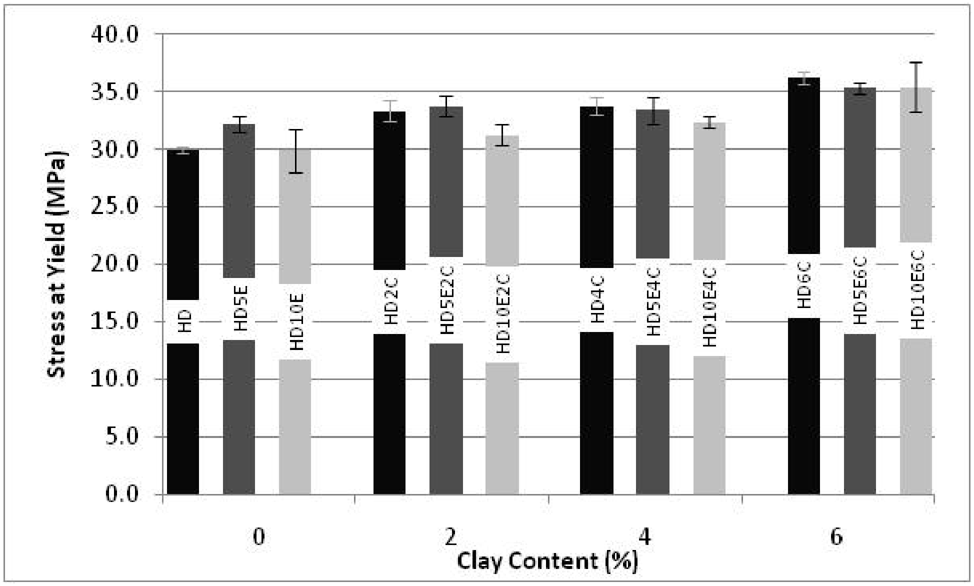

Figure 4.36 Stress at yield values of HDPE nanocomposites

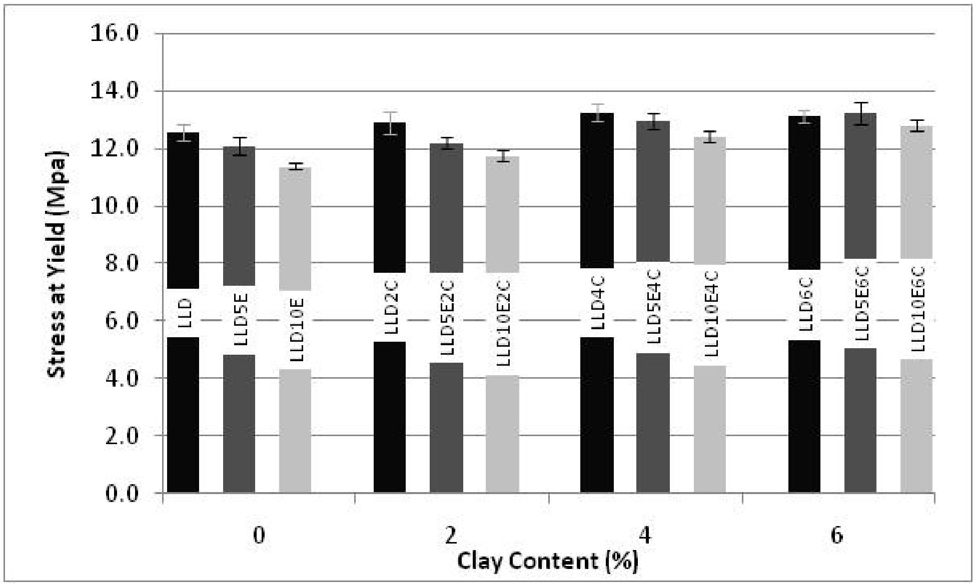

Figure 4.37 Stress at yield values of LLDPE nanocomposites

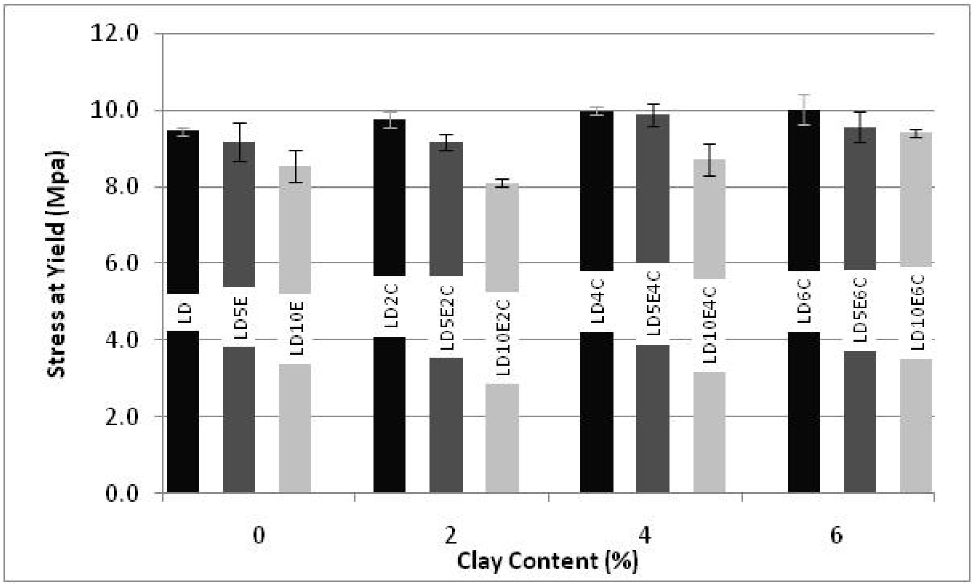

Figure 4.38 Stress at yield values of LDPE nanocomposites

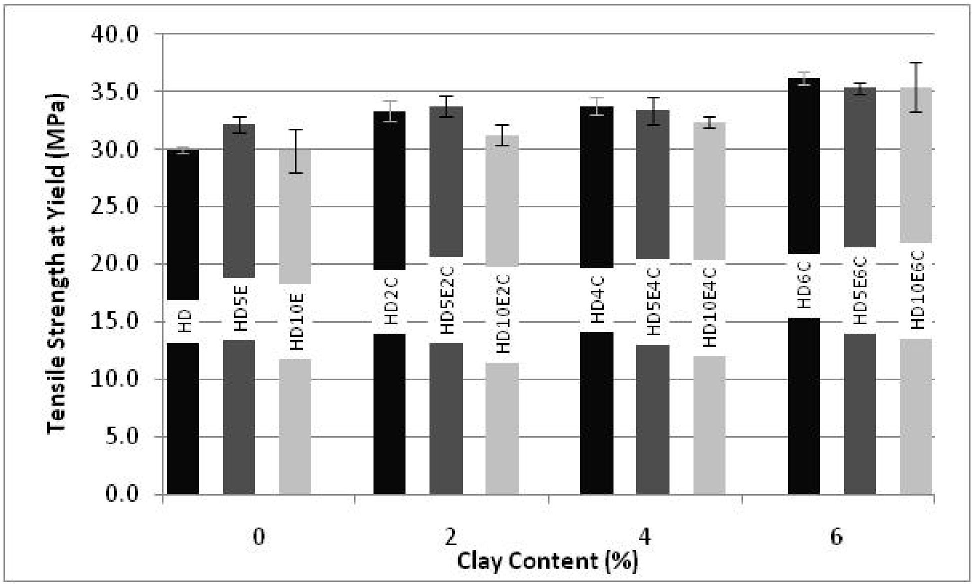

Figure 4.39 Tensile strength at yield values of HDPE nanocomposites

Figure 4.39 shows the tensile strength values of HDPE nanocomposites. These nanocomposites do not exhibit “strain hardening”, thus they exhibit maximum stress values at yield point. At higher clay loadings, tensile strength at yield values of HDPE nanocomposites are higher, see Figure 4.39. Nanocomposites of LDPE and LLDPE matrices exhibit “strain hardening”, thus the stress at break values are higher than the stress at yield values.

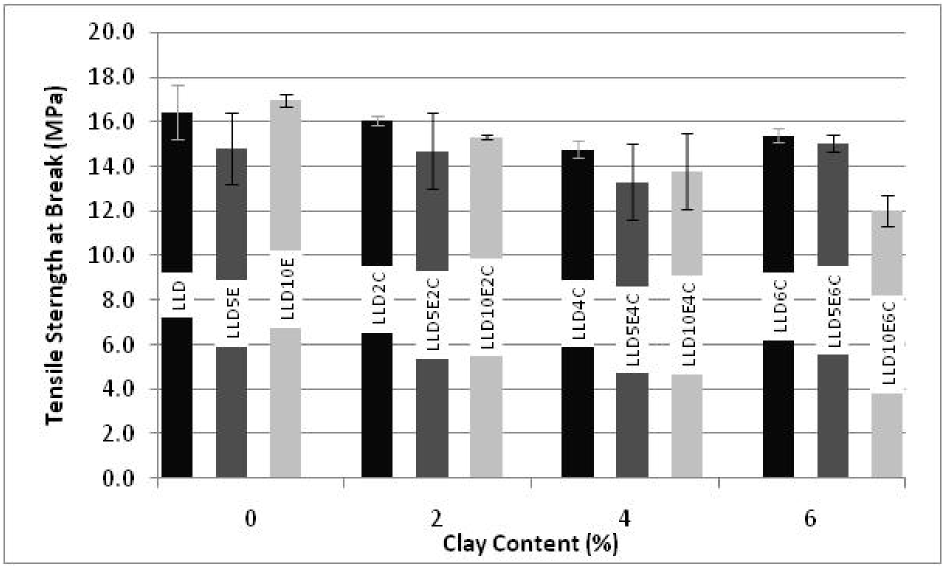

Figure 4.40 Tensile strength at break values of LLDPE nanocomposites

In LLDPE nanocomposites, see Figure 4.40, tensile strength at break decreases with increasing clay content.

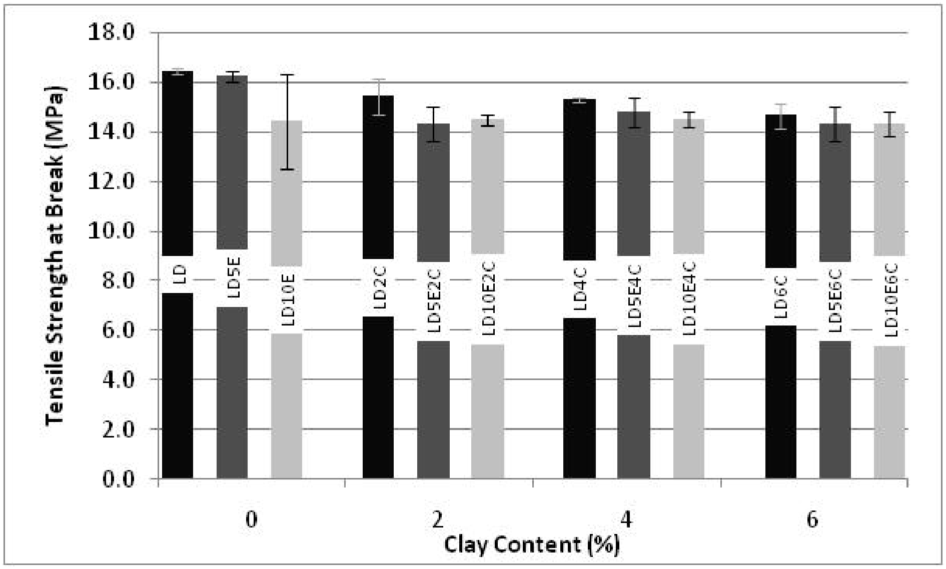

Figure 4.41 Tensile strength at break values of LDPE nanocomposites

Tensile strength at break values of LDPE nanocomposites decrease with increasing compatibilizer content, see Figure 4.41, since the compatibilizer has lower tensile strength than LDPE.

4.3.2 Flexural Properties

Three point bending test was performed on the injection molded samples. The results are tabulated in Appendix C, Table C.13 through C.15.

During the tests, no samples were broken and the tests were terminated manually.

As clay content is increased in ternary nanocomposites, flexural strength increases, however the material becomes more brittle. As compatibilizer content is increased, flexural strength decreases with the exception of LDPE/compatibilizer blend, see Figure 4.42 through Figure 4.44.

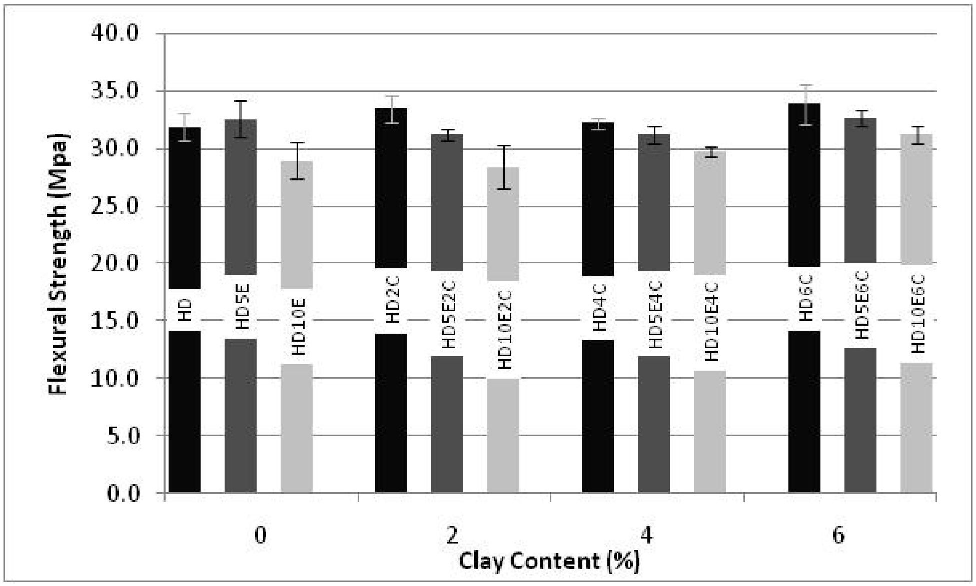

Figure 4.42 Flexural strength values of HDPE nanocomposites

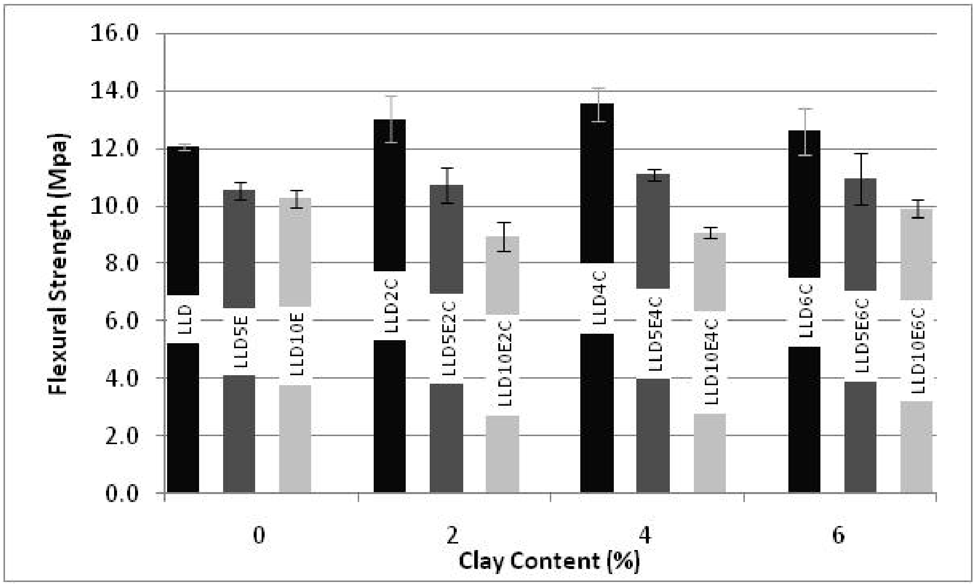

Figure 4.43 Flexural strength values of LLDPE nanocomposites

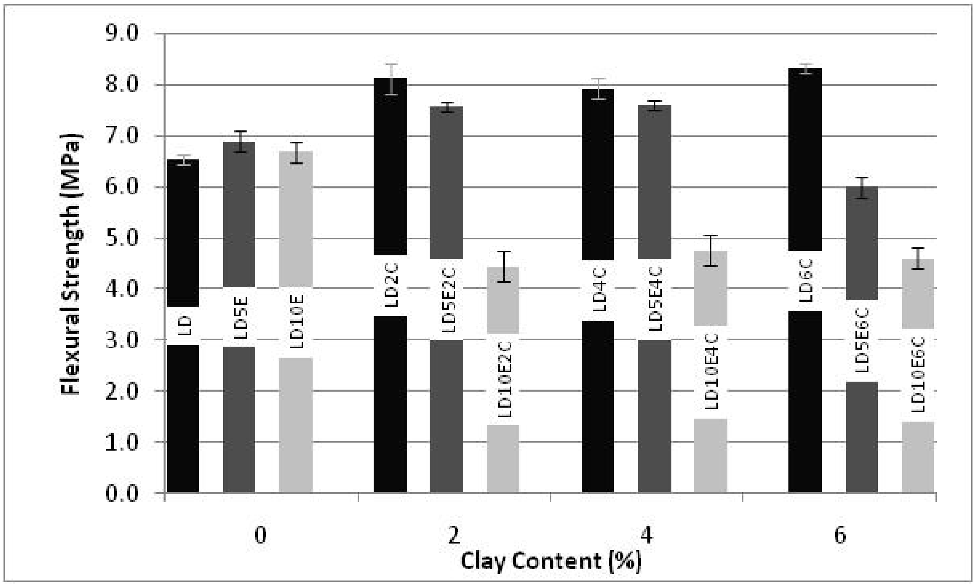

Figure 4.44 Flexural strength values of LDPE nanocomposites

Flexural modulus has the same tendency as the flexural strength. It increases with the clay concentration owing to the filler effect and decreases with the compatibilizer concentration since the compatibilizer has lower modulus than PE's, see Figure 4.45 through Figure 4.47.

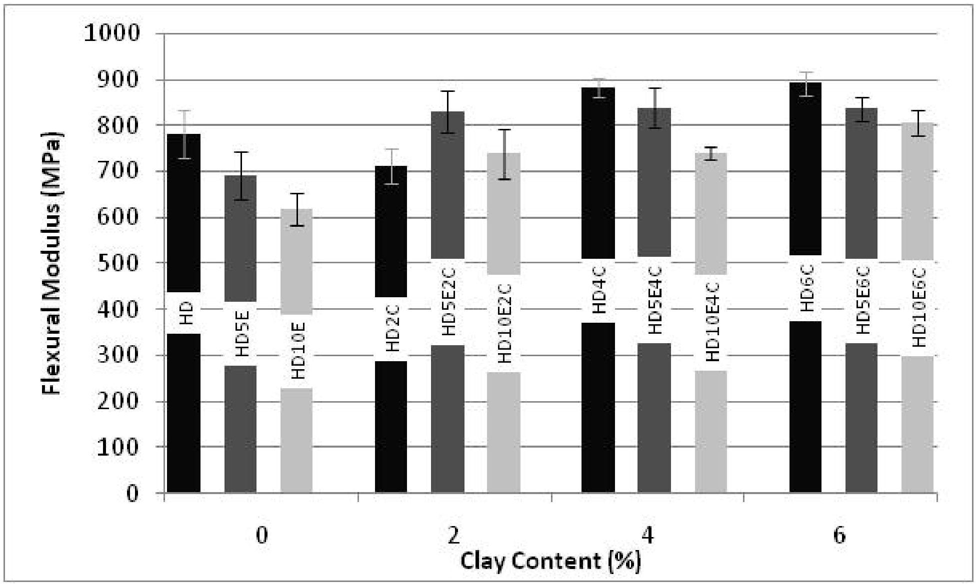

Figure 4.45 Flexural modulus values of HDPE nanocomposites

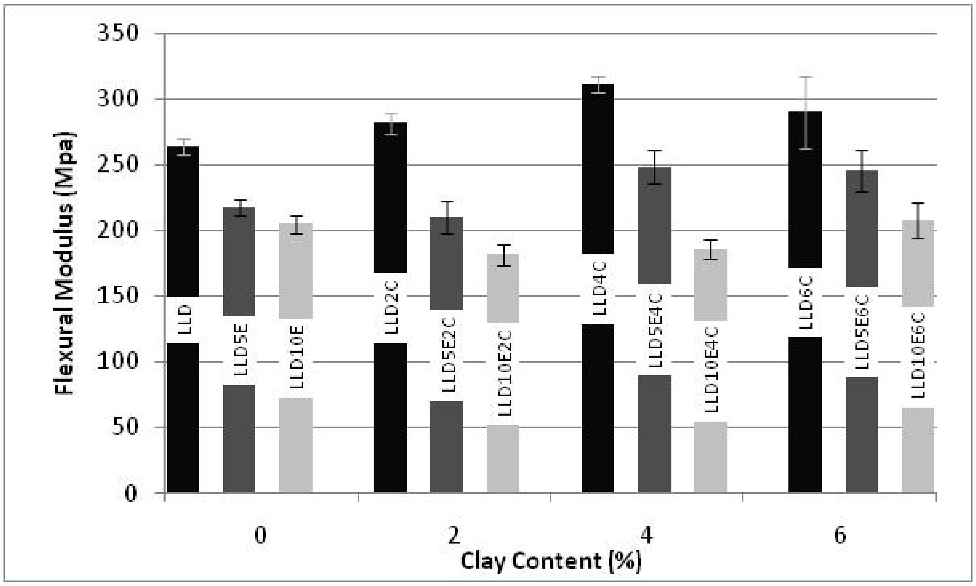

Figure 4.46 Flexural modulus values of LLDPE nanocomposites

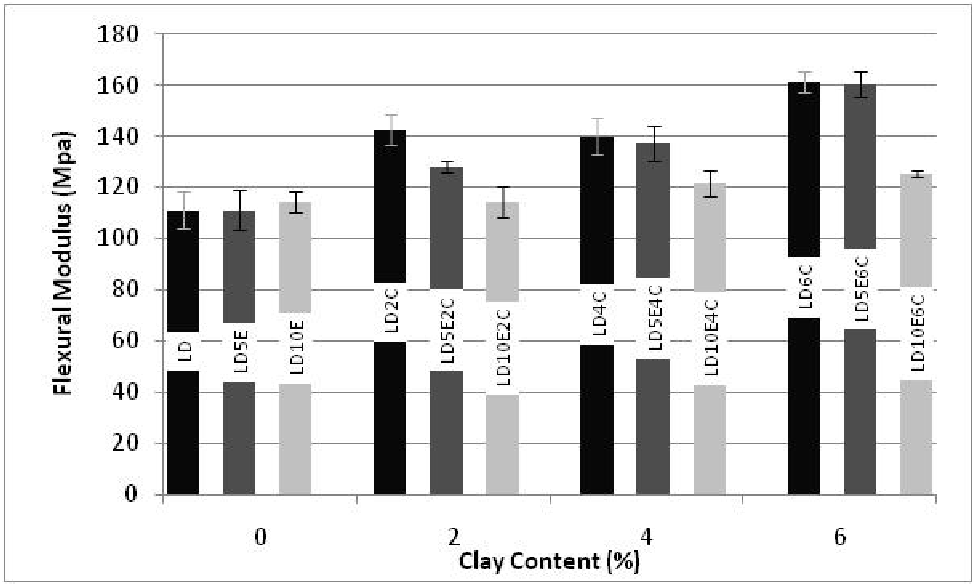

Figure 4.47 Flexural modulus values of LDPE nanocomposites

4.3.3 Impact Properties

The impact test results are presented in Appendix C, Table C.16 through C.18.

As the compatibilizer increases in binary systems, impact strength also increases, in fact Lotader® AX8900 (compatibilizer) is an impact modifier. The greatest increase is achieved at HDPE, 83% increase at 10% compatibilizer, however addition of clay decreases impact strength in HDPE nanocomposites, see Figure 4.48.

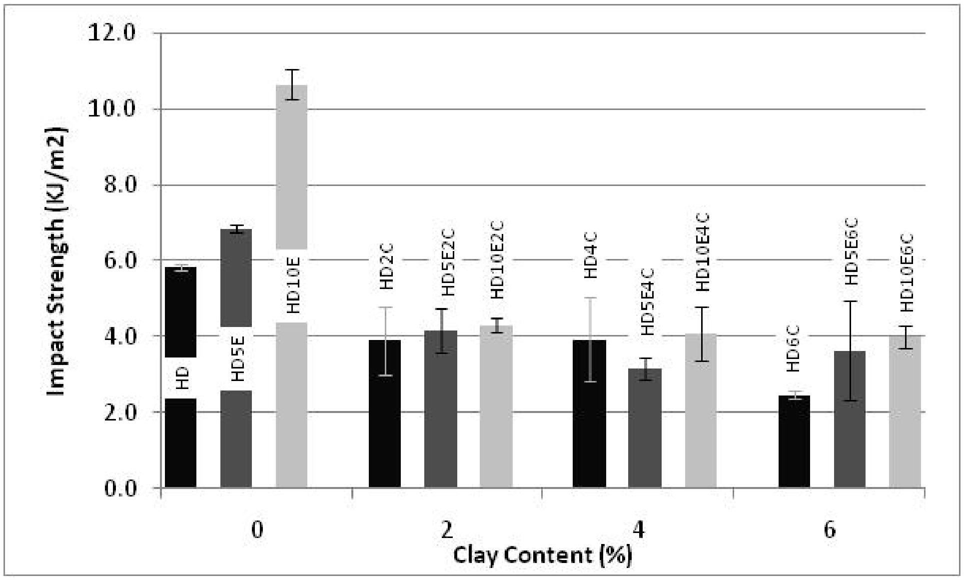

Figure 4.48 Impact strength values of HDPE nanocomposites

On the other hand, as the clay content increases above 2% in LLDPE and LDPE nanocomposites, impact strength decreases severely, as the undispersed tactoids and intercalants lead to poor interactions with the matrix. LDPE and LLDPE suffer more than HDPE from increasing clay content, see Figure 4.49 and Figure 4.50.

No ternary nanocomposite has higher impact strength than the neat polymers. Among the ternary nanocomposites for all the polyethylene grades, the materials with 10% compatibilizer, 2% organoclay shows the best performance. They also have the greatest increase in inter-laminar spacings as X-Ray tests show, which supports that they have the best organoclay dispersion among the samples.

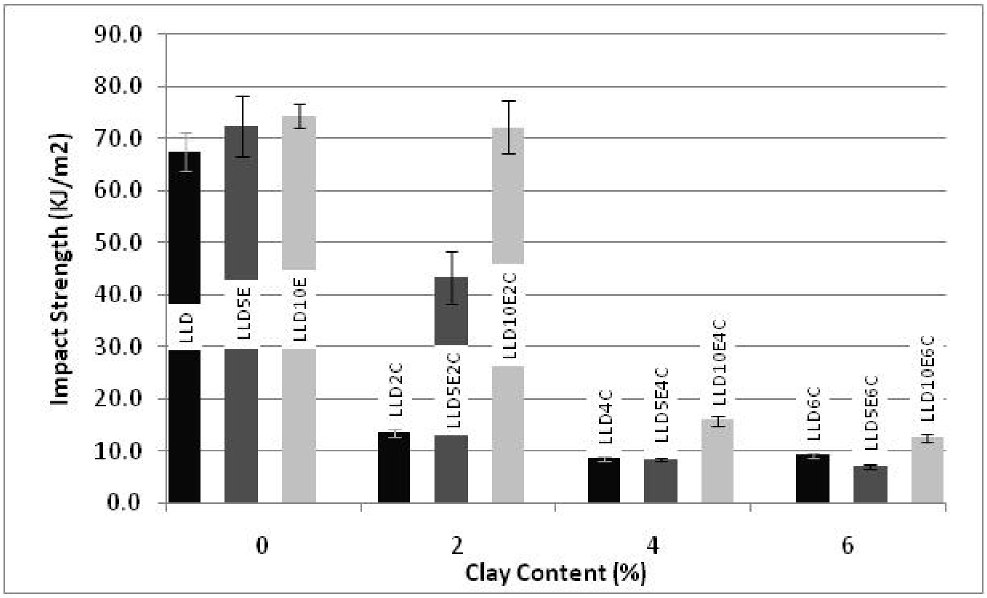

Figure 4.49 Impact strength values of LLDPE nanocomposites

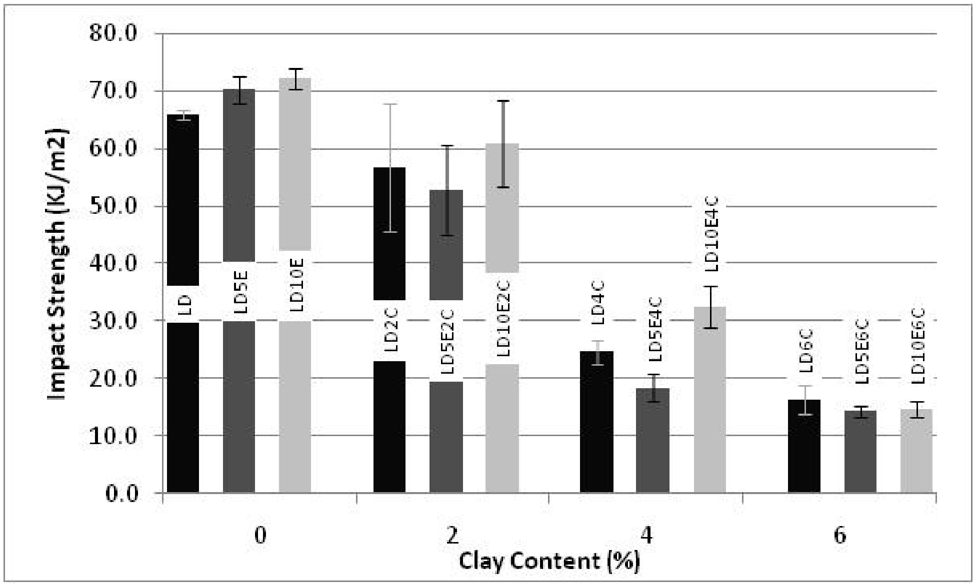

Figure 4.50 Impact strength values of LDPE nanocomposites

4.4 Flow Characteristics

MFI was performed on all the mixtures, to understand the flow properties, 2.16 kg weight was used at the temperature 190 ^{0}C and the results are presented in Table C.19.

Figure 4.51 through Figure 4.53 show the MFI values of HDPE, LLDPE and LDPE nanocomposites respectively.

Both clay and compatibilizer decrease MFI, thus increase the viscosity. The proposed mechanism is that compatibilizer promotes adhesion to the metals, so the blends stick the walls more [30], however clay reduces free volume, which prevents the flow [4]. As it is proposed, highest increase in viscosity is at 10% compatibilizer plus 6% clay content.

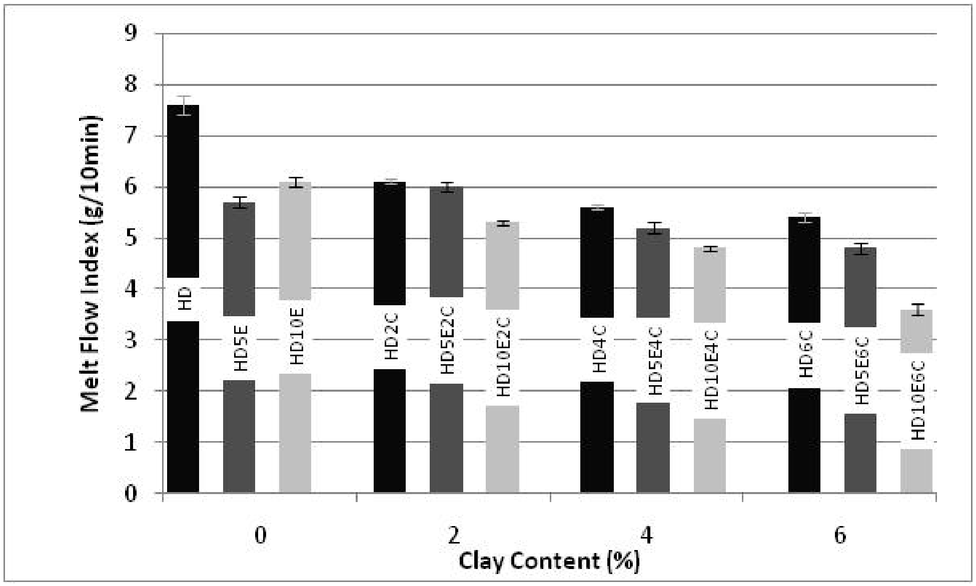

Figure 4.51 Melt flow index values of HDPE nanocomposites

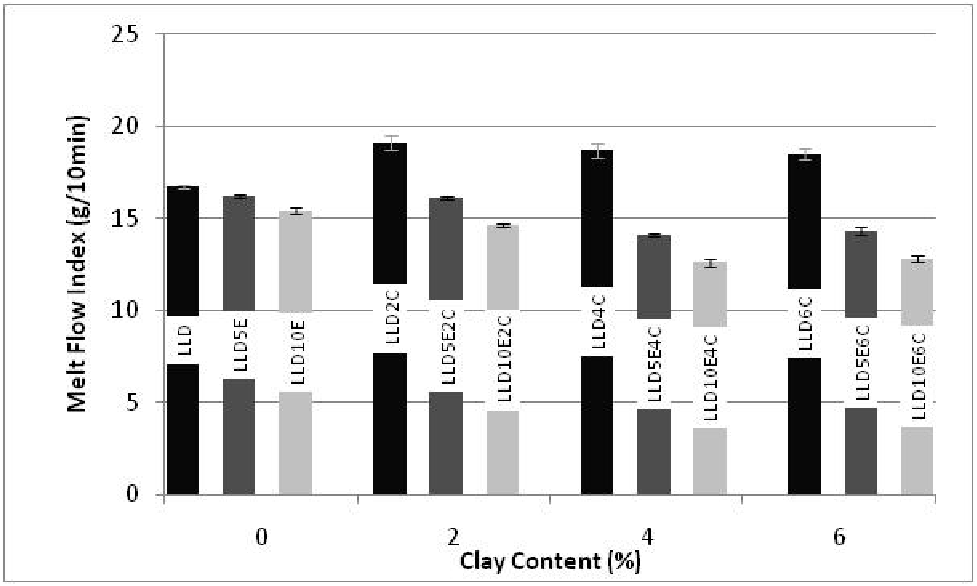

Figure 4.52 Melt flow index values of LLDPE nanocomposites

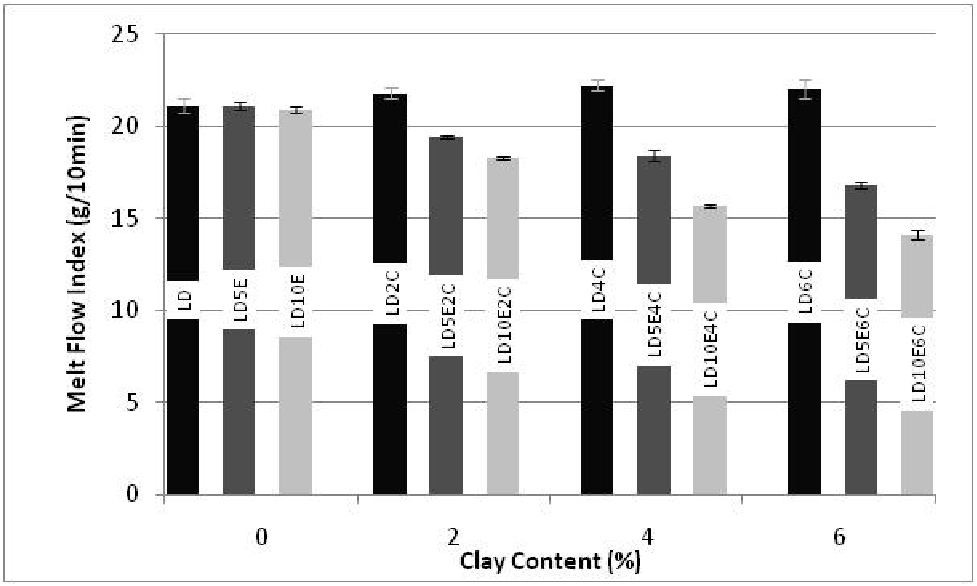

Figure 4.53 Melt flow index values of LDPE nanocomposites

CONCLUSIONS

Ternary nanocomposites of high density polyethylene, linear low density polyethylene and low density polyethylene were produced with organically modified montmorillonite clay and terpolymer of ethylene-methyl acrylate-glycidyl methacrylate as compatibilizer by means of melt compounding method. Effects of polyethylene type, organoclay and compatibilizer loading, on the morphology, rheology, thermal properties and mechanical properties were investigated.

According to X-ray diffraction patterns and SEM micrographs, in all ternary compositions intercalated structures were obtained, however no exfoliated nanocomposite was obtained.

For HDPE, 5% compatibilizer and 6% clay containing nanocomposite showed the highest yield stress, elastic modulus, flexural strength and flexural modulus; however the best impact strength results were obtained using 10% compatibilizer and 2% clay.

For LLDPE, 5% compatibilizer and 6% clay showed the highest yield stress, elastic modulus, strain at break, and flexural strength and modulus values; however the highest tensile and impact strength results were obtained using 10% compatibilizer and 2% clay.

For LDPE, 5% compatibilizer and 4% clay showed the highest yield stress, elastic modulus, tensile stress, however highest strain at break and impact strength results were obtained using 10% compatibilizer and 2% clay.

At higher clay loadings, high yield stress, elastic modulus, flexural strength, flexural modulus were obtained; however, poor impact strength, stress at break and strain at break values were observed. These results were obtained since clay could not be dispersed sufficiently at higher weight fractions and started to agglomerate causing early failure.

While investigating the effect of polyethylene type on the nanocomposite morphology, it was observed that only with high density polyethylene, intercalated nanocomposite was obtained without the use of compatibilizer. As HDPE has very few branches, it can enter into clay galleries easier. X-ray diffraction patterns showed, lowering of peaks and shifting of the first and second peaks to lower angles indicating intercalated structure. On the other hand, in binary clay/LDPE or LLDPE nanocomposites, decrease in basal spacing was observed. The reason for the collapse of clay galleries are thermal degradation and/or high pressure applied during the injection molding.

DSC data indicate that, T_m did not change, on the other hand percent crystallinity did. It is observed that organoclay used had no nucleation effect on polyethylene and compatibilizer decreased the crystallinity slightly.

According to MFI measurements, addition of clay increases viscosity by reducing the free volume. At the same clay content, compatibilizer increases dispersion and interaction of the clay and polymer, resulting in higher viscosity.

REFERENCES

1. Akovali G., “Handbook of Composite Fabrication”, Rapra Technology, Shawbury, UK, 2001.
2. Ajayan P. M., Schadler L. S. and Braun P. V., “Nanocomposite Science and Technology”, Wiley-VCH, Weinheim, Germany, 2003.
3. Okamoto M., ”Polymer/Layered Silicate Nanocomposites”, Rapra Review Reports, vol.14 no.7, 2003.
4. Utracki L. A., “Clay-Containing Polymeric Nanocomposites”, Shawbury, UK, 2004.
5. Vasile C. and Pascu M., ”Practical Guide to Polyethylene”, Rapra Technology Ltd., Shawbury, UK 2005.
6. Wing M. Y. and Zhong-Zhen Y., ‘’Polymer Nanocomposites’’, Woodhead Publishing and Maney Publishing, Cambridge, UK, 2006.
7. Lubin G., ‘’Handbook of Composites’’ , Van Nostrand Reinhold Company Ltd., New York, USA, 1969.
8. Wetzel B., Haupert F., Friedrich K., Zhang M.Q., Rong M. Z., “Mechanical and tribological properties of microparticulate and nanoparticulate reinforced polymer composites”, Proc. 13th ICCM, Beijing, 1021, 2001.
9. Klaus F., Stoyko F., Zhong Z., ”Polymer composites : from nano-to-macro-scale”, Springer, New York, USA, 2005.
10. Kissin Y.V., Kirk-Othmer Encycl. Chem. Technol. Vol. 17, Wiley Interscience, 724, 1996.
11. Beach D. L. and Kissin Y.V., Encycl. Polym. Sci. Eng., Wiley Interscience, vol 6, 454,1986.
12. Schutt J. H., Plast. World , vol. 55(1), 8, 1997.
13. Heinemann J., Reichert P., Thomann R. and Mhulhaupt R., ”Macromol Rapid Commun”, 20, p. 423, 1999.
14. Bergman J. S., Chen H., Giannelis E. P., Thomas M. G. and Coates T. G., “Chem Commun” , p. 2179, 1999.

15. Alexandre M., Dubois P., Sun T., Garces J. M. and Jerome R., Polymer, 43 p. 2123, 2002.
16. Kurokawa Y., Yasuda H. and Oya A., J Mater Sci Lett,15 p. 1481, 1996.
17. Fischer H. R., Gielgens L. H. and Koster T. P. M., *Acta Polym*,50 , p. 122, 1999.
18. The Dow Chemical Company, http://www.dow.com, fast accessed April 2007.
19. Middleman S., "Fundemantals of Polymer Processing", McGraw-Hill, New York, USA, 1977.
20. Simon G. P., "Polymer Characterization Techniques and Their Application to Blends", Oxford University Press, New York, USA, 2003.
21. Rauwendaal C., "Polymer Extrusion", Hanser Publishers, Munich, Germany, 1994.
22. Rubin I. I., "Injection Molding Theory and Practice", Wiley-Interscience, New York, USA ,1972.
23. Billmeyer F., "Text Book of Polymer Science", John Wiley & Sons, New York, USA, 1984.
24. Morgan J. G., Journal of Applied Polymer Science ., vol. 87, 1329-1338, 2003.
25. Schmitz J. V., "Testing of Polymers", Interscience Publishers, New York, 1965.
26. Alyamaç E., "Impact Modified Poly(ethylene-terephtalate)- Organoclay Nanocomposites", M.Sc. Thesis, Middle East Technical University, Ankara, Turkey, 2004.
27. Hunt B. J. and James M. I., "Polymer Characterisation", Blackie Academic & Professional, Glasgow, UK, 1993.
28. Boersma S. L., J. Amer. Ceramic Soc., vol. 38, 281, 1955.
29. Simonds H. R. and Weith A.J., "Extrusion of Plastics, Rubber and Metals", Reinhold Publishing, New York, USA, 1952.
30. Işık F., "Nanocomposites Based on Blends of Polyethylene", M.Sc. Thesis, Middle East Technical University, Ankara, Turkey, 2005.
31. Vaia R. A., Ishii, H., Giannelis E. P., Chemistry of Materials, vol. 5, 1694-1696, 1993.
32. Wang K. H., Choi M. H., Koo C. M., Choi Y.S., Chung I. J., Polymer, vol.42,9819-9826, 2001.

33. Southern Clay Products, http://nanoclay.com/publications.asp; fast accessed April 2007.
34. Kato M., Okamoto H., Hasegawa N., Tsukigase A. and Usuki A., Polymer Engineering and Science, vol.43 No.6, 1312-1316, 2003.
35. Liang G., Xu J., Bao S., Xu W., Journal of Applied Polymer Science, vol.91, 3974-3980, 2004.
36. Hotta S., Paul D.R., Polymer, vol.45 No.22, 7639-7654, 2004.
37. Wunderlich B., "Thermal Analysis of Polymeric Materials", Springer, Berlin, Germany 2005.
38. ASTM D638-91a, Standard Test Method for Tensile Properties of Plastics, "Annual Book of ASTM Standards", vol.8 No.1, 174-182, Philadelphia, USA, 1993.
39. Walter R., Friedrich K., Privalko V., Savadori A., J.Adhesion ,64, 87, 1997.
40. Arkema Company, http://lotader.com, fast accessed May 2007.
41. "Kirk-Othmer Encyclopedia of Chemical Technology", 4th Edition, vol. 24, 71-117, John Wiley and Sons, New York, USA,1993.
42. Vaia R.A., Jandt K.D., Kramer E.J., and Giannelis E.P., Chem.Mater.,Vol. 8 No.11, 2628, 1996.

APPENDICES

A. X-Ray Analysis

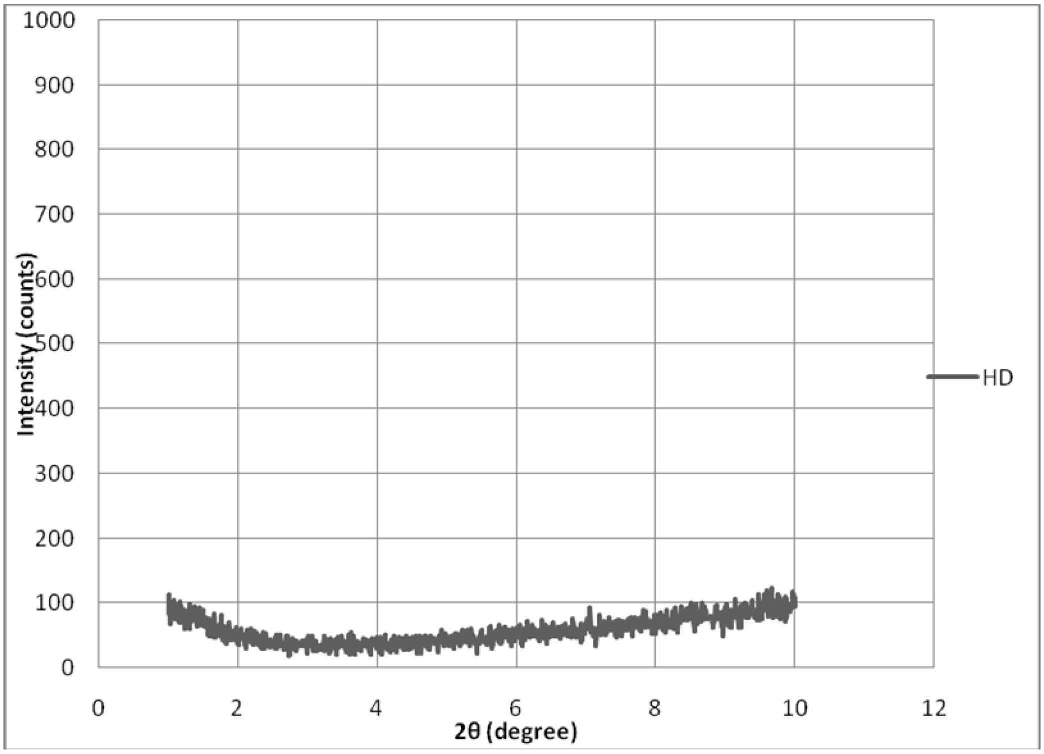

Figure A.1 X-Ray diffraction pattern of HDPE

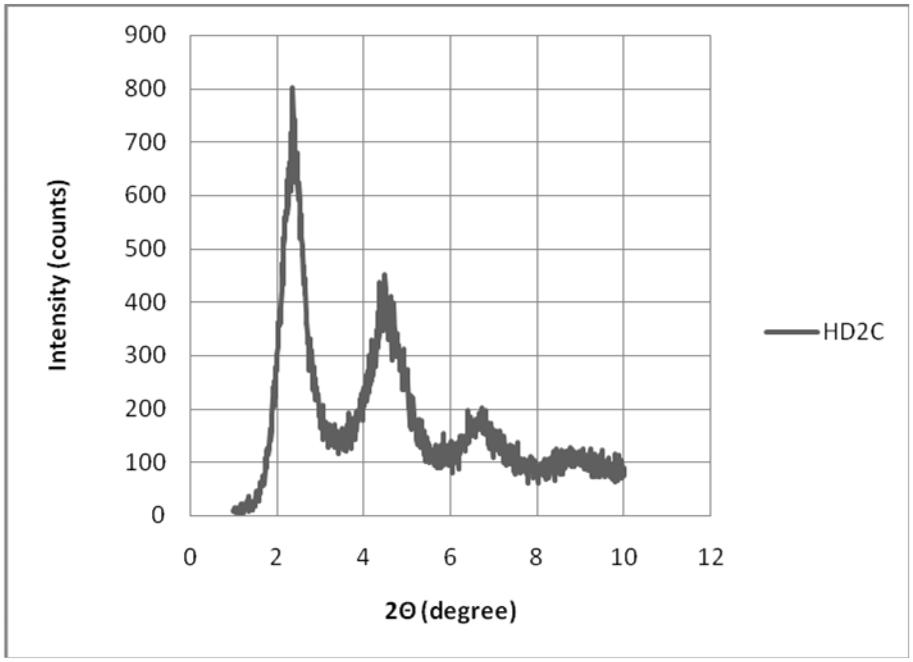

Figure A.2 X-Ray diffraction pattern of nanocomposite HD2C

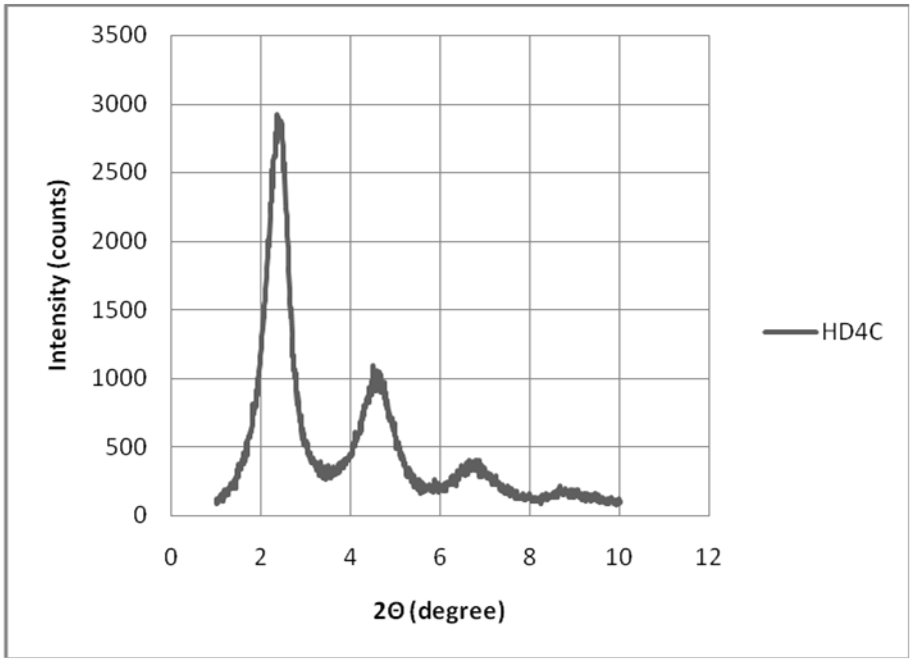

Figure A.3 X-Ray diffraction pattern of nanocomposite HD4C

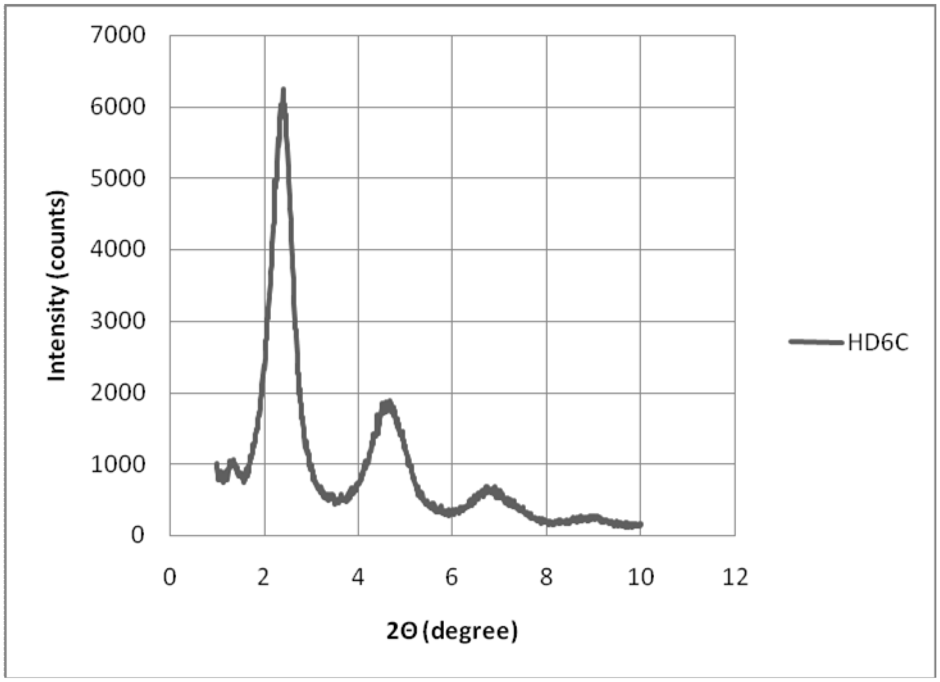

Figure A.4 X-Ray diffraction pattern of nanocomposite HD6C

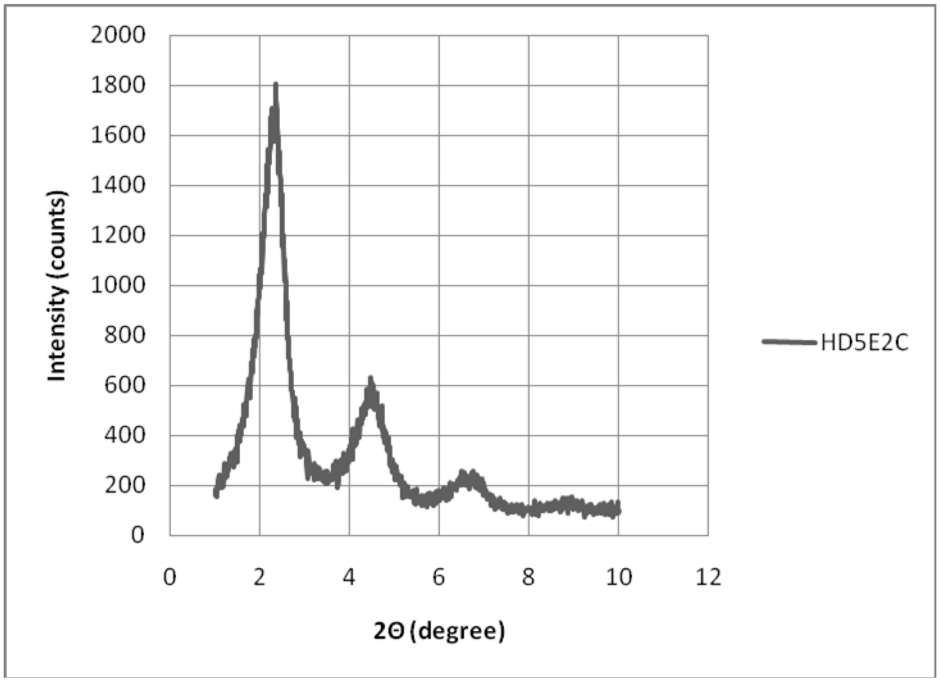

Figure A.5 X-Ray diffraction pattern of nanocomposite HD5E2C

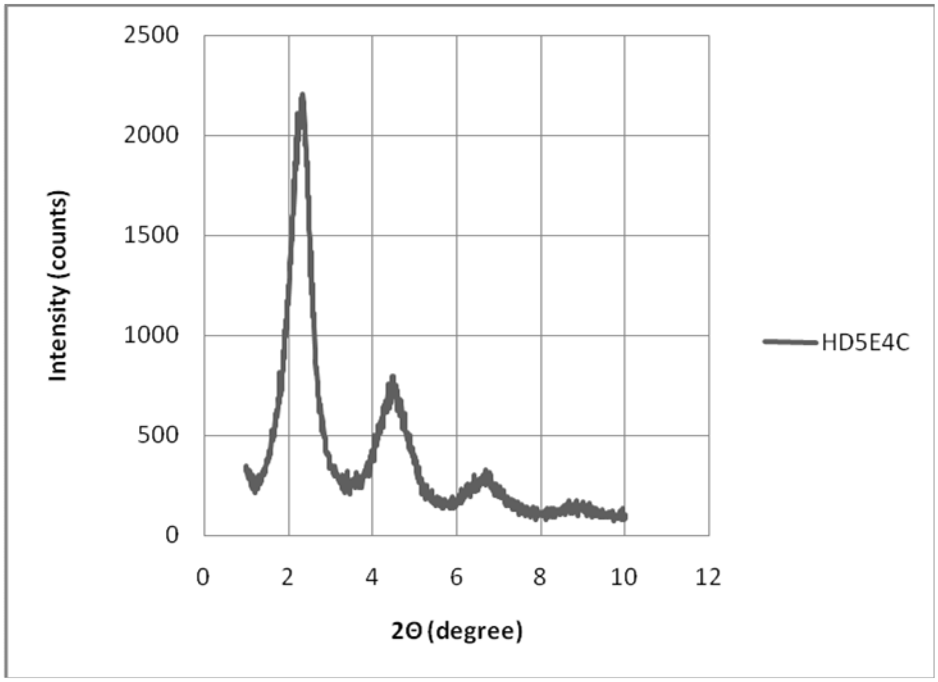

Figure A.6 X-Ray diffraction pattern of nanocomposite HD5E4C

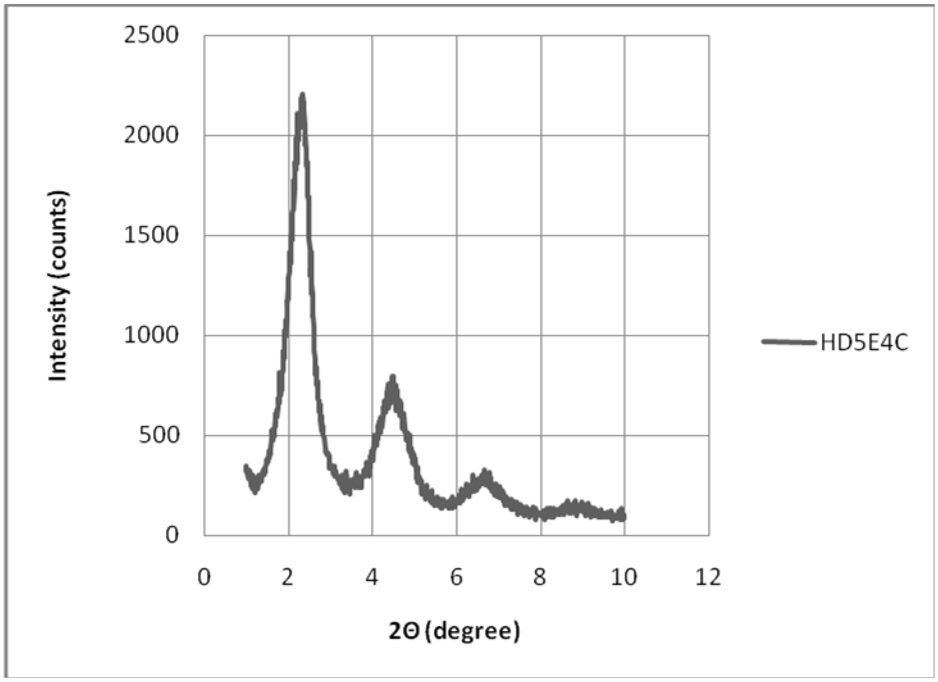

Figure A.7 X-Ray diffraction pattern of nanocomposite HD5E4C

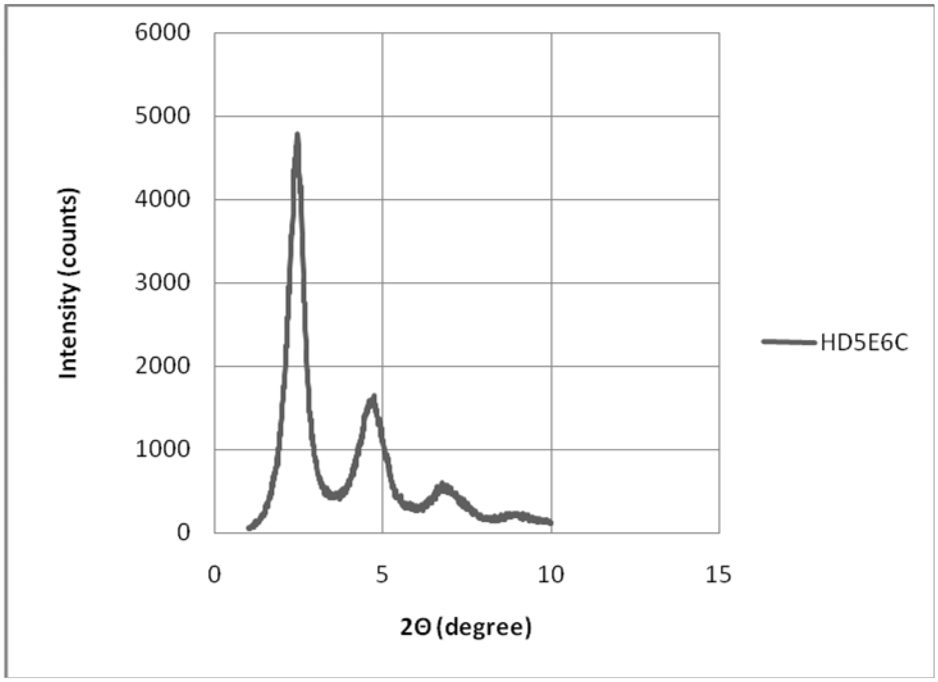

Figure A.8 X-Ray diffraction pattern of nanocomposite HD5E6C

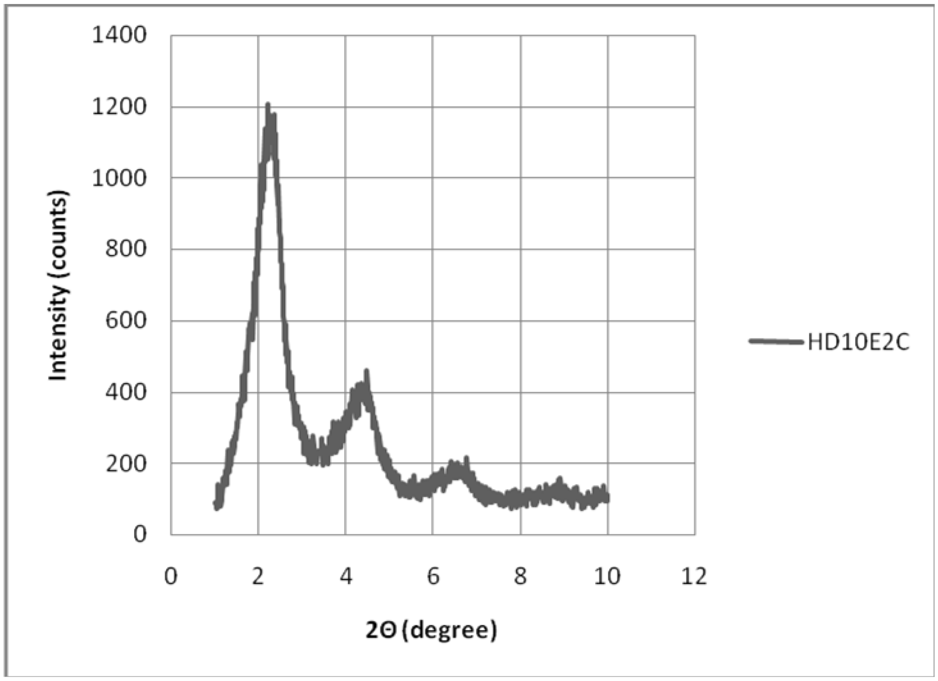

Figure A.9 X-Ray diffraction pattern of nanocomposite HD10E2C

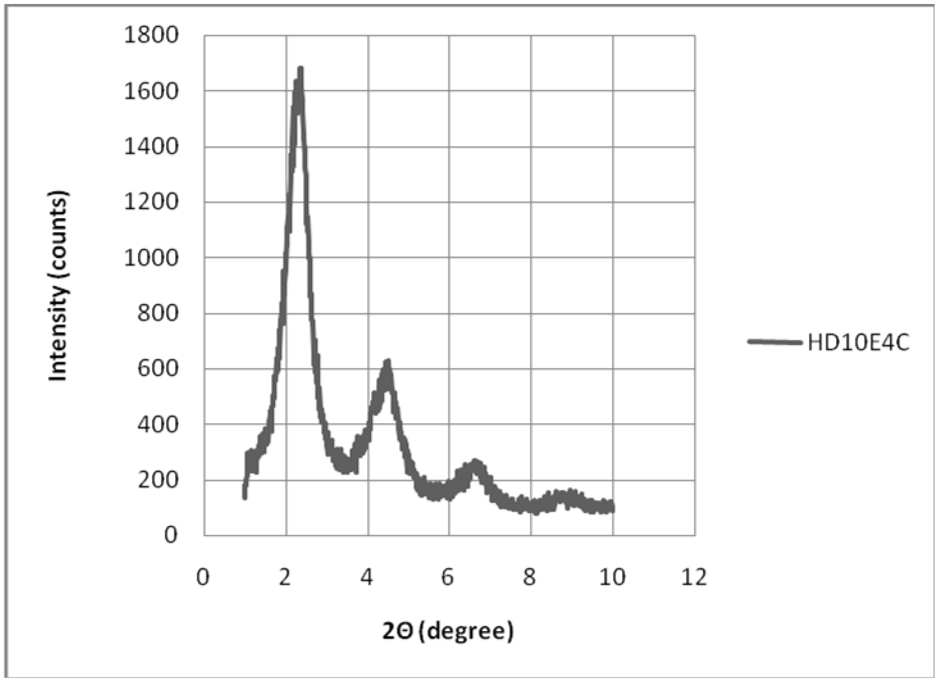

Figure A.10 X-Ray diffraction pattern of nanocomposite HD10E4C

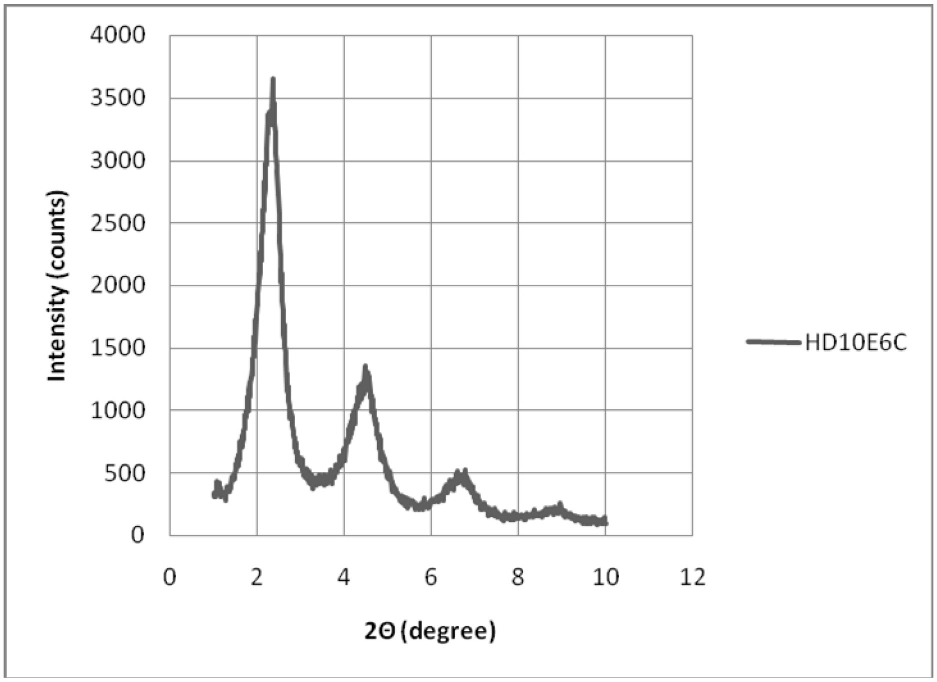

Figure A.11 X-Ray diffraction pattern of nanocomposite HD10E6C

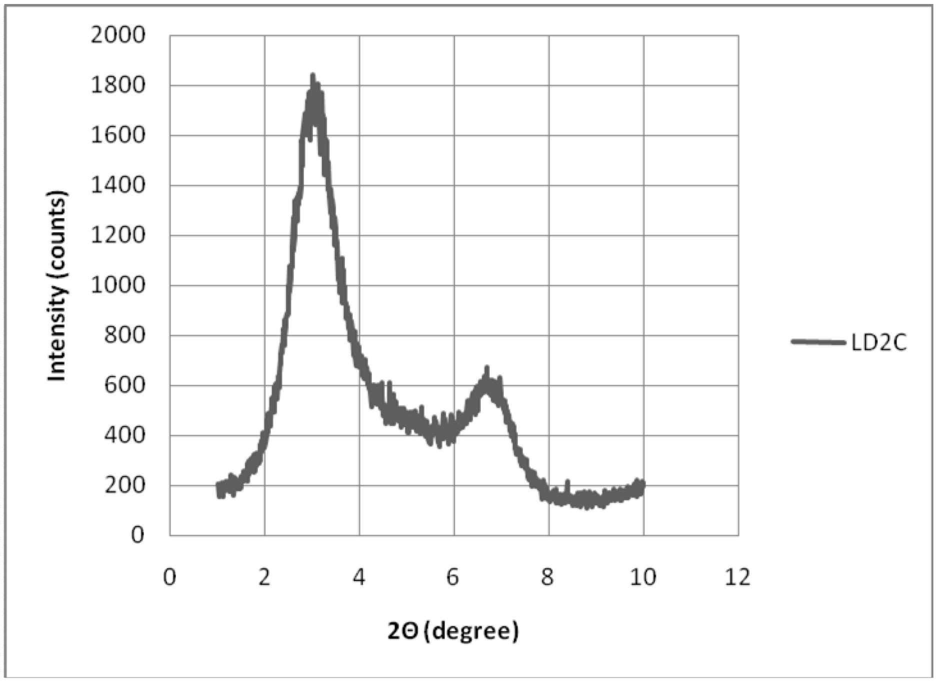

Figure A.12 X-Ray diffraction pattern of nanocomposite LD2C

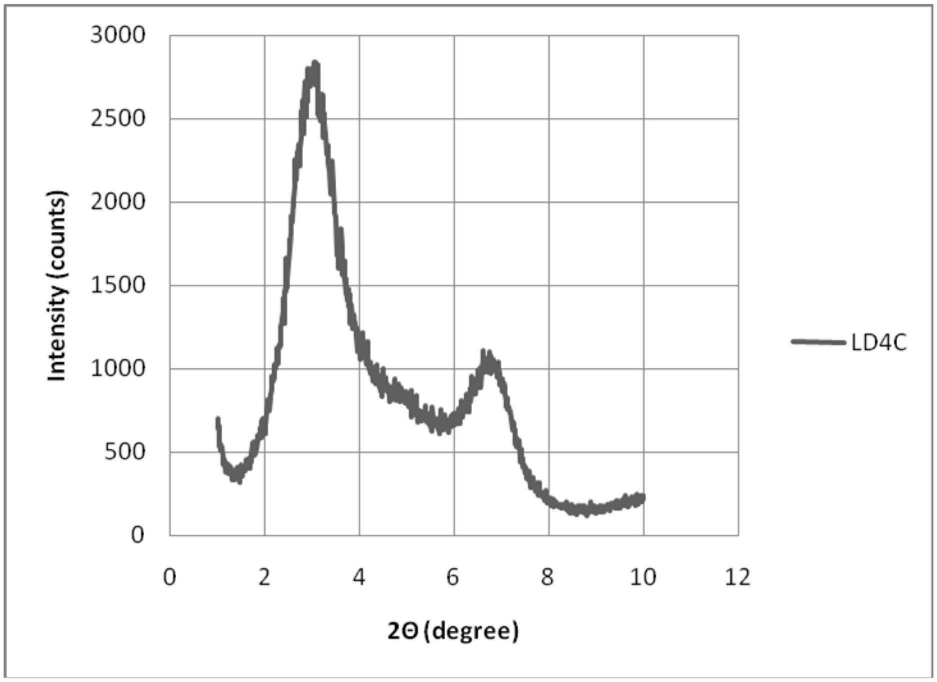

Figure A.13 X-Ray diffraction pattern of nanocomposite LD4C

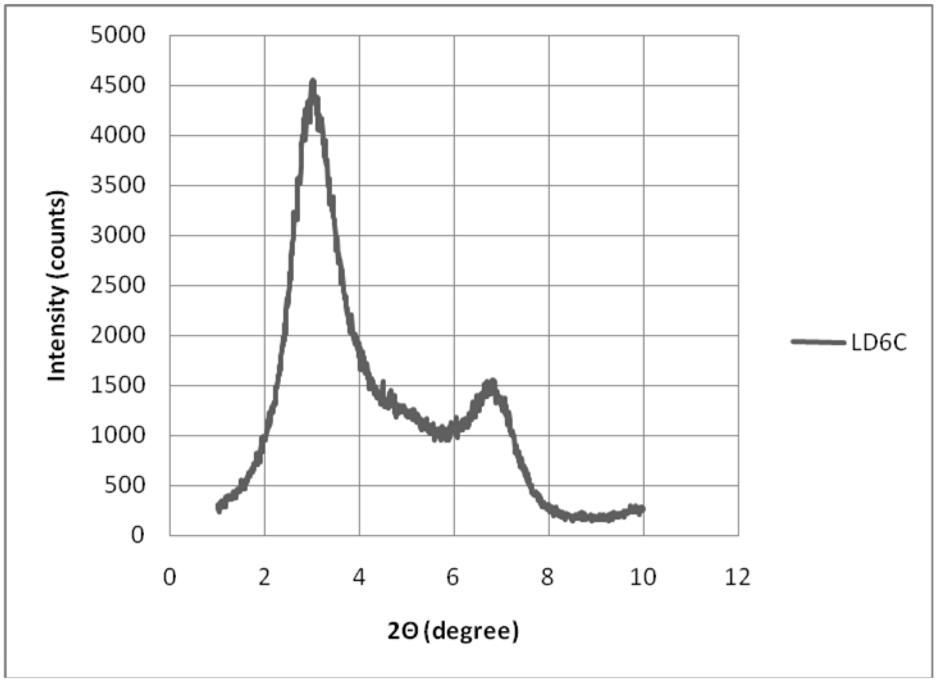

Figure A.14 X-Ray diffraction pattern of nanocomposite LD6C

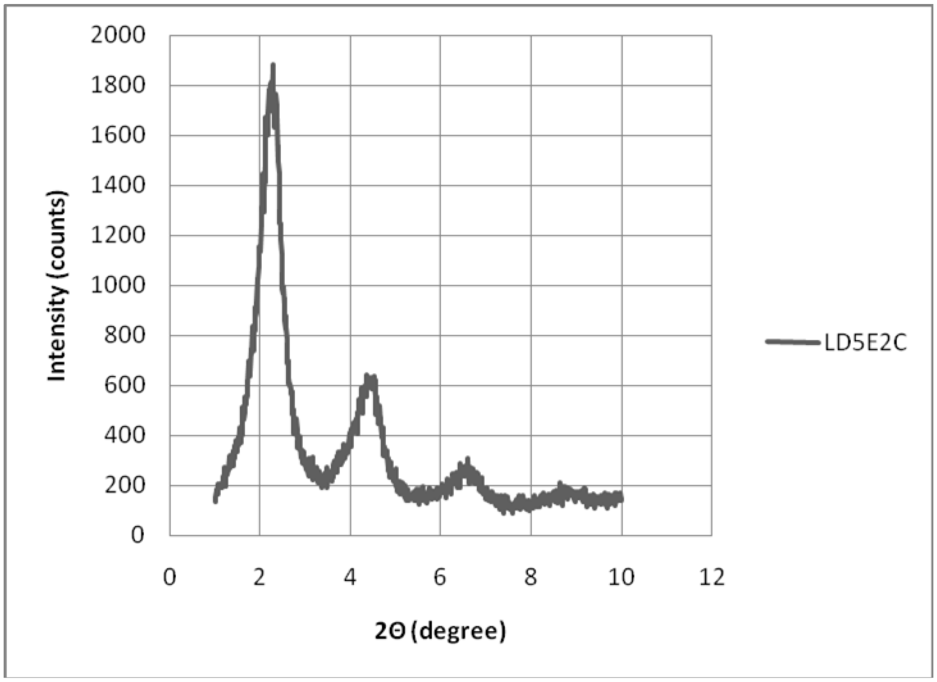

Figure A.15 X-Ray diffraction pattern of nanocomposite LD5E2C

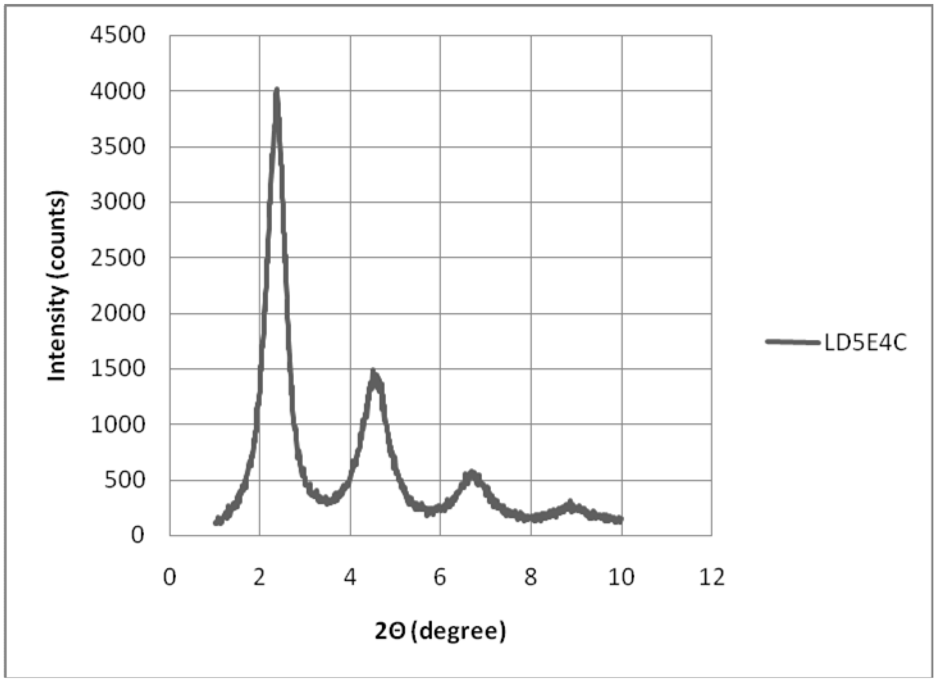

Figure A.16 X-Ray diffraction pattern of nanocomposite LD5E4C

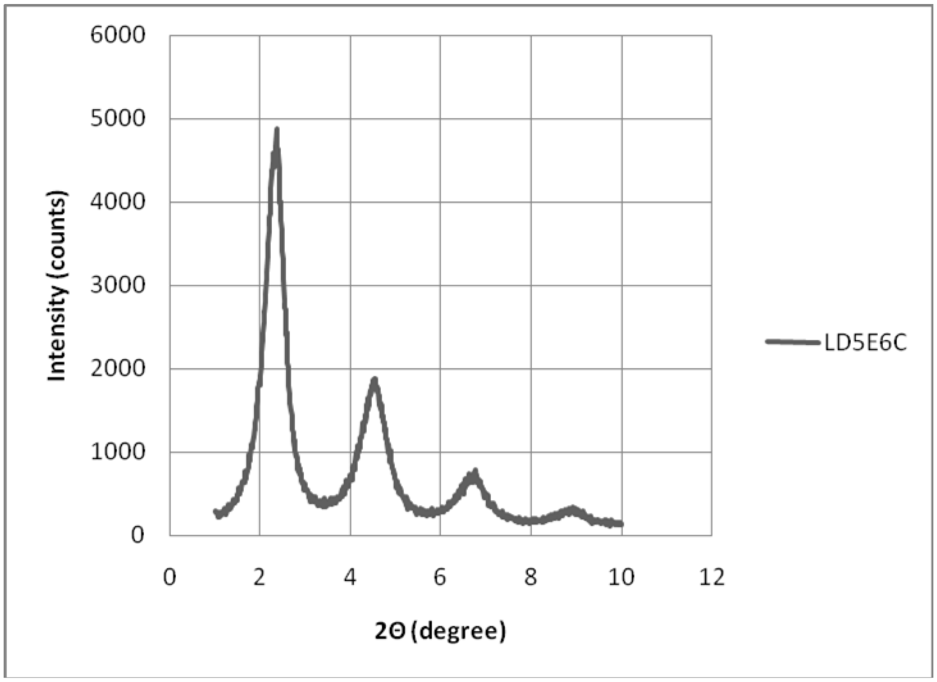

Figure A.17 X-Ray diffraction pattern of nanocomposite LD5E6C

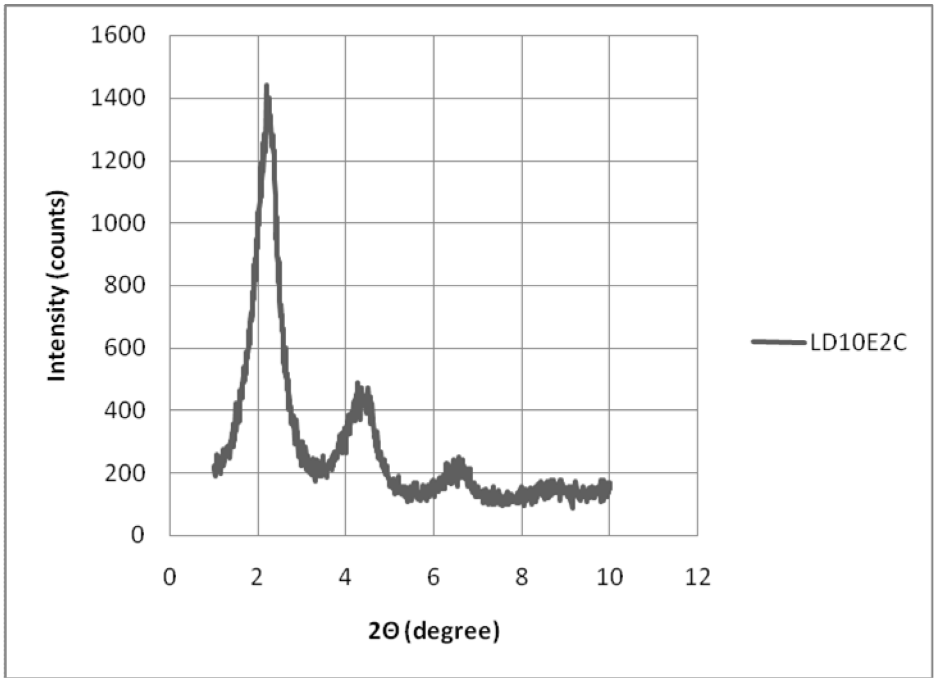

Figure A.18 X-Ray diffraction pattern of nanocomposite LD10E2C

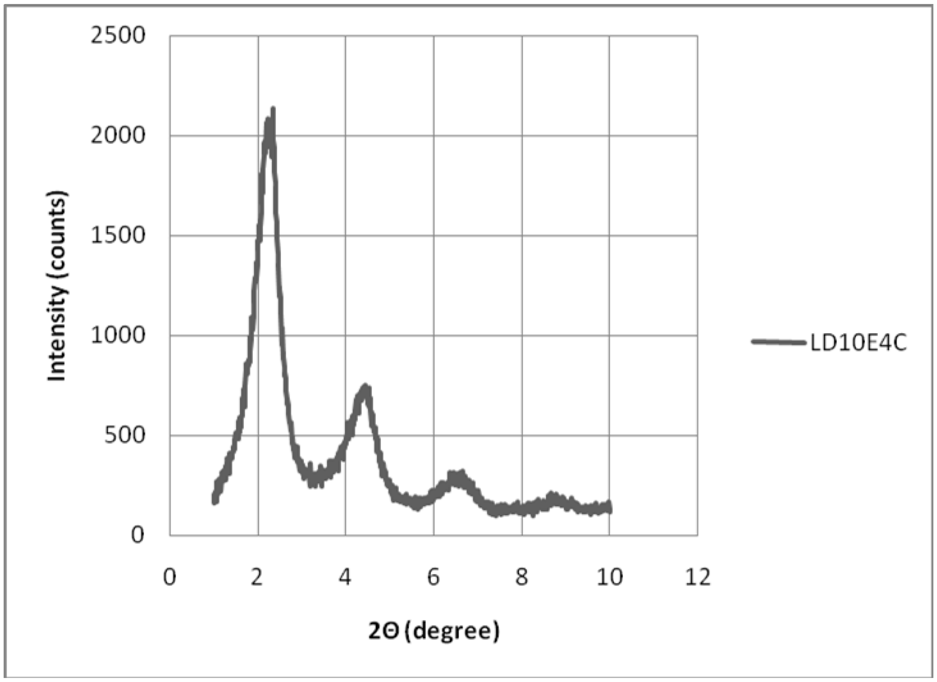

Figure A.19 X-Ray diffraction pattern of nanocomposite LD10E4C

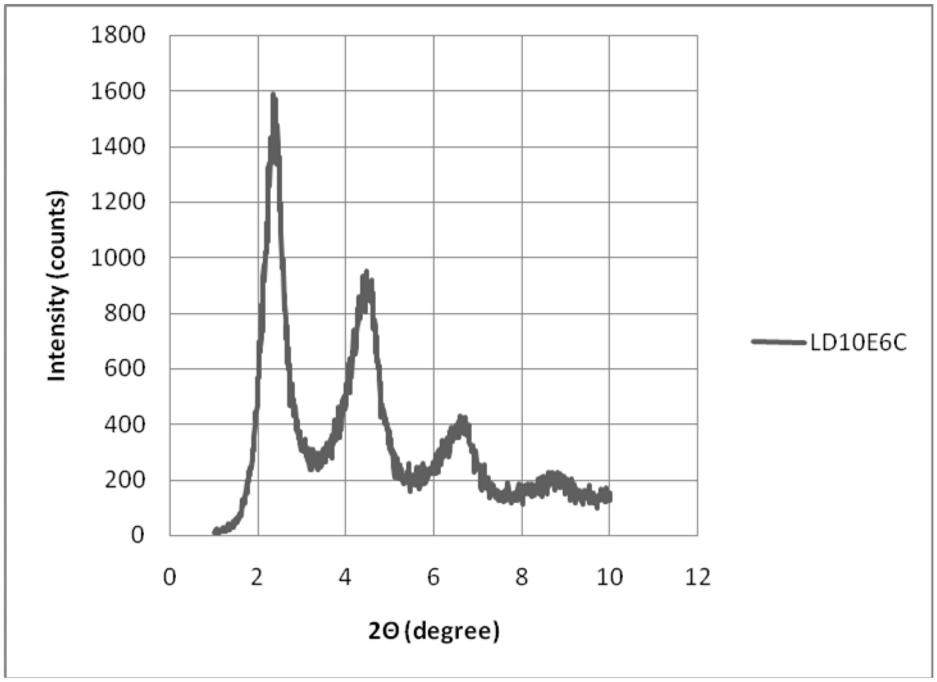

Figure A.20 X-Ray diffraction pattern of nanocomposite LD10E6C

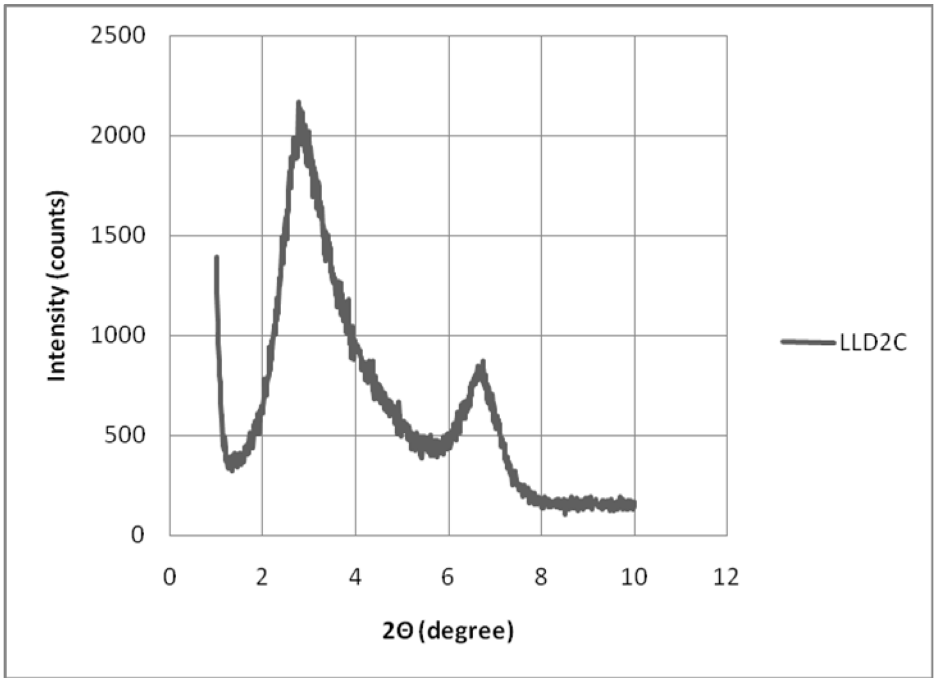

Figure A.21 X-Ray diffraction pattern of nanocomposite LLD2C

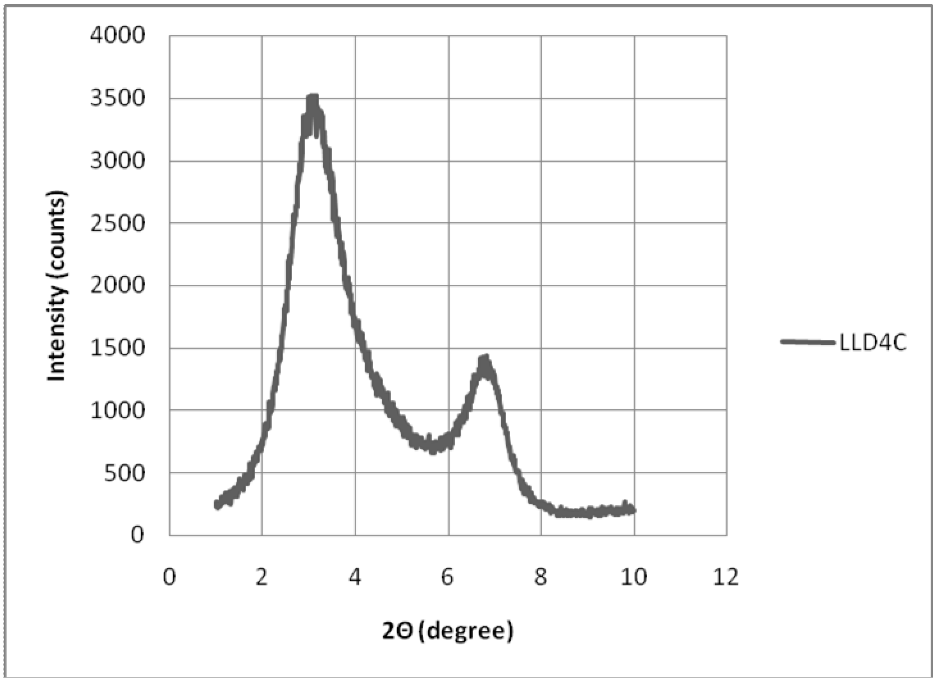

Figure A.22 X-Ray diffraction pattern of nanocomposite LLD4C

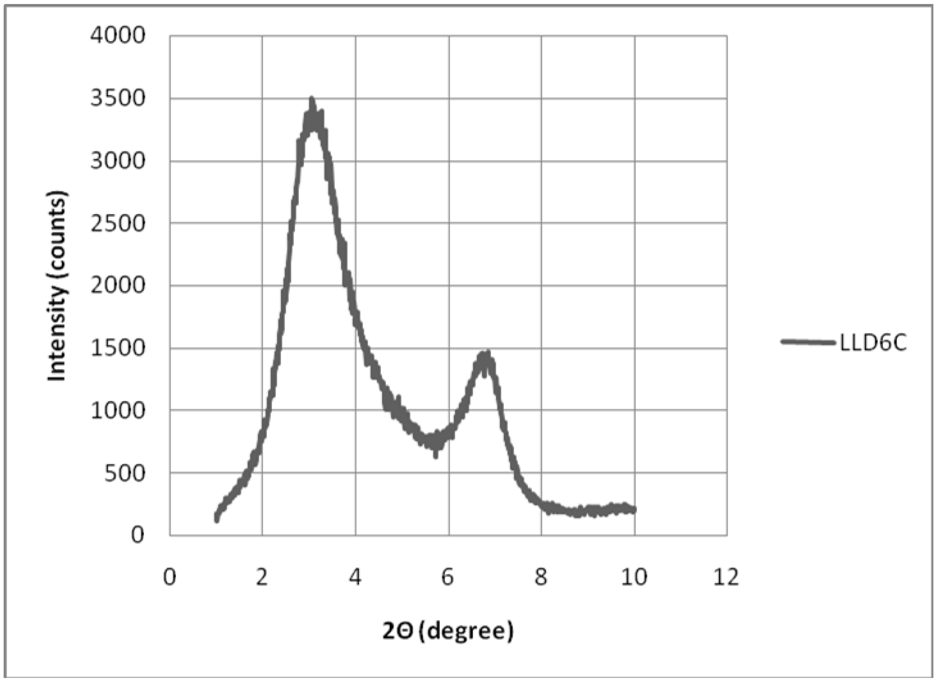

Figure A.23 X-Ray diffraction pattern of nanocomposite LLD6C

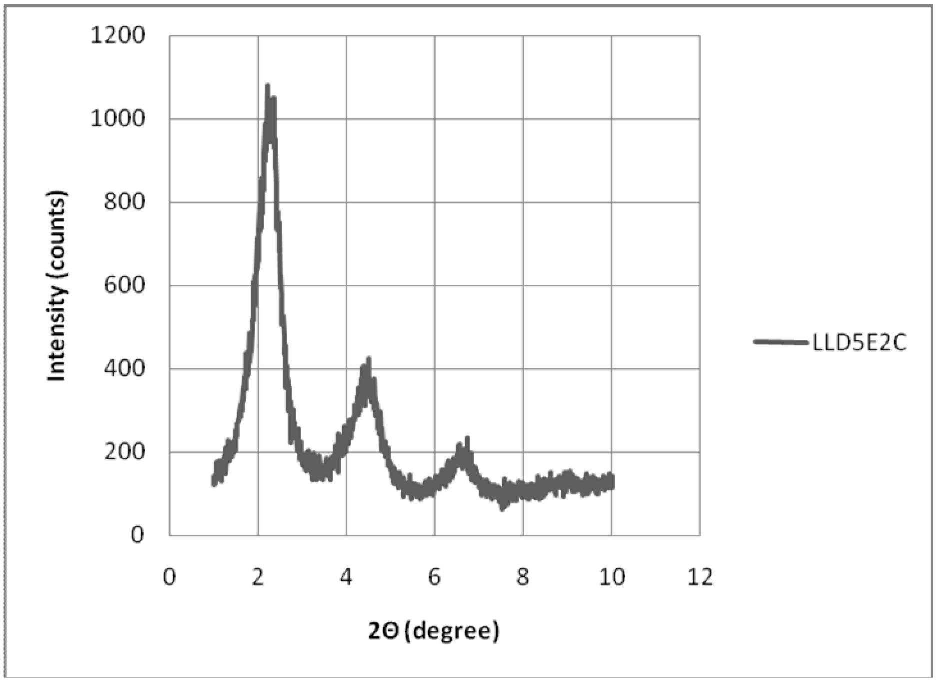

Figure A.24 X-Ray diffraction pattern of nanocomposite LLD5E2C

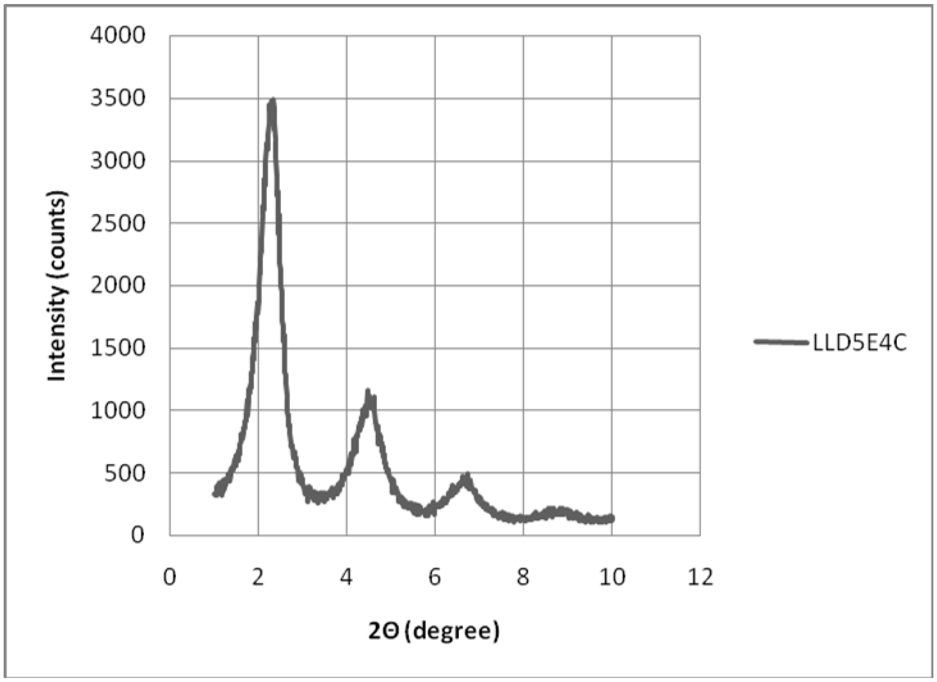

Figure A.25 X-Ray diffraction pattern of nanocomposite LLD5E4C

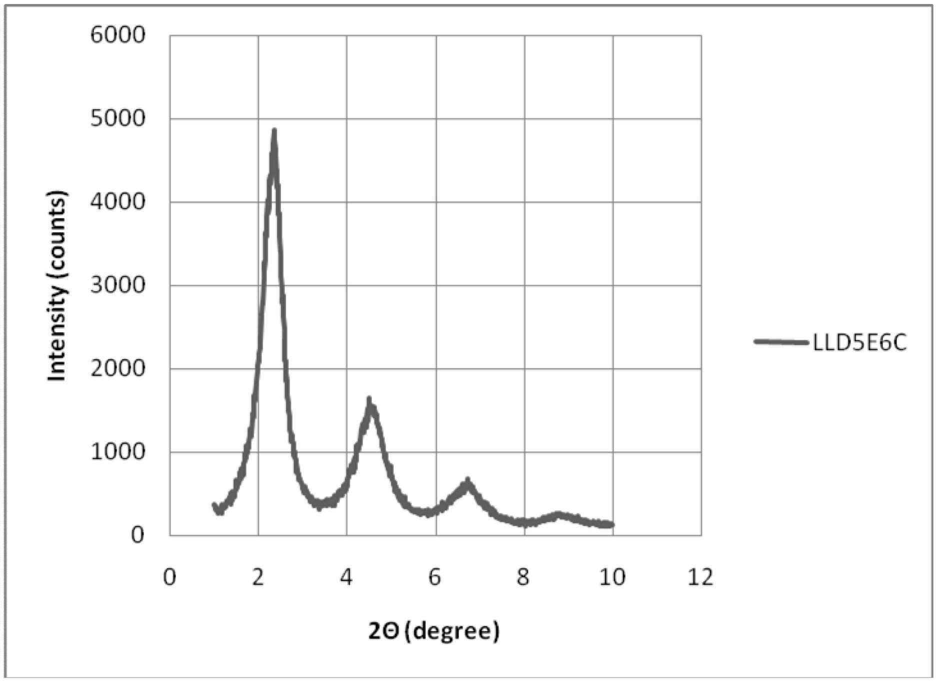

Figure A.26 X-Ray diffraction pattern of nanocomposite LLD5E6C

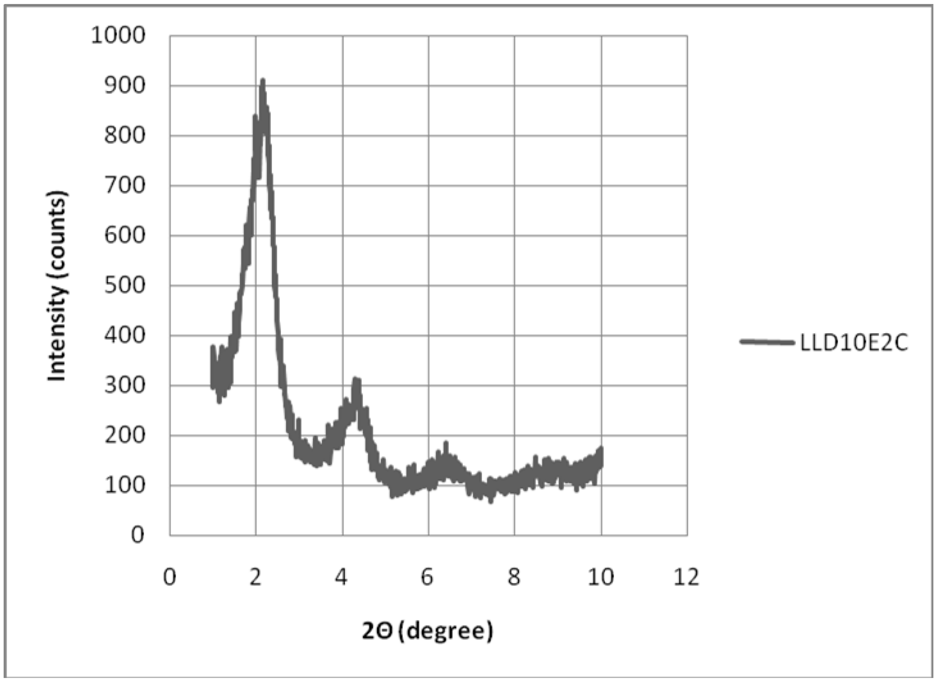

Figure A.27 X-Ray diffraction pattern of nanocomposite LLD10E2C

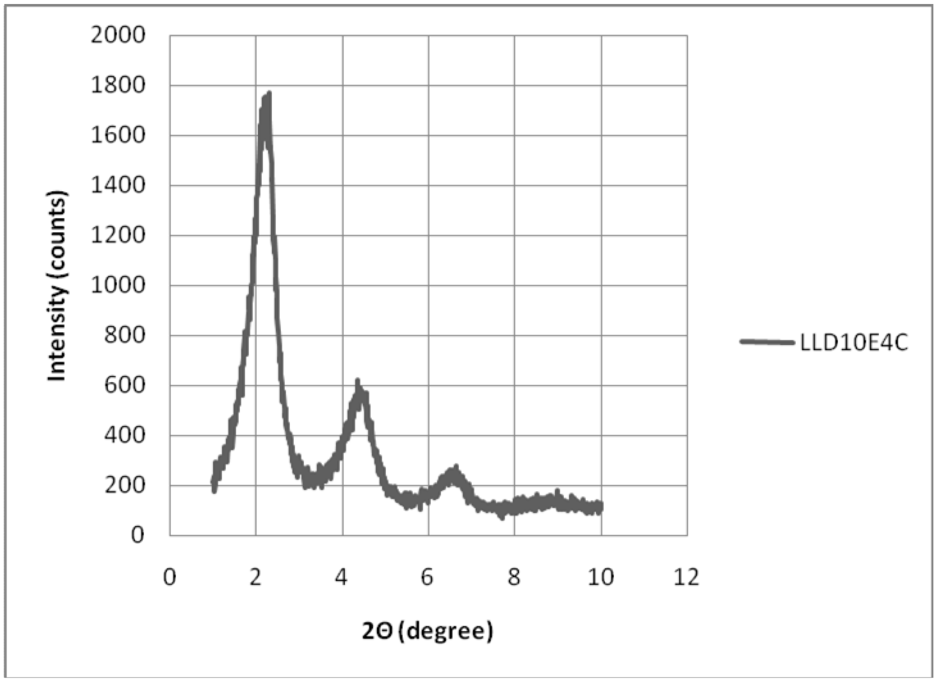

Figure A.28 X-Ray diffraction pattern of nanocomposite LLD10E4C

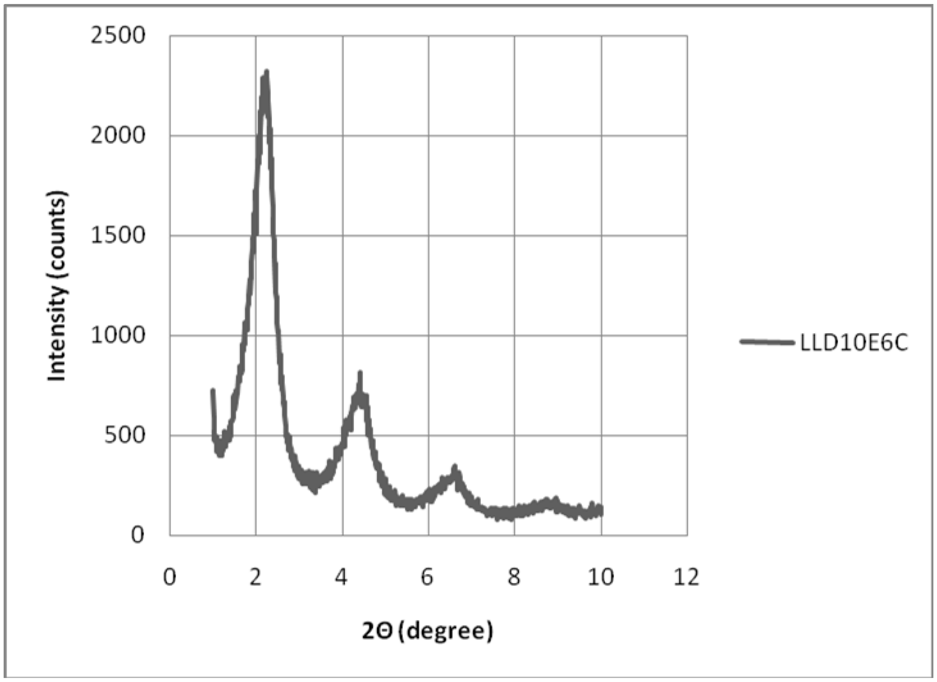

Figure A.29 X-Ray diffraction pattern of nanocomposite LLD10E6C

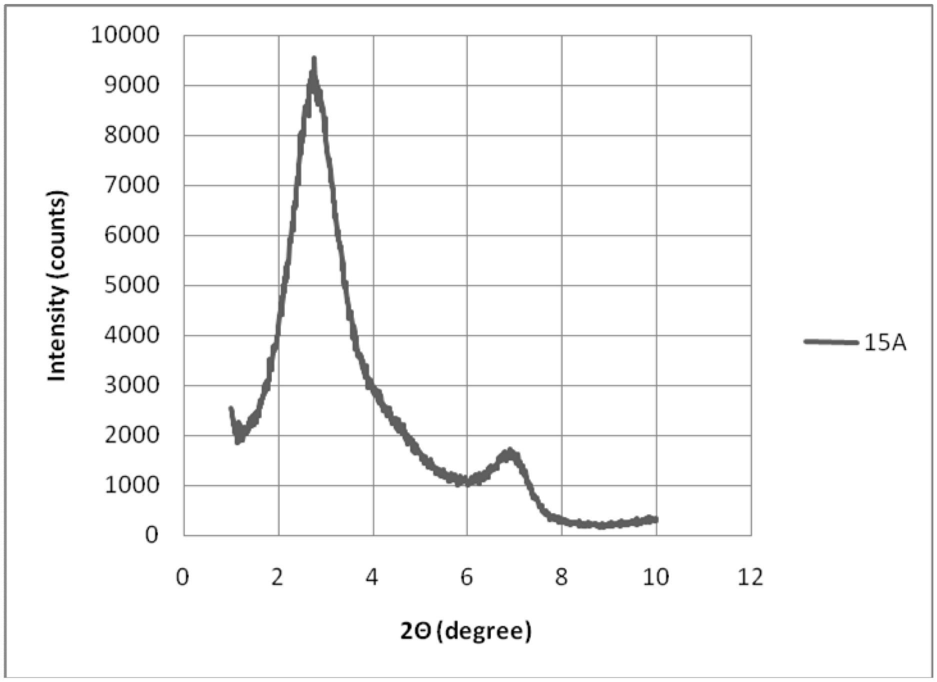

Figure A.30 X-Ray diffraction pattern of Organoclay Cloisite 15A

B. DSC Analysis

HD1

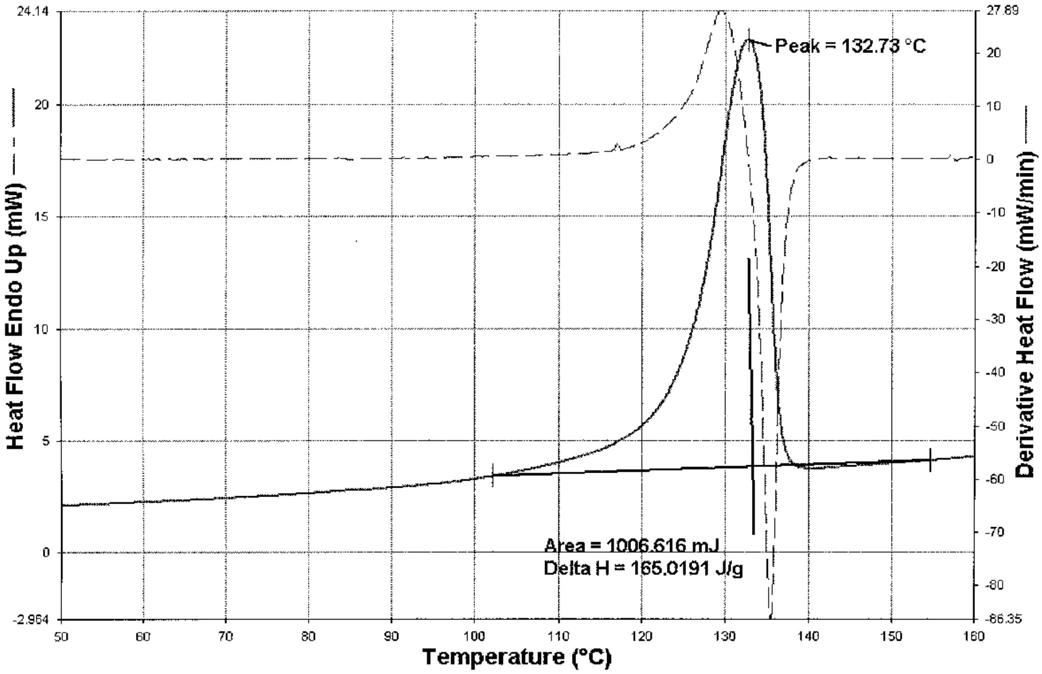

HD2

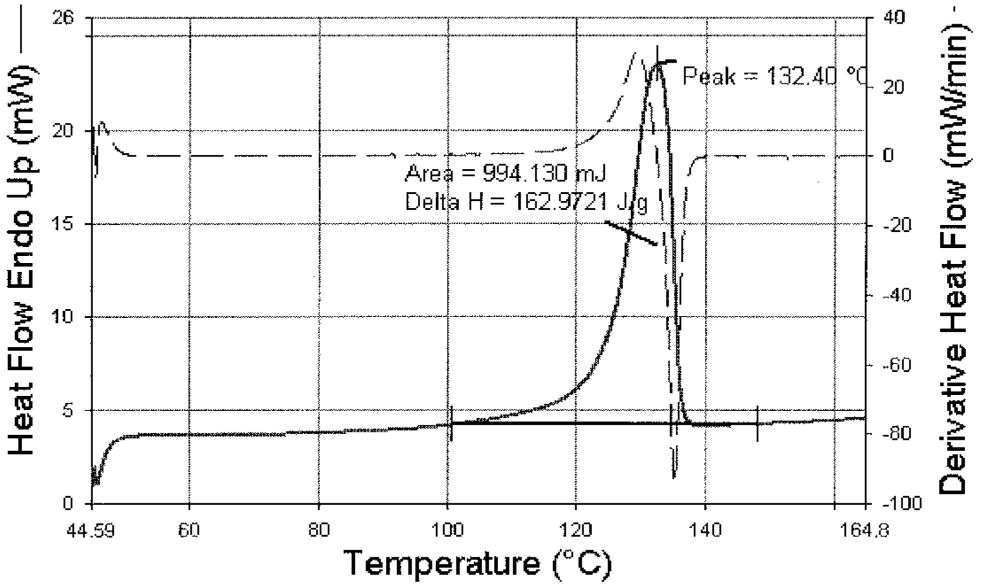

Figure B.1 DSC thermogram of HD (HD1) and HD5E (HD2)

HD3

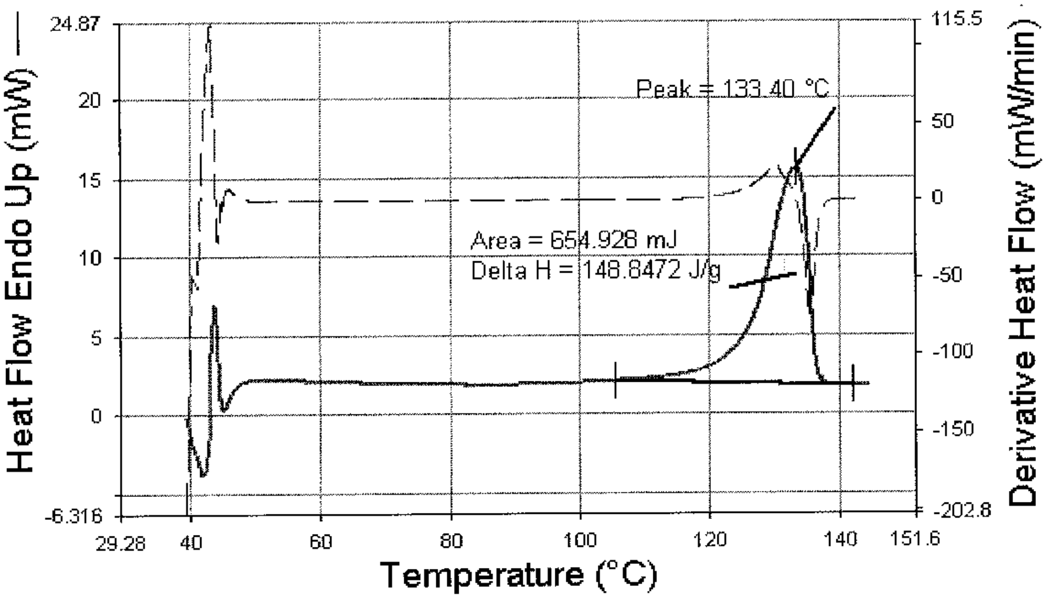

HD4

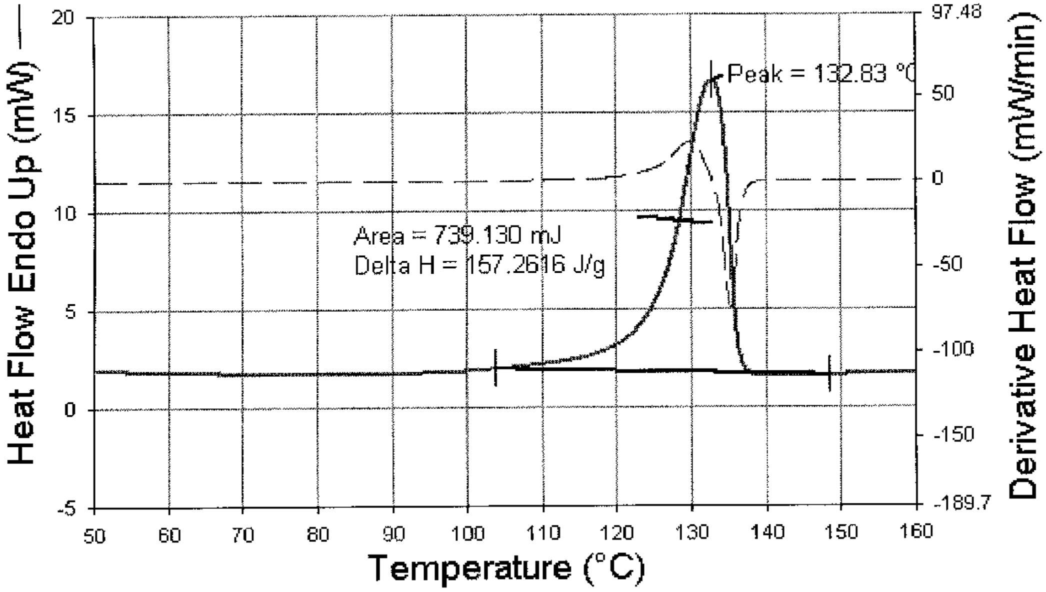

Figure B.2 DSC thermogram of HD10E (HD3) and HD2C (HD4)

HD5

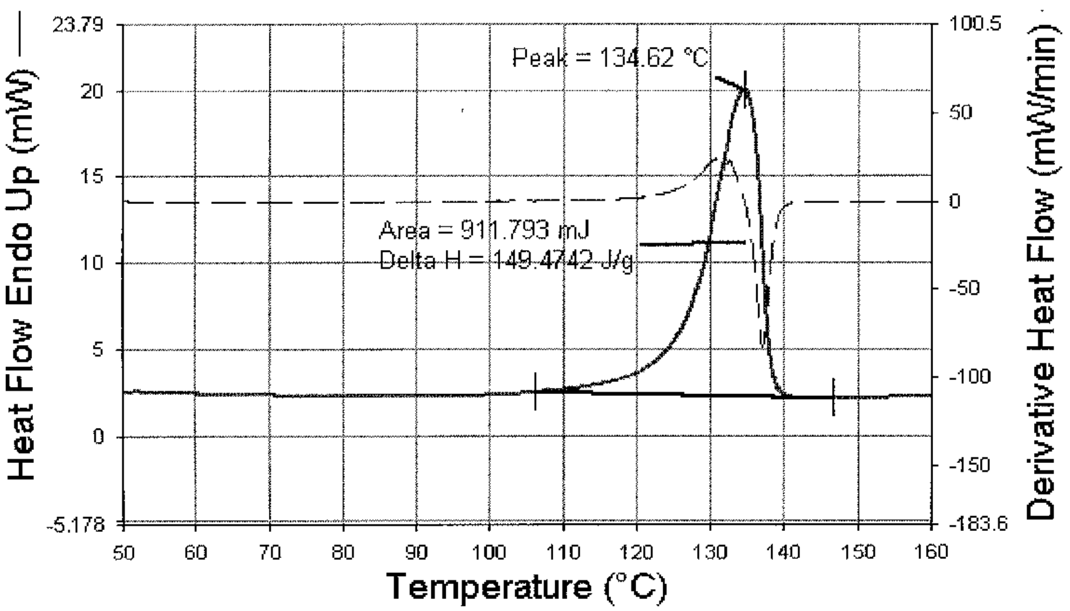

HD6

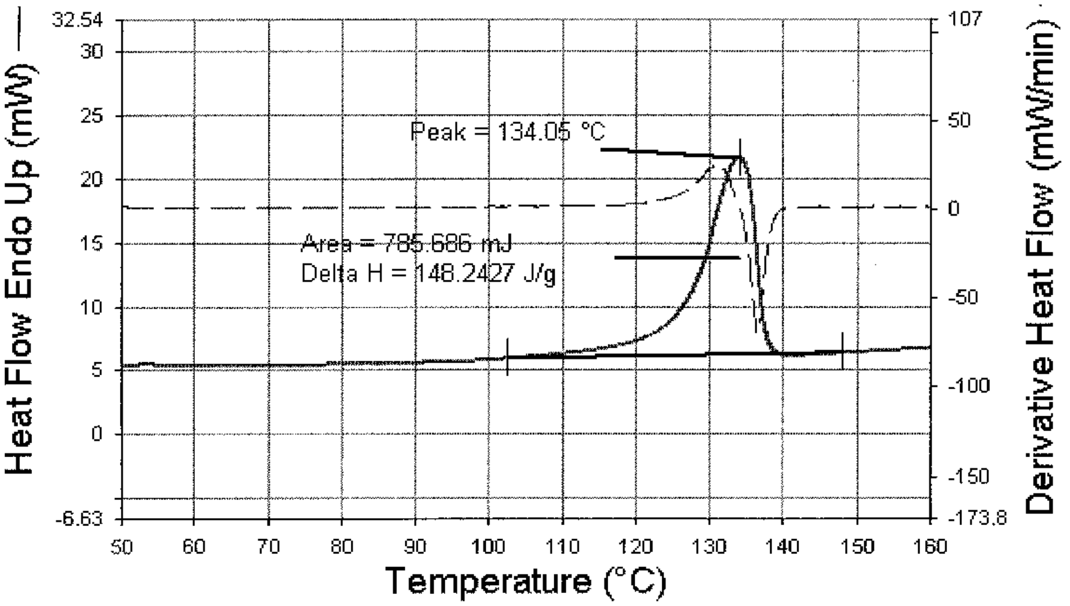

Figure B.3 DSC thermogram of HD4C (HD5) and HD6C (HD6)

HD7

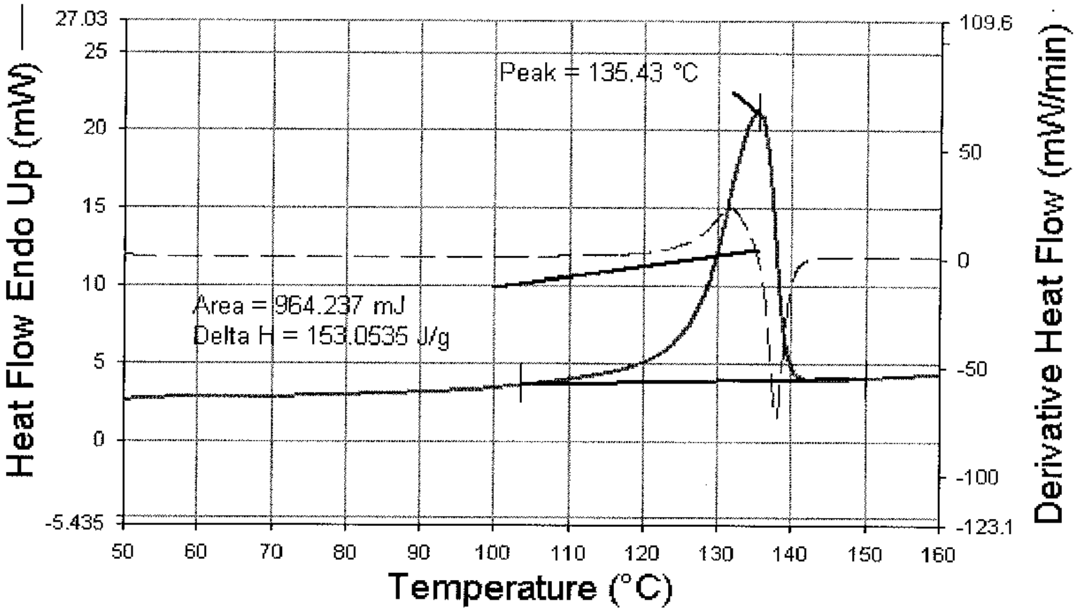

HD8

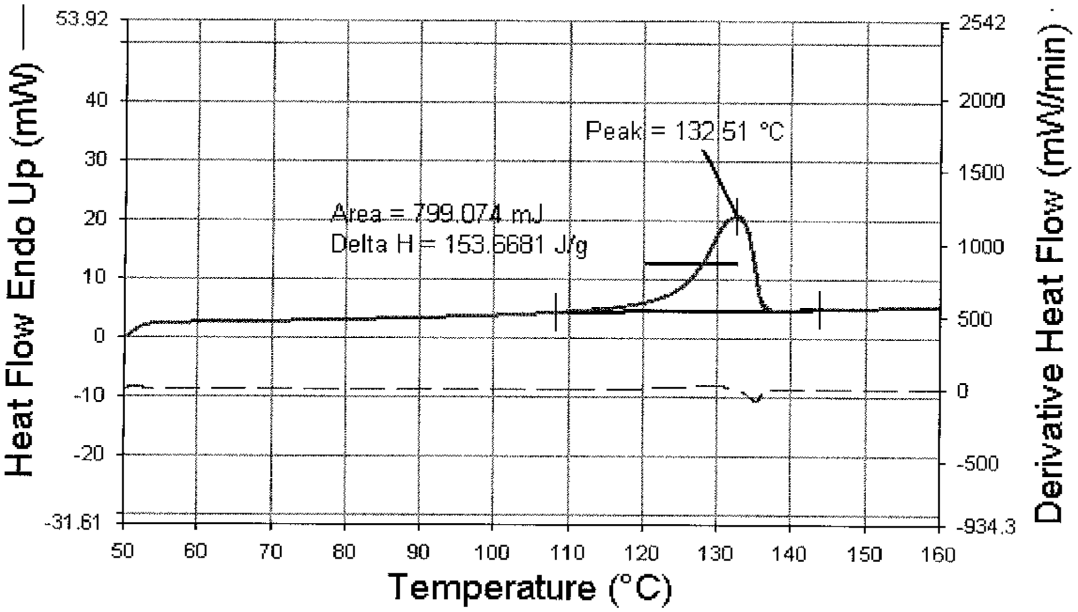

Figure B.4 DSC thermogram of HD5E2C (HD7) and HD5E4C (HD8)

HD9

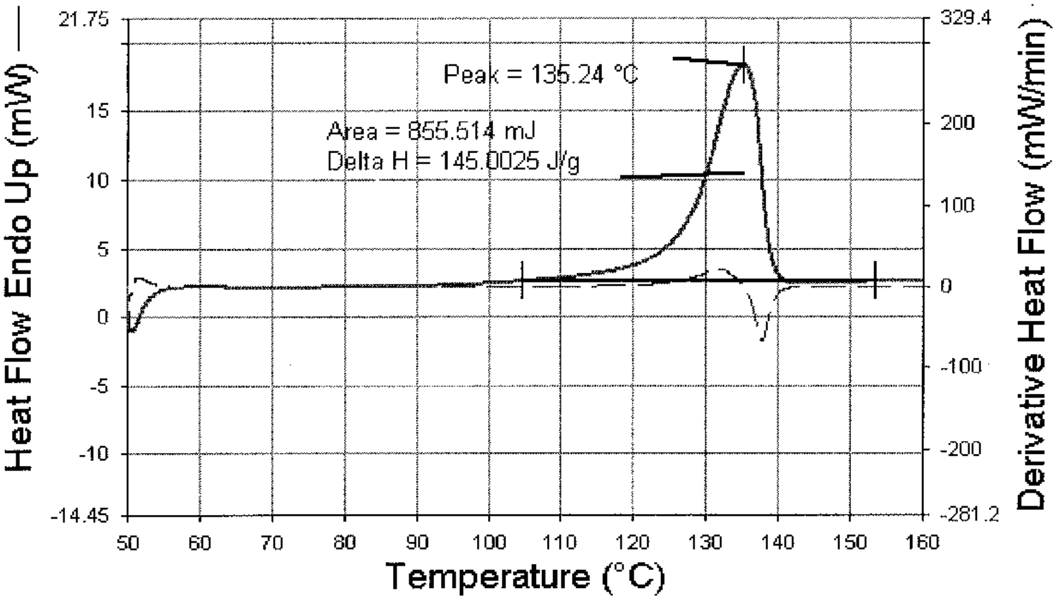

HD10

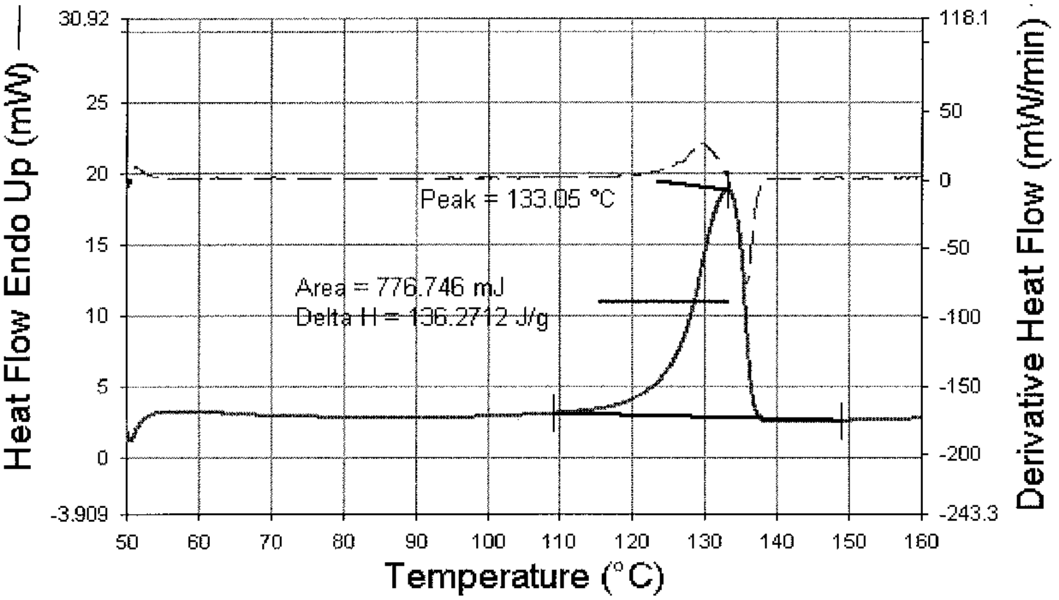

Figure B.5 DSC thermogram of HD5E6C (HD9) and HD10E2C (HD10)

HD11

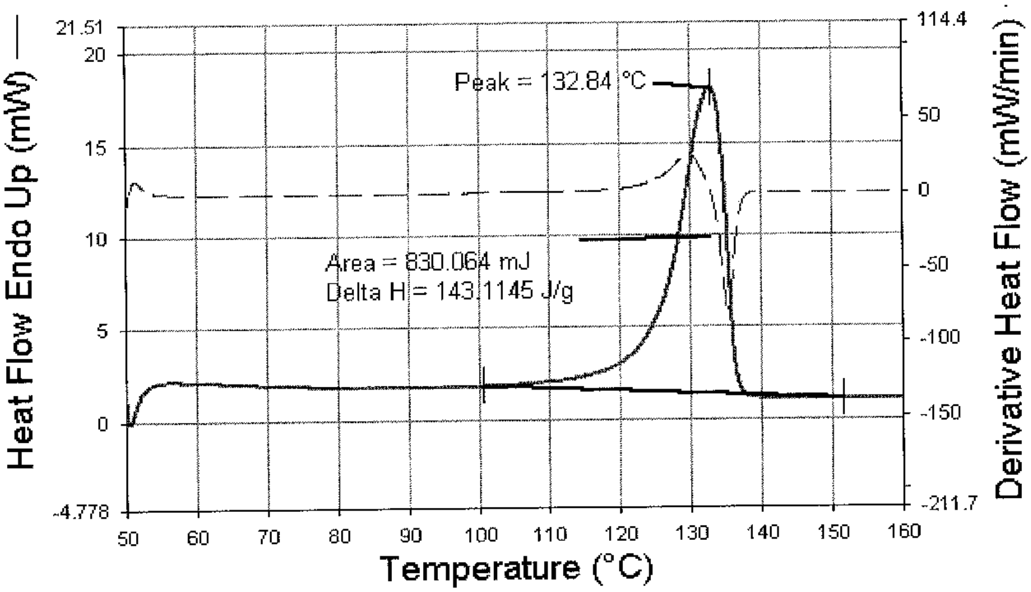

HD12

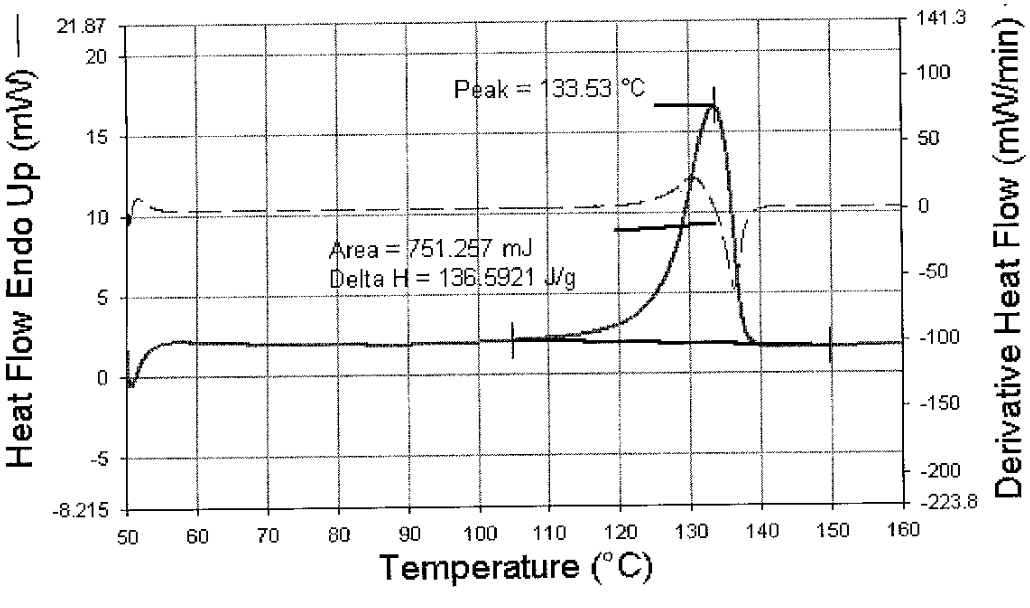

Figure B.6 DSC thermogram of HD10E4C (HD11) and HD10E6C (HD12)

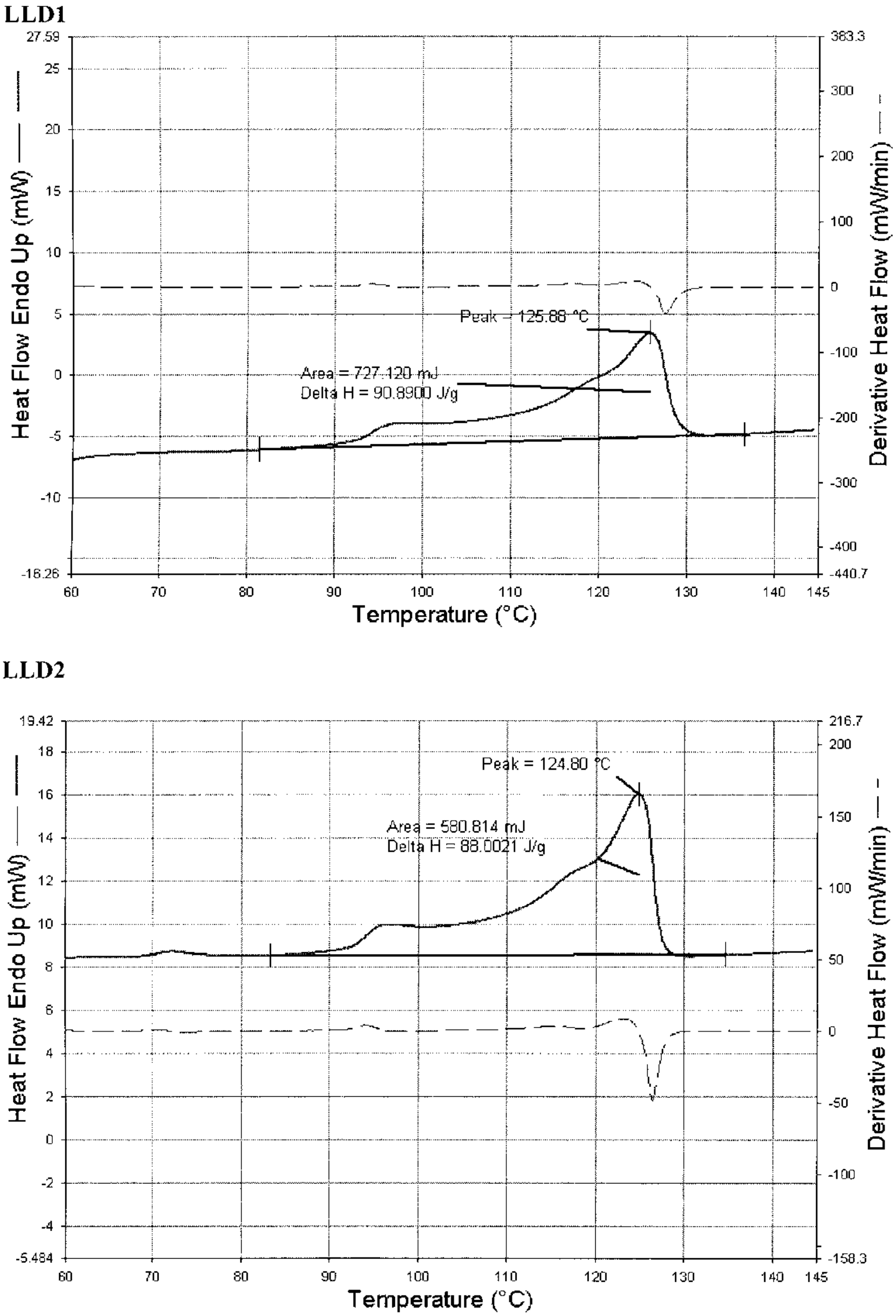

Figure B.7 DSC thermogram of LLD (LLD1) and LLD5E (LLD2)

LLD3

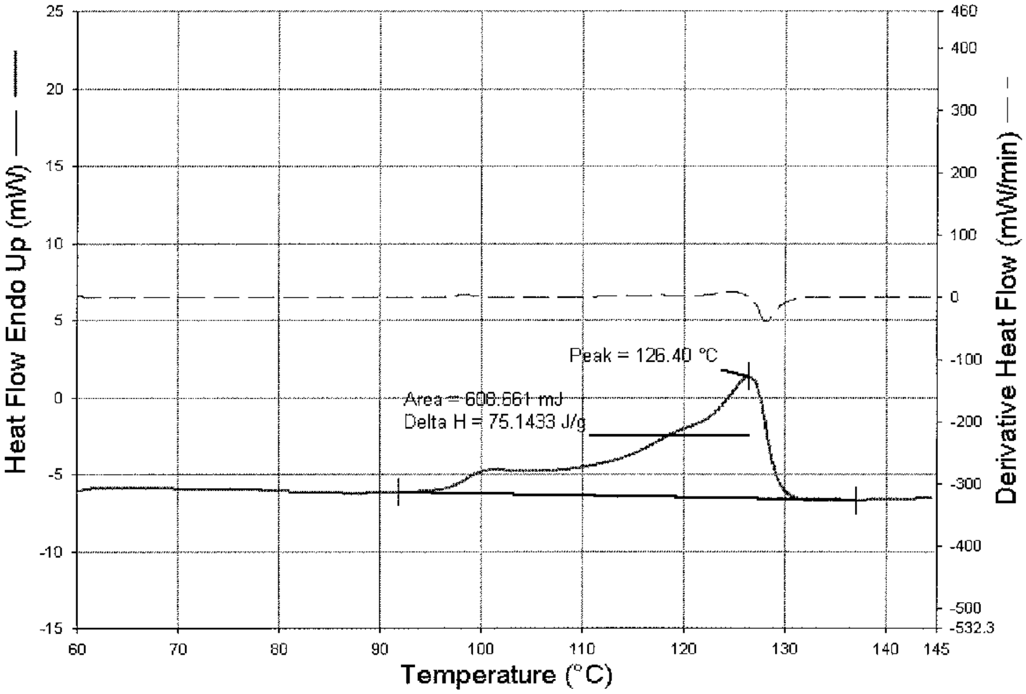

LLD4

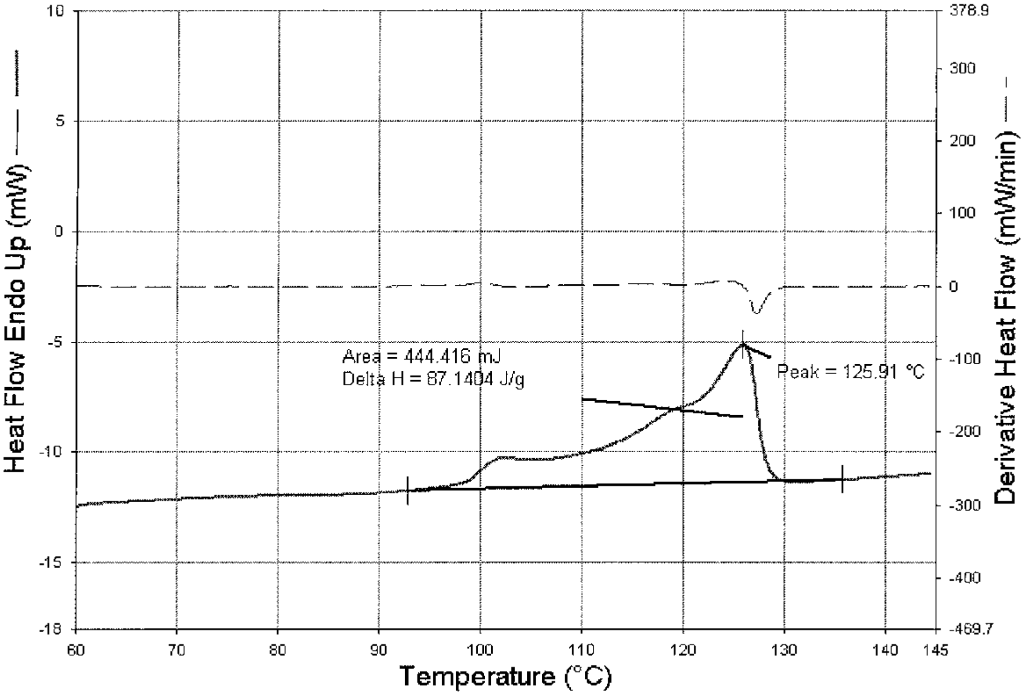

Figure B.8 DSC thermogram of LLD10E (LLD3) and LLD2C (LLD4)

LLD5

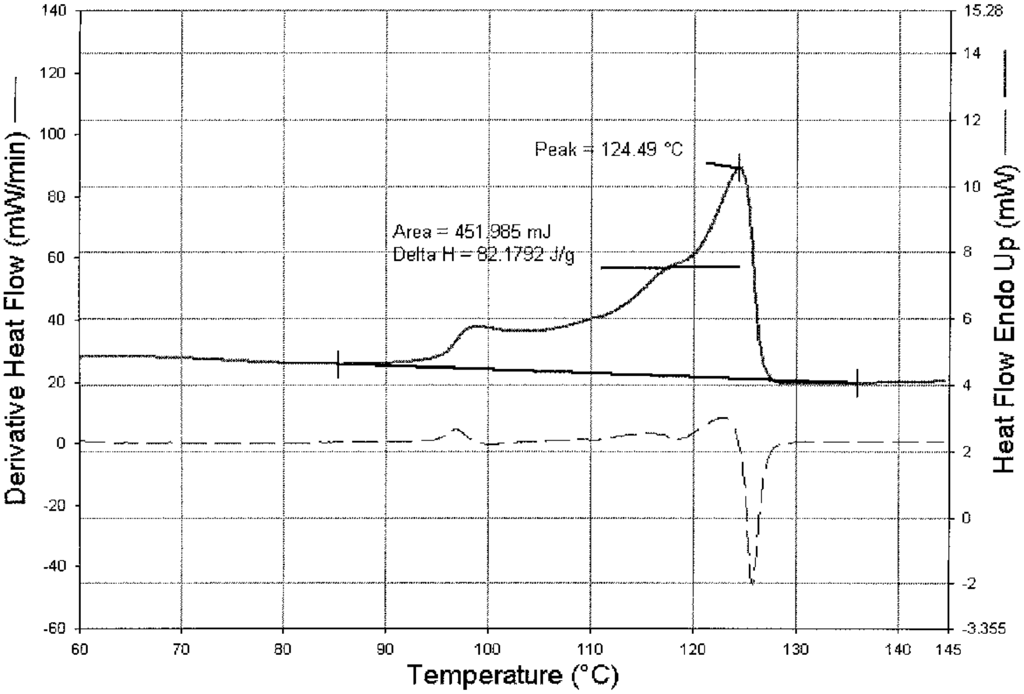

LLD6

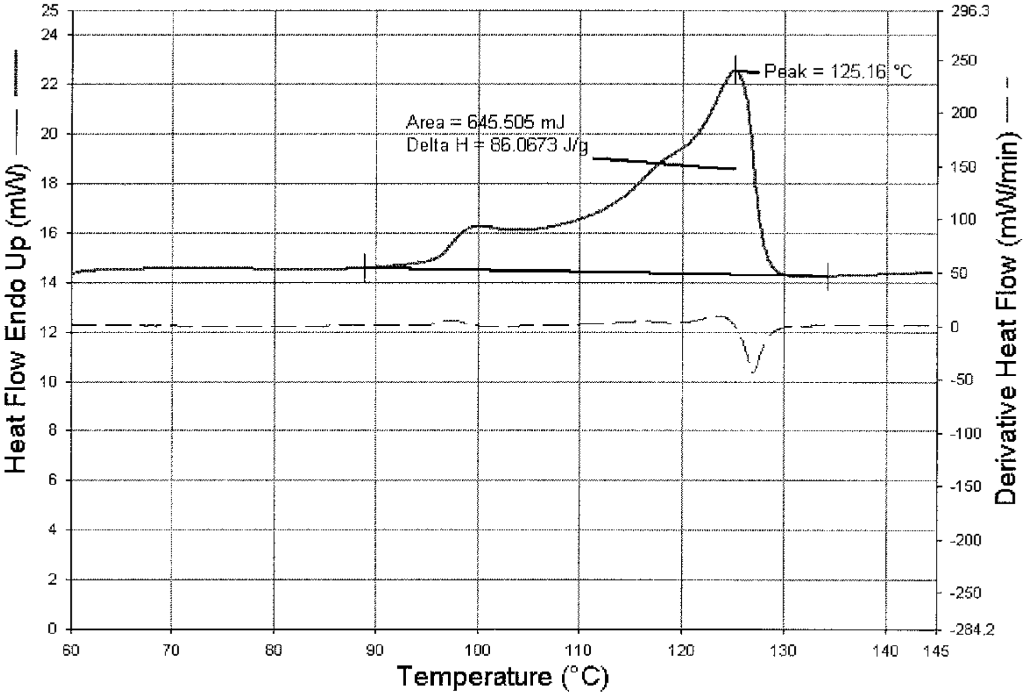

Figure B.9 DSC thermogram of LLD4C (LLD5) and LLD6C (LLD6)

LLD7

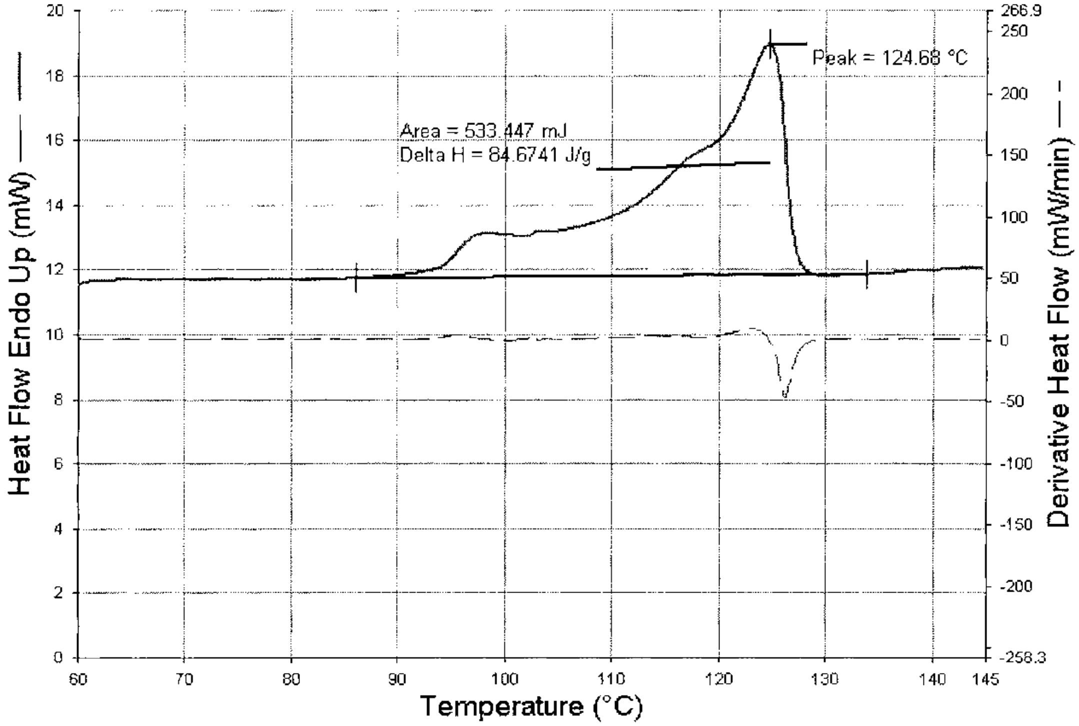

LLD8

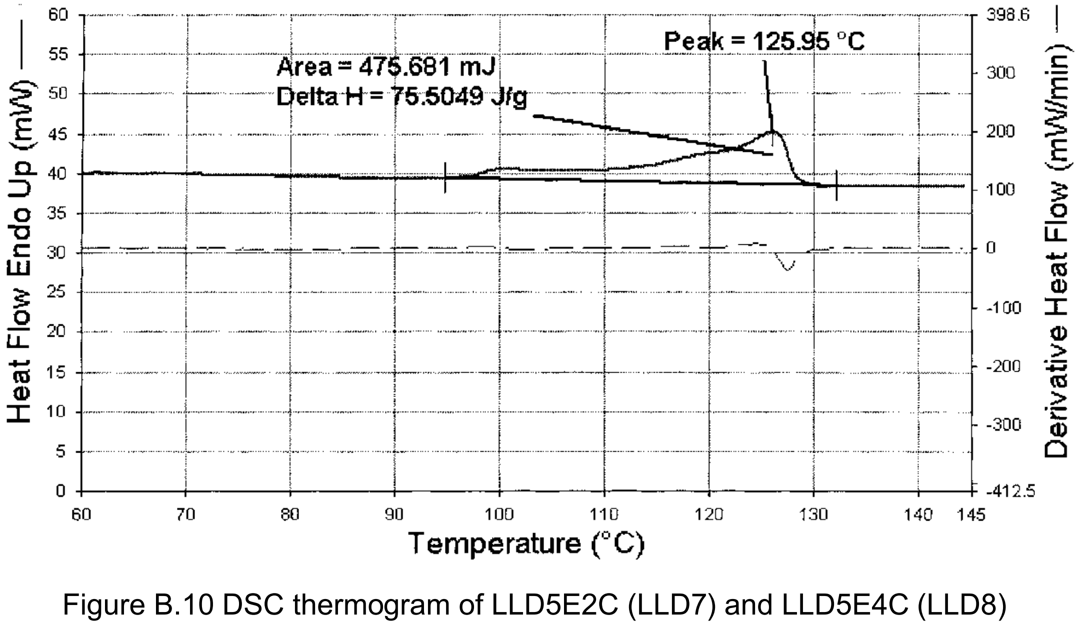

Figure B.10 DSC thermogram of LLD5E2C (LLD7) and LLD5E4C (LLD8)

LLD9

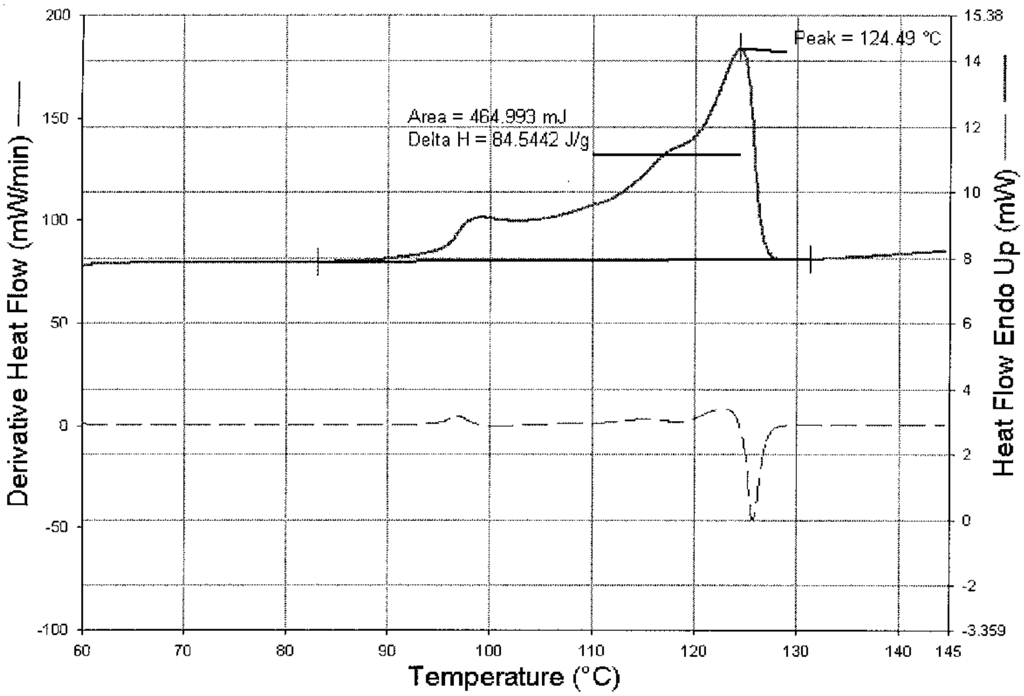

LLD10

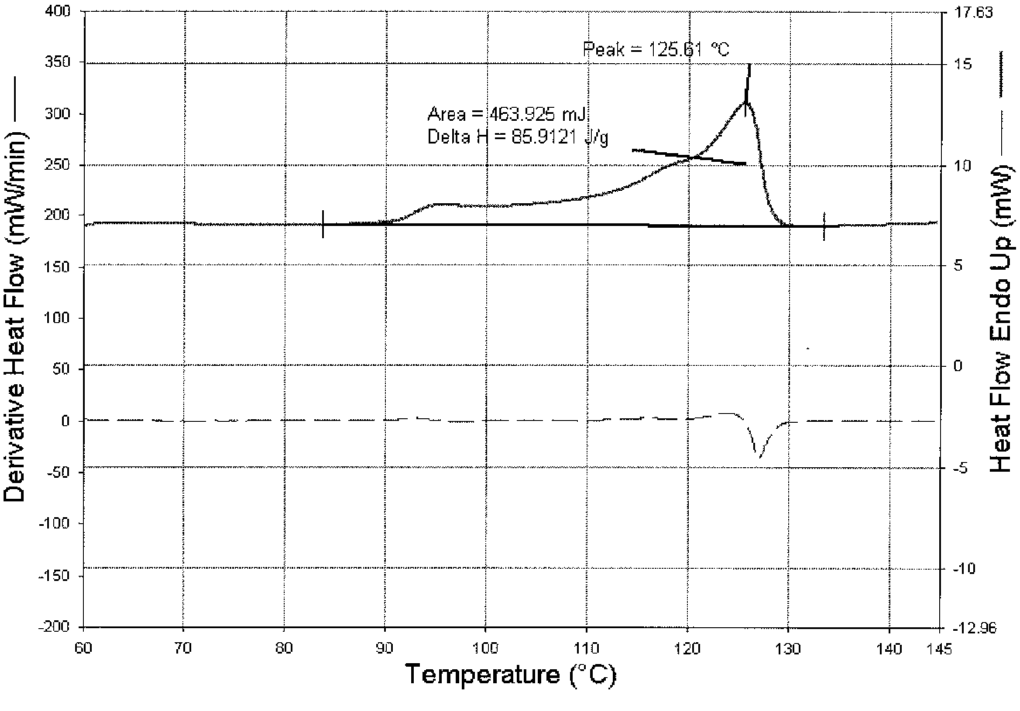

Figure B.11 DSC thermogram of LLD5E6C (LLD9) and LLD10E2C (LLD10)

LLD11

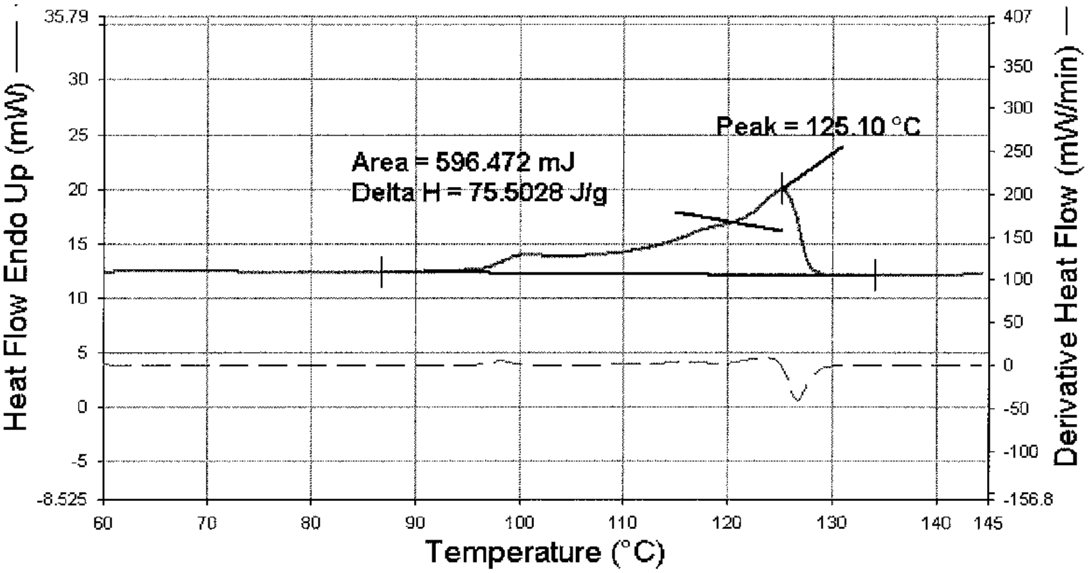

LLD12

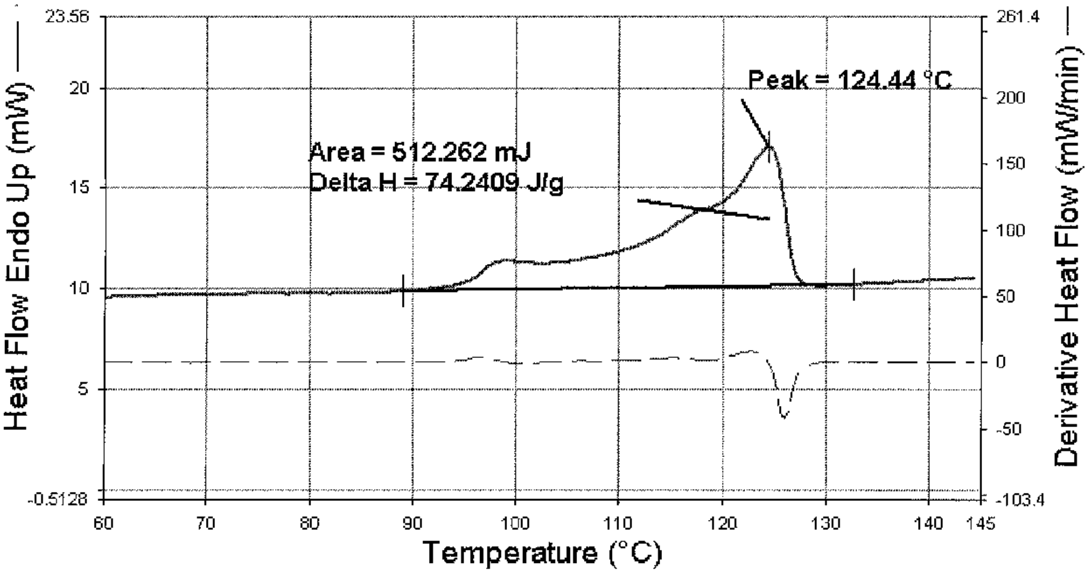

Figure B.12 DSC thermogram of LLD10E4C (LLD11) and LLD10E6C (LLD12)

LD1

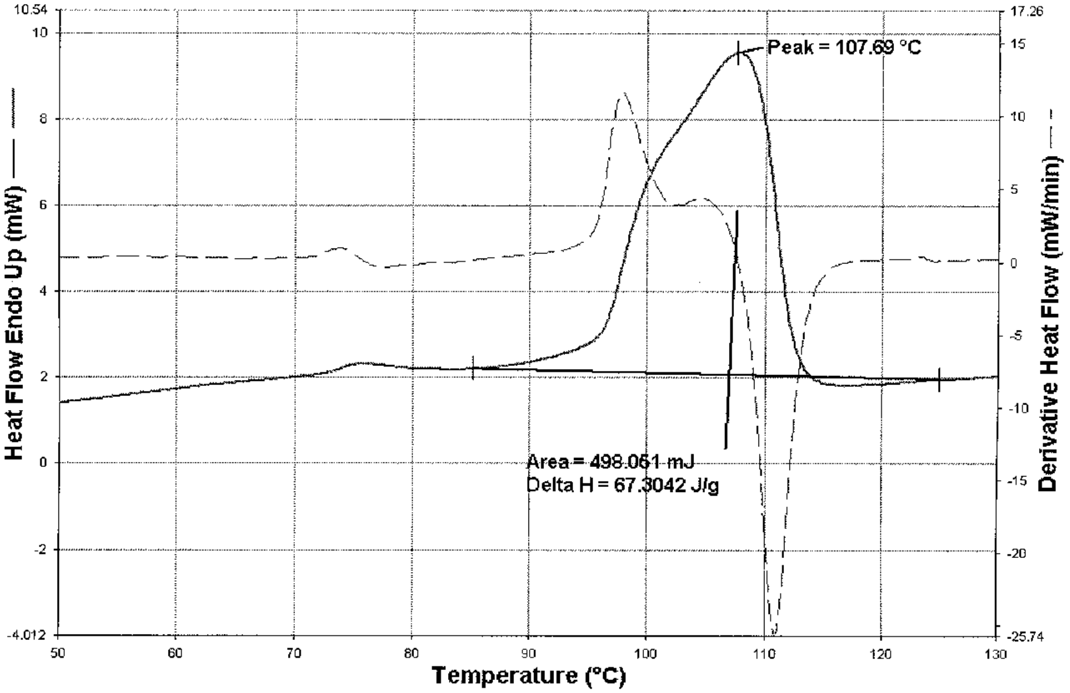

LD2

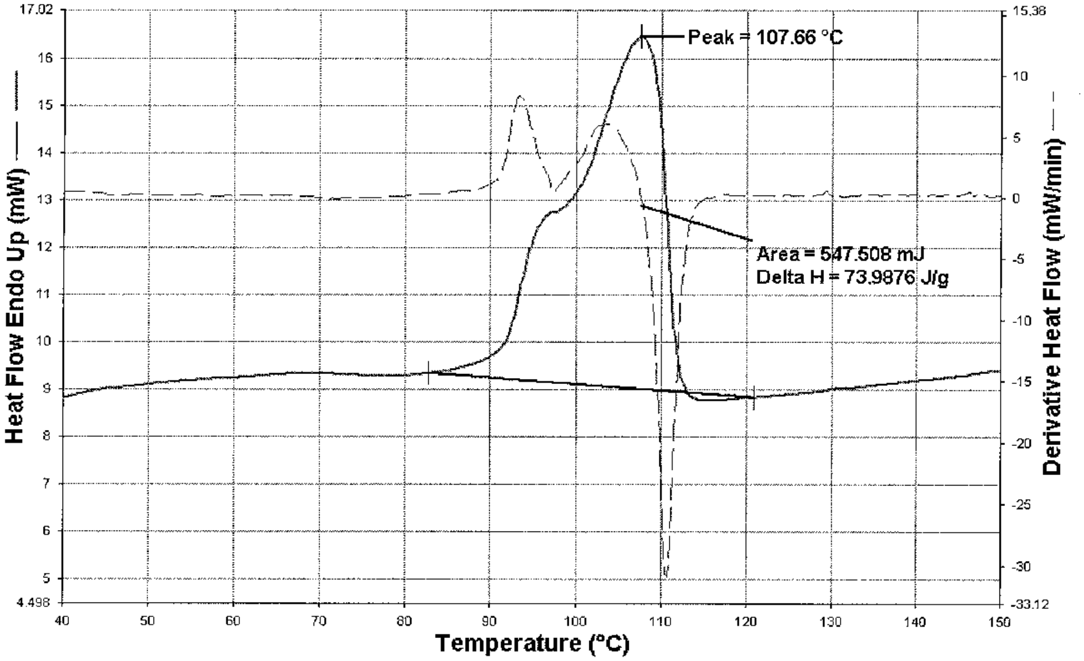

Figure B.13 DSC thermogram of LD (LD1) and LD5E (LD2)

LD3

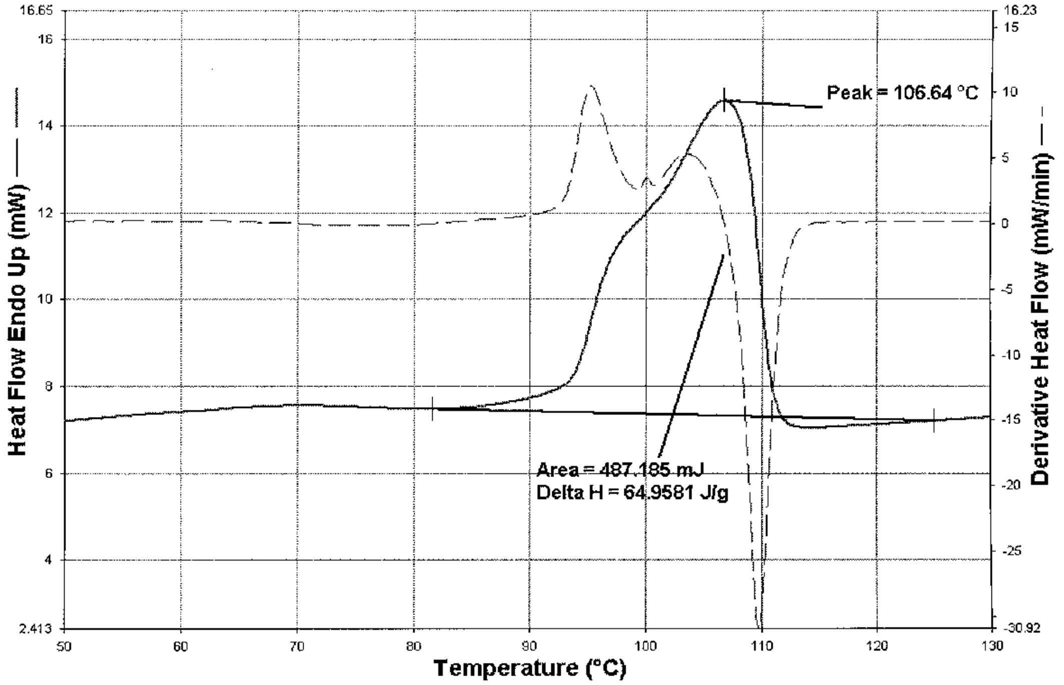

LD4

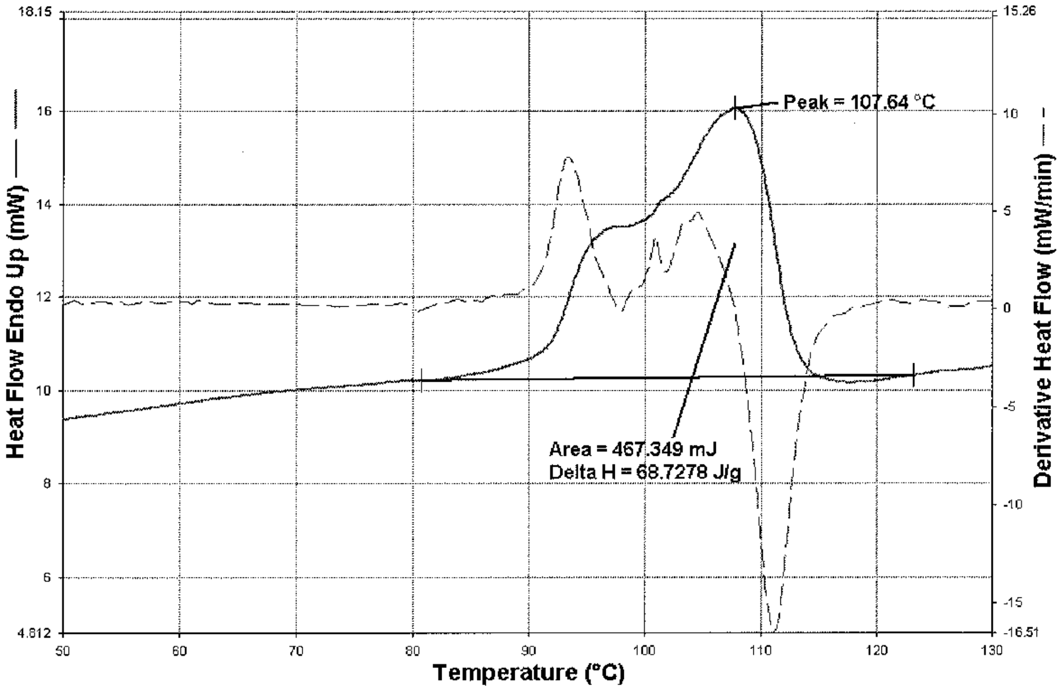

Figure B.14 DSC thermogram of LD10E (LD3) and LD2C (LD4)

LD5

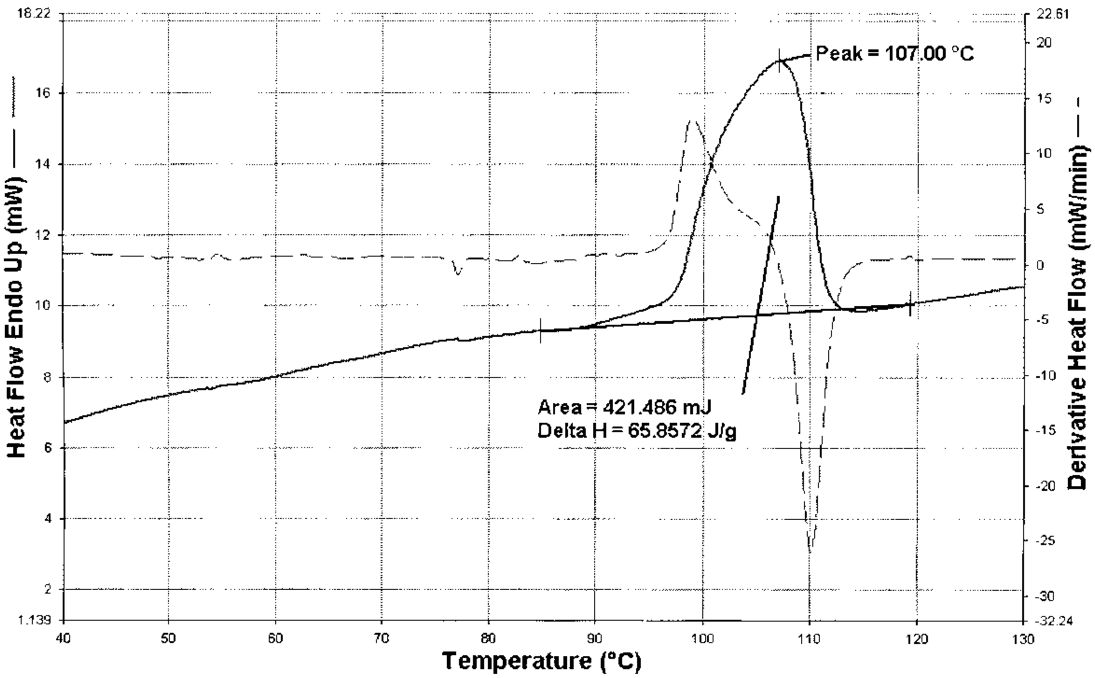

LD6

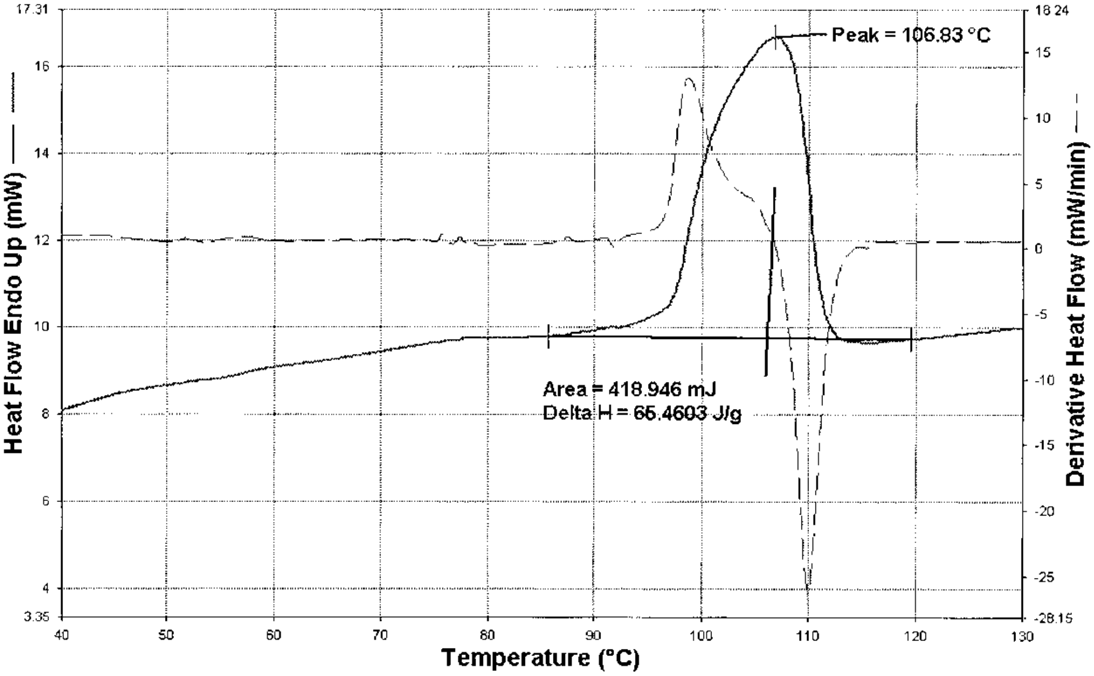

Figure B.15 DSC thermogram of LD4C (LD5) and LD6C (LD6)

LD7

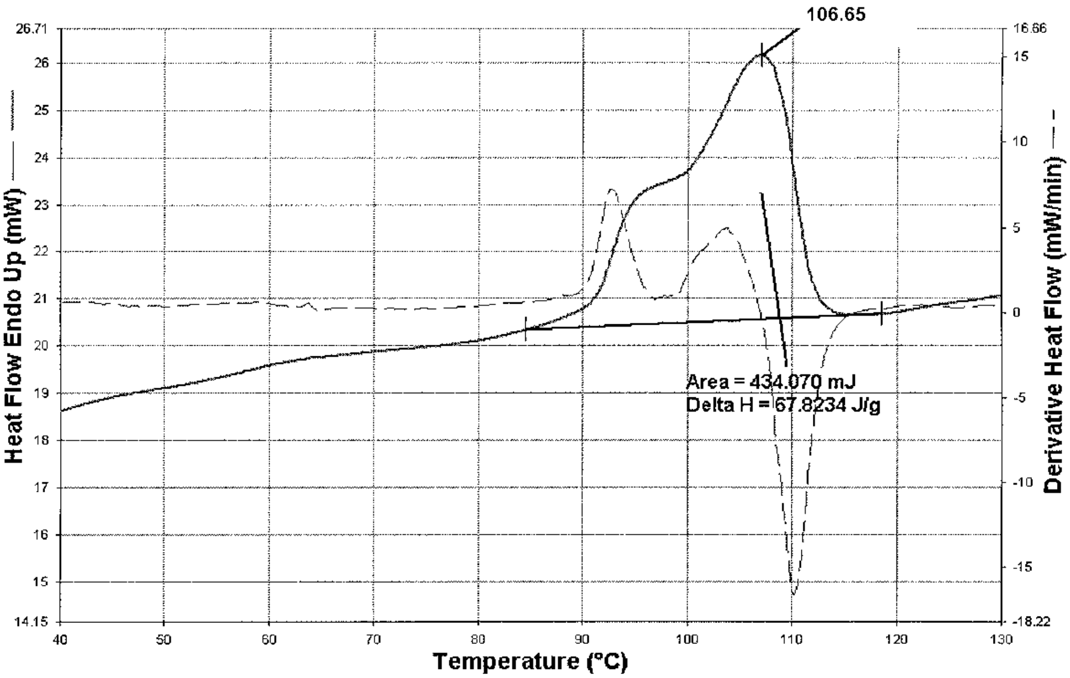

LD8

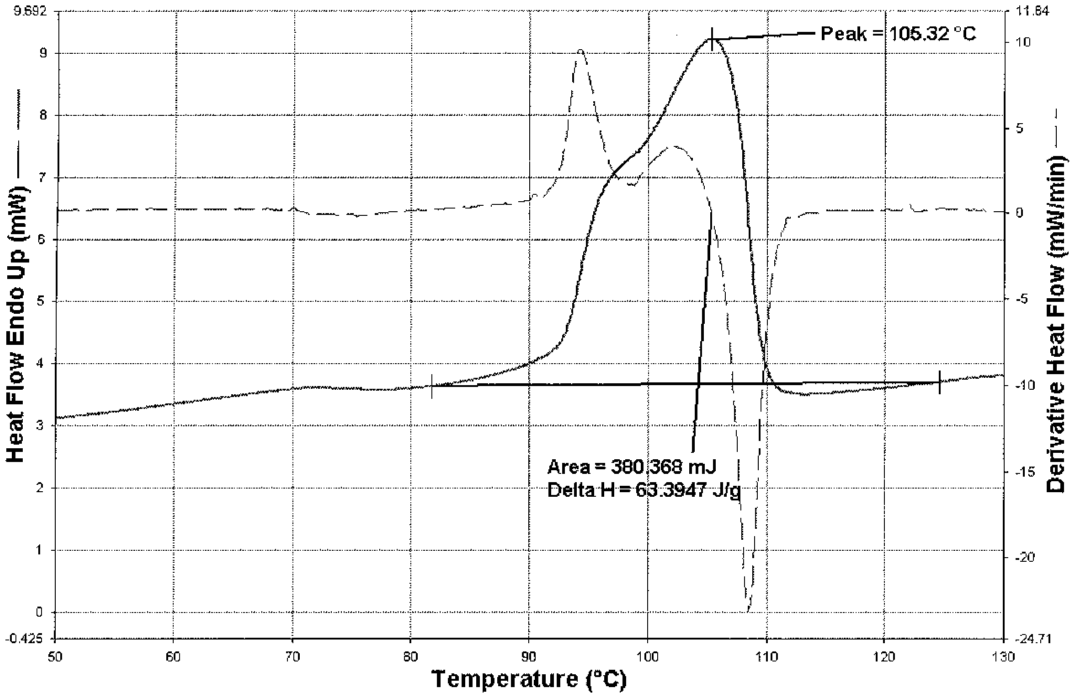

Figure B.16 DSC thermogram of LD5E2C (LD7) and LD5E4C (LD8)

LD9

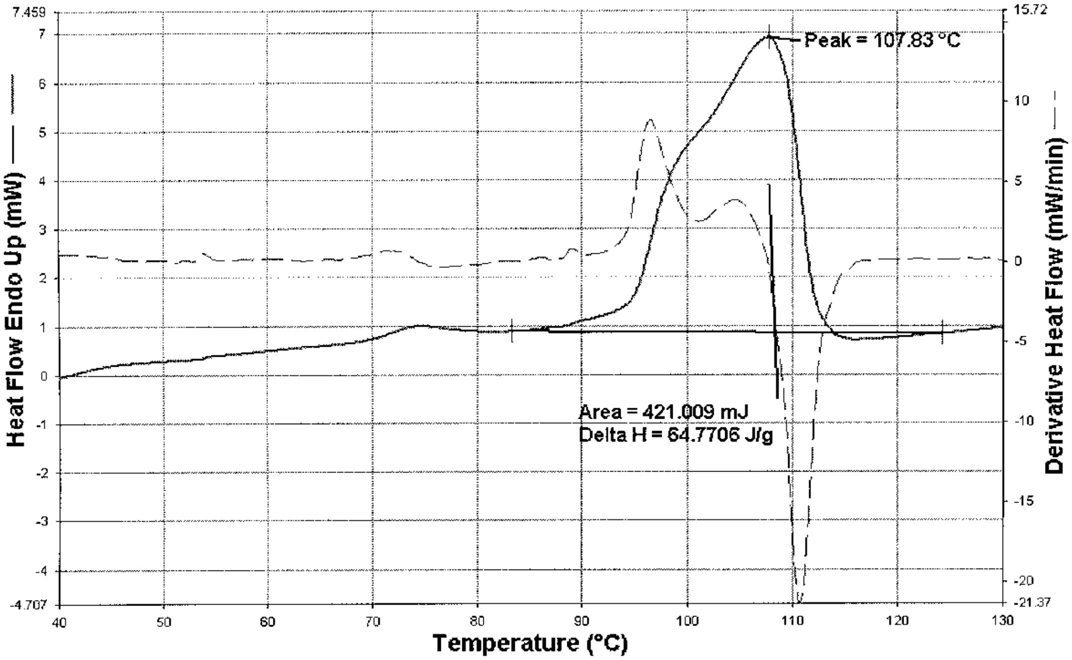

LD10

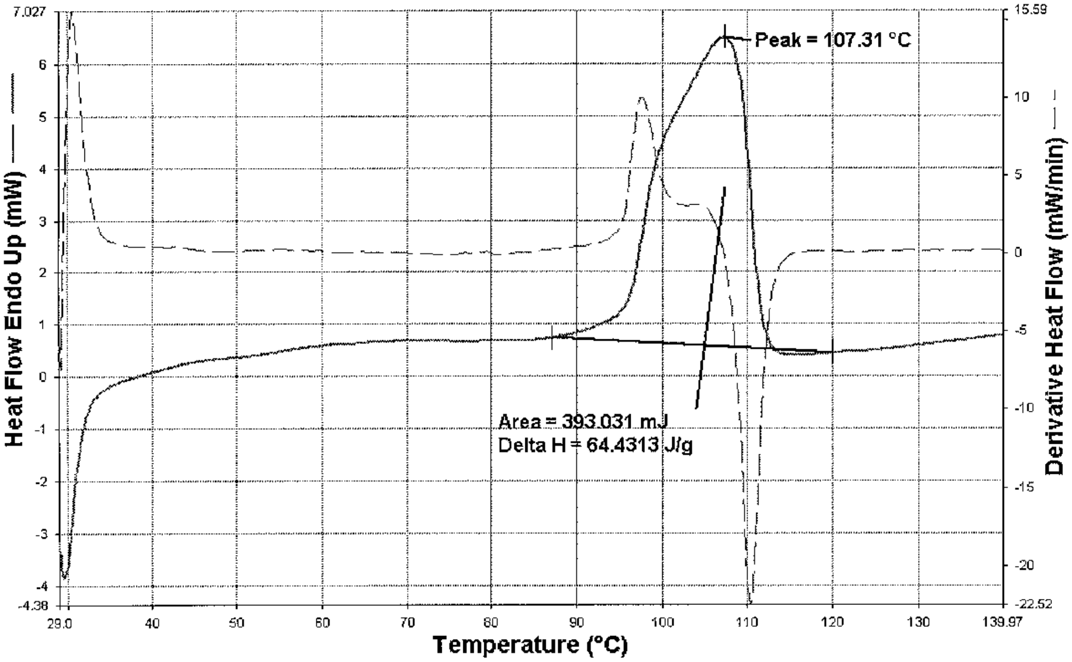

Figure B.17 DSC thermogram of LD5E6C (LD9) and LD10E2C (LD10)

LD11

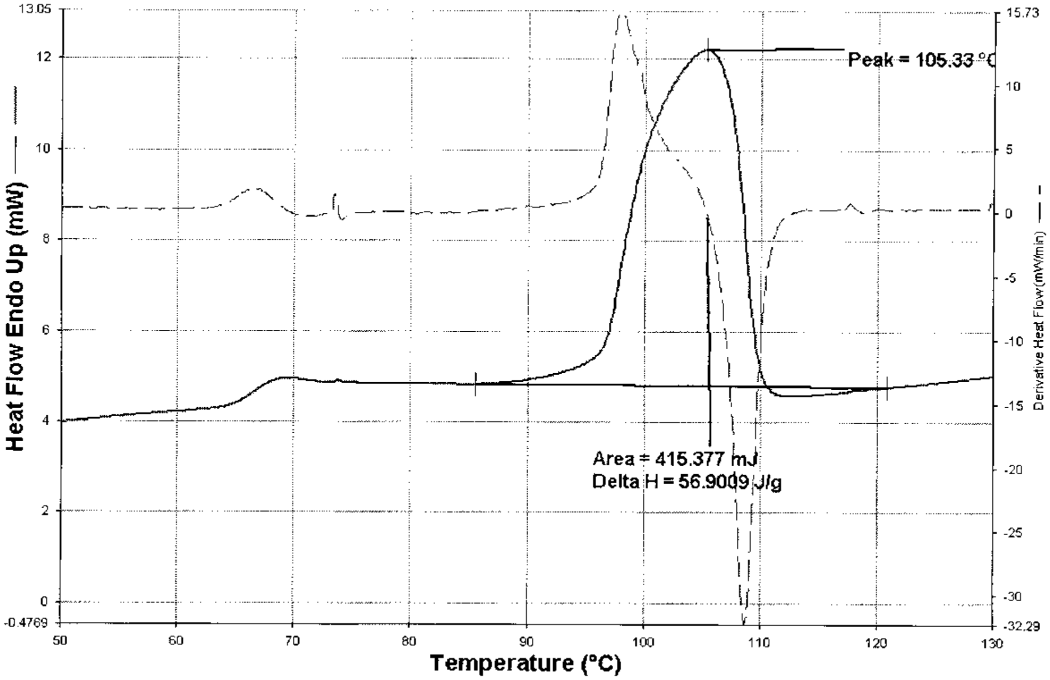

LD12

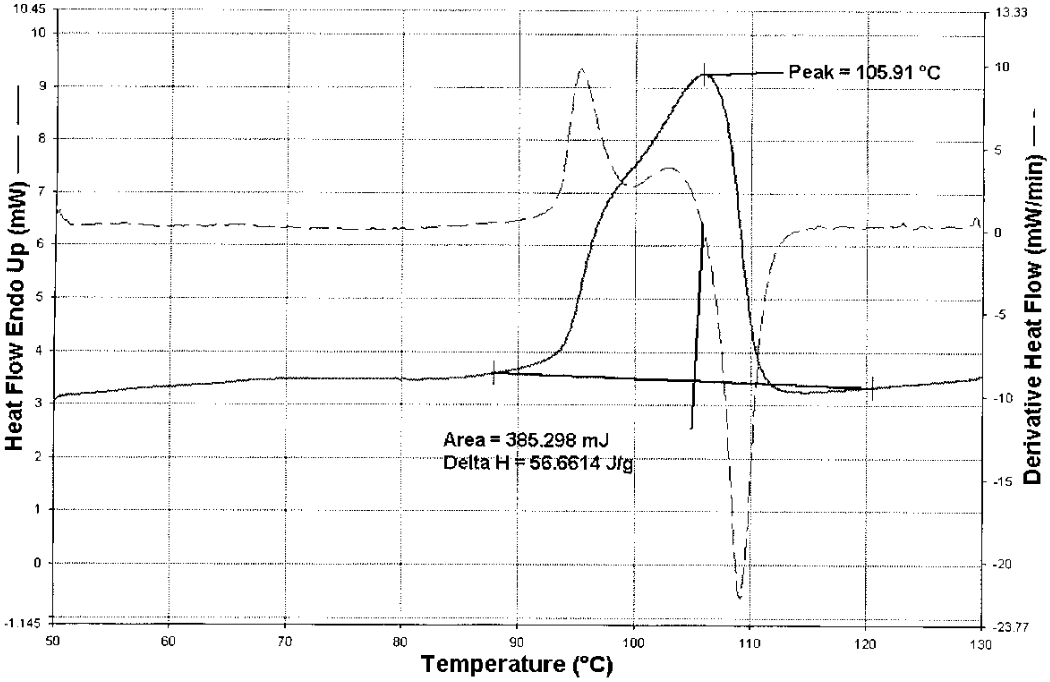

Figure B.18 DSC thermogram of LD10E4C (LD11) and LD10E6C (LD12)

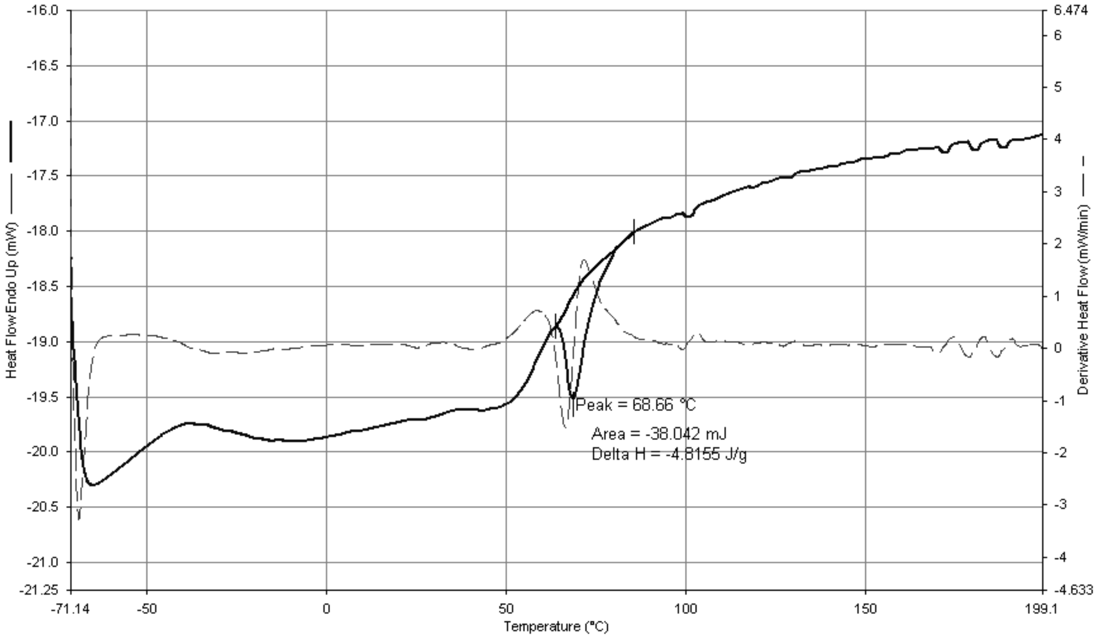

Figure B.19 DSC thermogram of compatibilizer E-MA-GMA (Lotader AX8900)

C. Test Results

Table C.1 HDPE Tensile Strength at Yield Data

Code	Compatibilizer %	Organoclay %	Tensile Strength at Yield (MPa)	St. Dev.
HD	0	0	30.0	0.3
HD5E	5	0	32.2	1.2
HD10E	10	0	29.9	1.9
HD2C	0	2	33.4	0.9
HD4C	0	4	33.8	0.8
HD6C	0	6	36.2	0.5
HD5E2C	5	2	33.8	0.9
HD5E4C	5	4	33.4	1.2
HD5E6C	5	6	35.3	0.5
HD10E2C	10	2	31.2	0.9
HD10E4C	10	4	32.4	0.5
HD10E6C	10	6	35.4	2.1

Table C.2 HDPE Tensile Strength at Break Data

Code	Compatibilizer %	Organoclay %	Tensile Strength at Break (MPa)	St. Dev.
HD	0	0	29.8	0.5
HD5E	5	0	34.9	1.2
HD10E	10	0	21.3	2.2
HD2C	0	2	26.4	3.9
HD4C	0	4	23.4	2.2
HD6C	0	6	21.5	2.2
HD5E2C	5	2	23.1	0.9
HD5E4C	5	4	22.5	1.2
HD5E6C	5	6	19.6	3.7
HD10E2C	10	2	22.2	0.8
HD10E4C	10	4	22.1	0.8
HD10E6C	10	6	19.2	1.2

Table C.3 LLDPE Tensile Strength at Yield Data

Code	Compatibilizer %	Organoclay %	Tensile Strength at Yield (MPa)	St. Dev.
LLD	0	0	12.6	0.3
LLD5E	5	0	12.1	0.3
LLD10E	10	0	11.4	0.1
LLD2C	0	2	12.9	0.4
LLD4C	0	4	13.3	0.3
LLD6C	0	6	13.1	0.2
LLD5E2C	5	2	12.2	0.2
LLD5E4C	5	4	13.0	0.3
LLD5E6C	5	6	13.2	0.4
LLD10E2C	10	2	11.8	0.2
LLD10E4C	10	4	12.4	0.2
LLD10E6C	10	6	12.8	0.2

Table C.4 LLDPE Tensile Strength at Break Data

Code	Compatibilizer %	Organoclay %	Tensile Strength at Break (MPa)	St. Dev.
LLD	0	0	16.5	1.2
LLD5E	5	0	14.8	1.6
LLD10E	10	0	17.0	0.3
LLD2C	0	2	16.1	0.4
LLD4C	0	4	14.8	0.4
LLD6C	0	6	15.4	0.3
LLD5E2C	5	2	14.7	1.7
LLD5E4C	5	4	13.3	1.7
LLD5E6C	5	6	15.0	0.4
LLD10E2C	10	2	15.3	0.1
LLD10E4C	10	4	13.8	1.7
LLD10E6C	10	6	12.0	0.2

Table C.5 LDPE Tensile Strength at Yield Data

Code	Compatibilizer %	Organoclay %	Tensile Strength at Yield (MPa)	St. Dev.
LD	0	0	9.4	0.1
LD5E	5	0	9.2	0.5
LD10E	10	0	8.5	0.4
LD2C	0	2	9.8	0.2
LD4C	0	4	10.0	0.1
LD6C	0	6	10.0	0.4
LD5E2C	5	2	9.2	0.2
LD5E4C	5	4	9.9	0.3
LD5E6C	5	6	9.6	0.4
LD10E2C	10	2	8.1	0.1
LD10E4C	10	4	8.7	0.4
LD10E6C	10	6	9.4	0.1

Table C.6 LDPE Tensile Strength at Break Data

Code	Compatibilizer %	Organoclay %	Tensile Strength at Break (MPa)	St. Dev.
LD	0	0	16.5	0.2
LD5E	5	0	16.2	0.2
LD10E	10	0	14.4	1.9
LD2C	0	2	15.4	0.7
LD4C	0	4	15.3	0.1
LD6C	0	6	14.7	0.5
LD5E2C	5	2	14.3	0.7
LD5E4C	5	4	14.8	0.6
LD5E6C	5	6	14.3	0.7
LD10E2C	10	2	14.5	0.2
LD10E4C	10	4	14.5	0.3
LD10E6C	10	6	14.3	0.5

Table C.7 HDPE Tensile Modulus Data

Code	Compatibilizer %	Organoclay %	Modulus MPa	St. Dev.
HD	0	0	622.8	56.3
HD5E	5	0	691.5	78.0
HD10E	10	0	630.8	167.6
HD2C	0	2	716.3	144.9
HD4C	0	4	544.1	51.3
HD6C	0	6	1008.3	59.7
HD5E2C	5	2	720.6	184.6
HD5E4C	5	4	853.2	53.8
HD5E6C	5	6	905.0	187.2
HD10E2C	10	2	723.8	142.6
HD10E4C	10	4	756.9	65.9
HD10E6C	10	6	793.0	117.4

Table C.8 LLDPE Tensile Modulus Data

Code	Compatibilizer %	Organoclay %	Modulus MPa	St. Dev.
LLD	0	0	262.8	36.5
LLD5E	5	0	200.3	41.9
LLD10E	10	0	193.6	45.4
LLD2C	0	2	188.6	11.5
LLD4C	0	4	236.4	28.4
LLD6C	0	6	265.3	64.2
LLD5E2C	5	2	195.6	41.7
LLD5E4C	5	4	223.2	61.7
LLD5E6C	5	6	235.4	37.8
LLD10E2C	10	2	204.9	20.0
LLD10E4C	10	4	170.3	31.9
LLD10E6C	10	6	220.9	42.5

Table C.9 LDPE Tensile Modulus Data

Code	Compatibilizer %	Organoclay %	Modulus MPa	St. Dev.
LD	0	0	108.9	4.7
LD5E	5	0	106.0	15.0
LD10E	10	0	110.1	6.2
LD2C	0	2	140.8	14.4
LD4C	0	4	150.6	24.9
LD6C	0	6	156.0	24.9
LD5E2C	5	2	118.3	10.5
LD5E4C	5	4	133.7	13.7
LD5E6C	5	6	126.6	21.4
LD10E2C	10	2	89.7	11.8
LD10E4C	10	4	104.5	6.7
LD10E6C	10	6	124.8	1.4

Table C.10 HDPE Elongation at Break Data

Code	Compatibilizer %	Organoclay %	Strain at Break %	St. Dev.
HD	0	0	658.3	47.5
HD5E	5	0	752.4	18.6
HD10E	10	0	366.0	128.8
HD2C	0	2	500.1	174.6
HD4C	0	4	270.6	238.5
HD6C	0	6	41.6	4.4
HD5E2C	5	2	310.9	199.0
HD5E4C	5	4	257.9	180.9
HD5E6C	5	6	44.3	9.9
HD10E2C	10	2	200.8	27.3
HD10E4C	10	4	139.8	87.0
HD10E6C	10	6	26.0	6.7

Table C.11 LLDPE Elongation at Break Data

Code	Compatibilizer %	Organoclay %	Strain at Break %	St. Dev.
LLD	0	0	614.4	74.0
LLD5E	5	0	541.3	90.6
LLD10E	10	0	698.0	23.3
LLD2C	0	2	621.0	29.9
LLD4C	0	4	549.0	3.6
LLD6C	0	6	590.6	24.4
LLD5E2C	5	2	560.0	63.3
LLD5E4C	5	4	479.7	91.9
LLD5E6C	5	6	583.7	18.0
LLD10E2C	10	2	568.5	53.8
LLD10E4C	10	4	436.7	165.8
LLD10E6C	10	6	383.2	131.6

Table C.12 LDPE Elongation at Break Data

Code	Compatibilizer %	Organoclay %	Strain at Break %	St. Dev.
LD	0	0	160.2	8.7
LD5E	5	0	160.6	24.4
LD10E	10	0	147.1	47.4
LD2C	0	2	136.5	13.8
LD4C	0	4	128.3	12.9
LD6C	0	6	103.4	18.1
LD5E2C	5	2	134.6	44.0
LD5E4C	5	4	108.9	17.0
LD5E6C	5	6	102.5	24.6
LD10E2C	10	2	143.1	7.2
LD10E4C	10	4	127.7	6.6
LD10E6C	10	6	115.6	11.2

Table C.13 HDPE Flexural Data

HDPE Comp. %	Clay %	Flexural strength MPa	Flexural strength St.Dev. MPa	Deflection at max load mm	Deflection at max load St.Dev.mm	Flexural modulus MPa	Flexural modulus St.Dev. MPa
0	0	31.9	1.2	13.5	0.7	783	52
5	0	32.5	1.6	12.7	0.7	691	52
10	0	28.9	1.6	13.5	0.3	618	36
0	2	33.5	1.2	13.0	1.6	712	39
0	4	32.2	0.5	13.2	0.7	882	21
0	6	33.8	1.7	13.2	0.6	891	25
5	2	31.2	0.5	12.9	0.6	831	45
5	4	31.2	0.8	13.2	0.4	838	43
5	6	32.6	0.7	12.5	0.3	836	27
10	2	28.4	1.9	13.2	0.5	738	53
10	4	29.7	0.4	13.2	0.6	740	14
10	6	31.2	0.7	12.8	0.4	807	28

Table C.14 LLDPE Flexural Data

LLDPE Comp. %	Clay %	Flexural strength MPa	Flexural strength St.Dev. MPa	Deflection at max load mm	Deflection at max load St.Dev.mm	Flexural modulus MPa	Flexural modulus St.Dev. MPa
0	0	12.1	0.1	14.0	0.7	264	6
5	0	10.5	0.3	15.0	0.5	218	6
10	0	10.3	0.3	14.4	0.9	205	7
0	2	13.0	0.8	14.1	0.6	282	8
0	4	13.5	0.6	14.4	0.8	311	6
0	6	12.6	0.8	14.0	0.9	290	27
5	2	10.7	0.6	14.4	0.7	210	12
5	4	11.1	0.2	13.5	0.3	248	13
5	6	11.0	0.9	13.6	0.7	246	16
10	2	8.9	0.5	13.8	1.2	182	8
10	4	9.1	0.2	13.6	0.7	186	7
10	6	9.9	0.3	13.9	0.5	208	13

Table C.15 LLDPE Flexural Data

LDPE Comp. %	Clay %	Flexural strength MPa	Flexural strength St.Dev. MPa	Deflection at max load mm	Deflection at max load St.Dev.mm	Flexural modulus MPa	Flexural modulus St.Dev. MPa
0	0	111	7	15.5	0.7	111	7
5	0	111	8	14.2	0.4	111	8
10	0	114	4	14.5	0.8	114	4
0	2	143	6	14.5	0.6	143	6
0	4	140	7	14.8	0.6	140	7
0	6	161	4	13.8	0.3	161	4
5	2	128	2	15.9	0.6	128	2
5	4	137	7	14.3	0.3	137	7
5	6	161	5	9.5	0.3	161	5
10	2	114	6	9.5	0.6	114	6
10	4	122	5	9.6	0.4	122	5
10	6	125	1	9.1	0.5	125	1

Table C.16 HDPE Notched Charpy Impact Test Results

Code	Compatibilizer %	Organoclay %	Impact Strength kJ/m^2	St. Dev.
HD	0	0	5.8	0.1
HD5E	5	0	6.8	0.1
HD10E	10	0	10.6	0.4
HD2C	0	2	3.9	0.9
HD4C	0	4	3.9	1.1
HD6C	0	6	2.5	0.1
HD5E2C	5	2	4.2	0.6
HD5E4C	5	4	3.2	0.3
HD5E6C	5	6	3.6	1.3
HD10E2C	10	2	4.3	0.2
HD10E4C	10	4	4.1	0.7
HD10E6C	10	6	4.0	0.3

Table C.17 LLDPE Notched Charpy Impact Test Results

Code	Compatibilizer %	Organoclay %	Impact Strength kJ/m^2	St. Dev.
LLD	0	0	67.6	3.7
LLD5E	5	0	72.5	5.8
LLD10E	10	0	74.3	2.3
LLD2C	0	2	13.6	0.7
LLD4C	0	4	8.5	0.5
LLD6C	0	6	9.1	0.4
LLD5E2C	5	2	43.4	5.0
LLD5E4C	5	4	8.4	0.4
LLD5E6C	5	6	7.0	0.4
LLD10E2C	10	2	72.2	5.0
LLD10E4C	10	4	15.9	0.9
LLD10E6C	10	6	12.6	0.8

Table C.18 LDPE Notched Charpy Impact Test Results

Code	Compatibilizer %	Organoclay %	Impact Strength kJ/m^2	St. Dev.
LD	0	0	65.8	0.8
LD5E	5	0	70.2	2.3
LD10E	10	0	72.1	1.9
LD2C	0	2	56.7	11.1
LD4C	0	4	24.6	2.0
LD6C	0	6	16.3	2.6
LD5E2C	5	2	52.8	7.8
LD5E4C	5	4	18.4	2.4
LD5E6C	5	6	14.3	1.0
LD10E2C	10	2	60.8	7.4
LD10E4C	10	4	32.5	3.6
LD10E6C	10	6	14.7	1.4

Table C.19 Melt flow index of all samples

Comp. %	Clay %	HDPE g/10min	St. Dev.	LLDPE g/10min	St. Dev.	LDPE g/10min	St. Dev.
0	0	7.6	0.2	16.7	0.1	21.1	0.4
5	0	5.7	0.1	16.2	0.1	21.1	0.2
10	0	6.1	0.1	15.4	0.2	20.9	0.2
0	2	6.1	0.1	19.1	0.4	21.8	0.3
0	4	5.6	0.1	18.7	0.4	22.2	0.3
0	6	5.4	0.1	18.5	0.3	22.0	0.5
5	2	6.0	0.1	16.1	0.1	19.4	0.1
5	4	5.2	0.1	14.1	0.1	18.4	0.3
5	6	4.8	0.1	14.3	0.2	16.8	0.2
10	2	5.3	0.1	14.6	0.1	18.3	0.1
10	4	4.8	0.1	12.6	0.2	15.7	0.1
10	6	3.6	0.1	12.8	0.2	14.1	0.3